Space Sci Rev (2015) 192:145–208
DOI 10.1007/s11214-015-0187-2

The Earth: Plasma Sources, Losses, and Transport Processes

Daniel T. Welling[1] · Mats André[2] · Iannis Dandouras[3] · Dominique Delcourt[4] · Andrew Fazakerley[5] · Dominique Fontaine[4] · John Foster[6] · Raluca Ilie[1] · Lynn Kistler[7] · Justin H. Lee[8] · Michael W. Liemohn[1] · James A. Slavin[1] · Chih-Ping Wang[9] · Michael Wiltberger[10] · Andrew Yau[11]

Received: 7 March 2015 / Accepted: 13 July 2015 / Published online: 17 September 2015

Abstract This paper reviews the state of knowledge concerning the source of magnetospheric plasma at Earth. Source of plasma, its acceleration and transport throughout the system, its consequences on system dynamics, and its loss are all discussed. Both observational and modeling advances since the last time this subject was covered in detail (Hultqvist et al., Magnetospheric Plasma Sources and Losses, 1999) are addressed.

Keywords Magnetosphere · Plasma · Ionosphere · Solar wind

✉ D.T. Welling
dwelling@umich.edu

M. André
mats.andre@irfu.se

I. Dandouras
Iannis.Dandouras@irap.omp.eu

D. Delcourt
dominique.delcourt@lpp.polytechnique.fr

A. Fazakerley
a.fazakerley@ucl.ac.uk

D. Fontaine
dominique.fontaine@lpp.polytechnique.fr

J. Foster
jcf@haystack.mit.edu

R. Ilie
rilie@umich.edu

L. Kistler
lynn.kistler@unh.edu

J.H. Lee
Justin.H.Lee@aero.org

M.W. Liemohn
liemohn@umich.edu

J.A. Slavin
jaslavin@umich.edu

1 Introduction

Earth, being our most extensively explored solar system body, has decades of work dedicated to the sources, losses, and circulation of plasma within its magnetosphere. Indeed, a previous International Space Science Institute review book has already been dedicated to this topic (Hultqvist et al. 1999). This book painted a picture of the balance between ionospheric and solar wind plasma at every major magnetospheric region, from the high latitude ionosphere to the plasma sheet and inner magnetosphere. It is a comprehensive review of modeling and observational work performed up to the point of its publication.

Over the past decade and a half since the book's release, the community has continued to make significant strides in understanding the near-Earth plasma environment (see Chappell 2015 for history and current status). This review summarizes these advances. It will begin by focusing on recent advances in our knowledge of the entry mechanisms for each source. The transport and acceleration of the relevant populations from source to key magnetospheric regions will be reviewed, as well as the consequences each source has on magnetospheric dynamics. The review will conclude with loss mechanisms for magnetospheric plasma, then address the outstanding questions that remain in this broad subject area.

2 Sources

There are two important sources of plasma in Earth's magnetosphere: the solar wind, which provides almost exclusively hydrogen, and the Earth's ionosphere, which is capable of delivering considerable amounts of hydrogen as well as heavy ions, such as helium and oxygen. Other sources, important at other solar system bodies, are either not applicable (e.g., surface sputtering) or contribute so little as to be considered negligible (e.g., plasma from natural satellites). Here, we review progress in our understanding of the entry mechanisms for high latitude ionospheric plasma, low latitude ionospheric plasma, and solar wind plasma.

C.-P. Wang
cat@atmos.ucla.edu

M. Wiltberger
wiltbemj@ucar.edu

A. Yau
yau@ucalgary.ca

1 University of Michigan, Ann Arbor, USA

2 Swedish Institute of Space Physics, Uppsala, Sweden

3 CNRS, IRAP, University of Toulouse, Toulouse, France

4 LPP, Ecole Polytechnique-CNRS, Université Pierre et Marie Curie, Paris, France

5 Mullard Space Science Laboratory, University College London, Holmbury St. Mary, UK

6 Massachusetts Institute of Technology Haystack Observatory Westford, Massachusetts, USA

7 University of New Hampshire, Durham, NH, USA

8 The Aerospace Corporation, El Segundo, CA, USA

9 University of California, Los Angeles, USA

10 National Center for Atmospheric Research, High Altitude Observatory, Boulder, CO, USA

11 University of Calgary, Calgary, Canada

2.1 High Latitude Ionospheric Plasma

The variety of observed ion outflows in the high-latitude ionosphere may be grouped into two categories: bulk ion flows with energies up to a few eV, in which all the ions acquire a bulk flow velocity, and suprathermal ion outflows in which in general a fraction of the ions are energized to much higher energies. The category of bulk ion flows includes the polar wind and auroral bulk O^+ up-flow from the topside auroral and polar-cap ionosphere. The category of suprathermal ion outflows includes ion beams, ion conics, transversely accelerated ions (TAI), and upwelling ions (UWI).

Observations of both thermal and superthermal ion outflows prior to the mid-1990 were the subject of the comprehensive review of Moore et al. (1999) under the ISSI Study Project on Source and Loss Processes. In this review, we shall focus on more recent outflow measurements from satellites and ground radar. These measurements were, in general, acquired in different phases in the 11-year solar cycle, and covered different ranges of both altitude and ion energy. It is important to take into account the relative phase in the solar cycle and the relative altitude and ion energy coverage between different measurements, as many ion outflow characteristics exhibit significant long-term variations as well as variability on the time scale of days within a solar rotation near solar maximum. For convenience in our discussions below, we will use the term "topside ionosphere" to refer to the altitude region below 1000 km, including the F-region, and the terms "low-", "mid-", and "high-altitude" to the regions between 1000–4000 km, between 4000–10,000 km, and above 10,000 km, respectively.

At both auroral and polar cap latitudes, a plasma flux tube undergoes a circulation cycle that begins with anti sunward flow and stretching in length, from $\sim$10 to $\sim$100 R_E. This occurs either as it disconnects from the conjugate hemisphere to connect into the solar wind during part of the Dungey cycle or as moves with the viscous flow in the low-latitude boundary layer. During the stretch part of the cycle, the ionospheric plasma can expand freely into the upper reaches of the flux tube because of the negligible plasma pressure there. This results in the formation of the polar wind: the spatial separation between the heavier ions and the electrons due to the Earth's gravitation produces a polarization electric field that acts to accelerate the ions in the upward direction. Additional acceleration mechanisms give rise to the so-called "non-classical" polar wind (Schunk 2007).

Polar wind ion observations have been made on a number of polar-orbiting satellites, including ISIS-2, DE-1, Akebono, and Polar; polar wind electron observations have also been made on DE-1 and Akebono. These observations spanned different phases of Solar Cycle 20 to 23, and a wide range of altitudes from 1000 km to $\sim$50,500 km (8 R_E) altitude (Yau et al. 2007). A composite picture of the polar wind emerges from these observations. The polar wind is regularly observed at all local times and polar latitudes, and is composed primarily of electrons and H^+, He^+ and O^+ ions; the ion composition varies with the solar cycle, and is dominated in density by O^+ ions up to 4000–7000 km. The dayside and the nightside velocity profiles are qualitatively similar for all three species, both having a monotonic increase in velocity with altitude, a similar mass dependence of the magnitude of the velocity, and the largest acceleration (increase of velocity with altitude) of the H^+ velocity below 4000 km.

Near solar maximum on the dayside, the altitude at which the ion reaches 1 km/s is near 2000 km for H^+, but near 3000 and 6000 km for He^+ and O^+, respectively; for all three species, the dayside velocity is significantly larger than on the nightside, being about 12, 6, and 4 km/s for H^+, He^+ and O^+ respectively, at 10,000 km, compared with $\sim$7, 4, and 3 km/s, respectively, on the nightside (Abe et al. 1993b). This is suggestive of

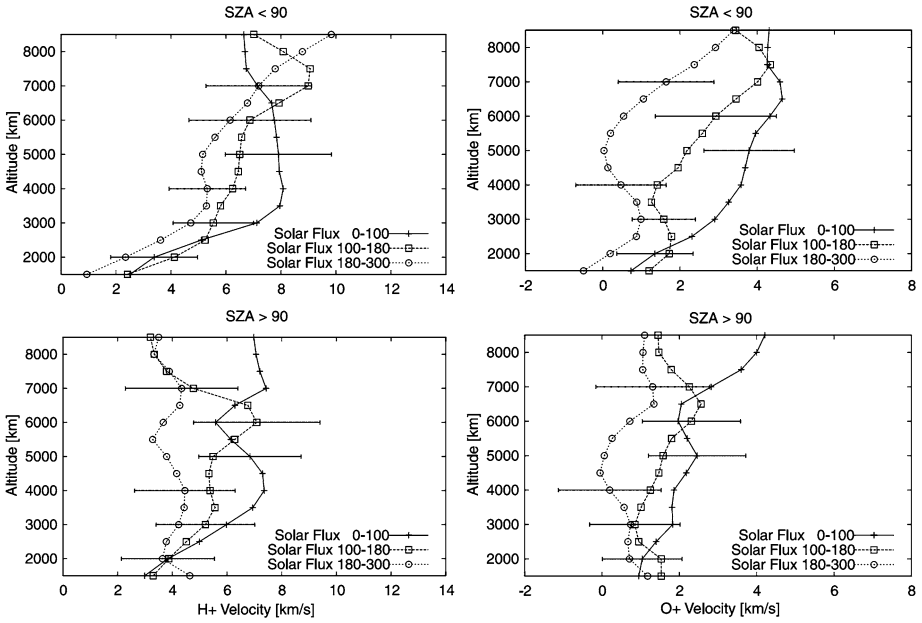

Fig. 1 Averaged H^+ (*left*) and O^+ (*right*) velocity observed on Akebono versus altitude for different solar flux levels: SZA $< 90°$ (*top row*) and SZA $> 90°$ (*bottom row*). From Abe (2004)

possible enhancement in the ambipolar electric field amplitude or presence of additional ion acceleration on the dayside due to escaping atmospheric photoelectrons (Tam et al. 2007). The averaged O^+ velocity begins to increase near 5000 km. This suggests that the O^+ ions above this altitude are predominantly upward; on the nightside, the averaged O^+ velocity starts to increase from zero at 7000 km. The magnitude of ion acceleration at a given altitude is found to correlate strongly with the electron temperature (Abe et al. 1993a). The ion velocity-to-electron temperature ratio also increases with altitude. This increase is consistent with the cumulative increase in ion velocity due to acceleration via ambipolar electric field along the field line. The variability (standard deviation) of the ion velocity is as much as 50 % of the mean during active times ($K_P \geq 3$), and larger during quiet times ($K_p \leq 2$). The mean velocity appears only weakly dependent on Kp for all three species.

Figure 1 shows the averaged H^+ and O^+ polar wind velocity at different solar flux levels (F10.7) as a function of altitude in the sunlit (SZA $< 90°$) and shadow (non-sunlit; SZA $> 90°$) regions, respectively. In the sunlit region, the H^+ velocity increases with altitude at all altitudes for all solar flux levels, except at low solar flux (F10.7 < 100), where it remains almost constant above 4000 km. However, the velocity gradient in different altitude regions varies with solar flux. At high solar flux (F10.7 > 180), the velocity increases continuously from 1500 km to 8500 km. In comparison, at low solar flux, the velocity increase with altitude is much larger below 3600 km and much smaller above 4000 km. As a result, the averaged velocity is about 50–60 % larger at 4000 km and comparable at ~7000 km. The O^+ velocity in the sunlit region remains below 1 km/s below 6000 km, but increases with altitude above that height at high solar flux. A similar transition in the velocity is observed at 4000 km at medium solar flux. At low solar flux, the velocity increases gradually with altitude from 1500 to 7000 km, reaching 4 km/s at 5000 km. In other words, the altitudinal gradients of both H^+ and O^+ velocity have very similar solar flux dependence and altitude

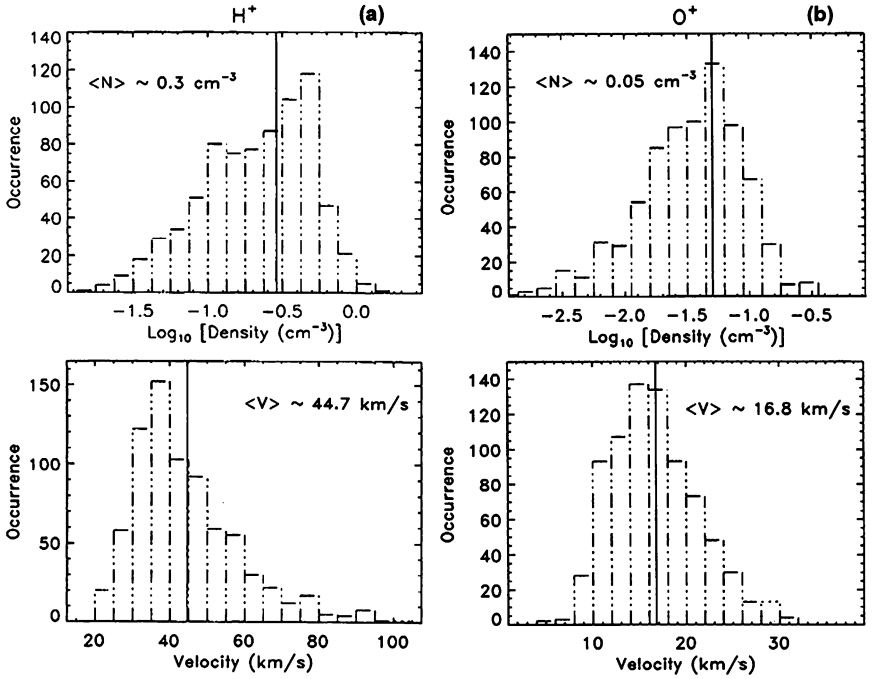

Fig. 2 Occurrence histograms of observed (**a**) H^+ and (**b**) O^+ polar wind density (*top*) and parallel velocity (*bottom*) on Polar at 50,500 km near solar minimum. From Su et al. (1998)

variations, namely, larger gradient below 5000 km and smaller gradient above 7000 km at low solar flux than at high solar flux. This results in generally higher H^+ and O^+ velocities below 7000 km and 8500 km, respectively, at low solar flux.

The observed ion outflow rate of H^+ and O^+ is also only weakly dependent on K_P, the O^+ rate at 6000–9000 km altitude increasing by a factor of 1.7 as K_P increases from 1 to 6 (Abe et al. 1996). The outflow rate of both species exhibits very similar IMF Bz dependence. It increases with B_Z under northward IMF conditions.

The magnetic local time (MLT) dependence of the polar wind ion flux strongly resembles that of the observed ion velocity: the ion flux is largest in the noon quadrant and smallest in the midnight quadrant. This is consistent with the larger ambipolar electric field in the sunlit polar wind. The polar wind H^+ flux (normalized to 2000 km altitude) in the noon quadrant is in the range of 1–20 $\times$ 10^7 $cm^{-2}\,s^{-1}$. The corresponding O^+ flux is typically a factor of 1.5–2.0 smaller. The fluxes of the different polar wind ion species have markedly different seasonal dependences in general. In the case of He^+, the flux has a winter-to-summer ratio of $\sim$20, which is attributed to the seasonal variations of neutral atmospheric helium and molecular nitrogen and the corresponding helium photo-ionization rate and He^+–N2 charge-exchange rate.

As the polar wind ions flow upward on open magnetic field lines to higher altitudes and undergo generally anti-sunward convection in the dayside cusp and the polar cap, they may be subject to a number of "non-classical" polar wind ion acceleration mechanisms (Yau et al. 2007). An example is centrifugal acceleration in the parallel direction due to strong $E \times B$ convection in regions of curved magnetic field at high altitudes above a few R_E. The result of this is that ions continue to increase in both drift speed and temperature. Figure 2 shows

the occurrence distributions of the polar wind H^+ and O^+ ions near the apogee of the Polar satellite at ∼50,050 km altitude, where the H^+ density averages ∼0.3 cm^{-3} and the H^+ parallel velocity averages 45 km/s near solar minimum (Su et al. 1998). The corresponding O^+ density and velocity are about a factor of 6 and 2.7 smaller (i.e. ∼0.05 cm^{-3} and ∼17 km/s) respectively.

The observed velocity ratio between ion species on both Akebono and Polar spacecraft spans a wide range of values, and on average lies between unity and the inverse square root mass ratio of the species, i.e. $1 < V_{\parallel,H^+}/V_{\parallel,O^+} < \sqrt{m_{O^+}/m_{H^+}} = 4$. This suggests that a number of processes of comparable energy gain may be contributing to the overall ion acceleration. The temperature of polar wind ions is generally low. On Akebono, the temperature was found to be in the range of 0.05–0.35 eV below 10,000 km (Drakou et al. 1997), and the parallel-to-perpendicular temperature ratio was less than unity at 5000 km. At Polar apogee (∼50,090 km), the averaged parallel H^+ and O^+ temperature is ∼1.7 and ∼7.5 eV, respectively, and the parallel-to-perpendicular temperature ratio is ∼1.5 for H^+ and ∼2.0 for O^+ (Su et al. 1998).

Interspersed with bulk polar flows is bulk auroral flow. Ion upflows at velocities exceeding 1 km/s have been observed in the topside ionosphere in both the nightside auroral zone and the dayside cleft on low-altitude polar-orbiting satellites, including the Dynamic Explorer 2 (DE-2) (Heelis et al. 1984) and the Hilat satellites, and from ground radars, including the Chatanika incoherent scatter radar and the European incoherent scatter radar (EISCAT) and EISCAT Svalbard radar (ESR). The term "upflow" is used instead of "outflow" to emphasize the very low (and below escape) energy nature of the flow. The observed ion upflow is highly variable in time and location, and generally confined to narrow latitude regions. Large upward ion flows often occur in regions of large ion convection velocities, and are dominated by O^+ and at times enhanced in molecular NO^+.

On DE-2 at 600–1000 km, the occurrence probability of upflow is generally larger than that of downflow in the auroral zone but smaller in the polar cap on both the dayside and the nightside. The peak probability spans the convection reversal on the dayside, and is more extended in latitude and located at lower latitude on the nightside. The probability for flows exceeding 100 m/s increases and moves equatorward with increasing K_P, from about 0.25 near 78° invariant at $K_P \leq 3-$ to about 0.35 near 70° at $K_P \geq 6$ on the dayside. In the polar cap (>78° invariant), the probability of upflow is several times larger during northward IMF than during southward IMF, and it is generally greater in the pre-noon sector than in the pre-midnight sector.

The observed upflow by EISCAT generally falls into two types. Type-1 upflow is associated with strong electric fields in regions of downward field-aligned currents and very low F-region electron densities adjacent to auroral arcs. It is characterized by ion temperature enhancements and perpendicular ion temperature anisotropy ($T_\perp > T_\parallel$). The latter is indicative of frictional heating of ions drifting through neutrals and production of strong pressure gradients, which push the ions upward. The type-2 upflow is typically observed above auroral arcs and is characterized by electron temperature enhancements, weak to moderate electric fields, and a stronger ion flux. All of these features are indicative of auroral electron precipitation and the resulting electron ionization occurs more frequently compared with type-1 upflow.

On average over the solar cycle, the field-aligned upflow occurrence probability at 500 km altitude is higher on the dusk side than on the dawn side, and peaks at ∼23 % in the pre-midnight sector. The upflow velocity increases monotonically with altitude starting from about 300 km, to values exceeding 100 m/s at 500 km in the majority (∼55 %) of cases (Foster et al. 1998). Roughly 50–60 % of the observed upflow events occurred during

intervals of enhanced ion temperature. The observed dawn-dusk asymmetry and midnight-sector peak is believed to reflect the combined effects of both MLT and latitudinal variations of upflow at the location of the EISCAT radar at Tromsø, which at 66.2° invariant latitude, lies within the nightside auroral oval and equatorward of the dayside oval.

In contrast, at the EISCAT Svalbard radar (ESR), which at 75.4° invariant lies within the dayside oval and poleward of the nightside oval, the upflow on the dayside starts or reaches an observable velocity at higher altitudes, and has a larger occurrence frequency than on the nightside above 400 km (Liu et al. 2001), as well as a dawn-dusk asymmetry that increases with altitude in favor of the dawn side over the dusk side. The starting altitude of ion upflow increases with solar activity level, with approximately 25 % and 16 % of the dayside upflow events below 400 km (55 % and 34 % below 450 km) altitude in period of low and high solar activity (F10.7 $<$ 140 and F10.7 $>$ 140), respectively. The upflow occurrence frequency at 500 km altitude increases with K_P, and peaks around geomagnetic noon at ∼11–21 %, where the averaged ion flux reaches 2×10^9 cm^{-2}s^{-1} and is relatively independent of geomagnetic activity level (K_P). During quiet and moderately active periods, the downflow frequency peaks in the dawn sector (03–09 MLT) at ∼5–6 %. During disturbed periods, the downflow frequency peaks in the noon sector (10–15 MLT), and the peak frequency of ∼25 % exceeds the upflow frequency, and is consistent with the ESR being equatorward of most of the upflow events.

Approximately half of the dayside ion upflow events are accompanied by increases of both ion and electron temperatures, compared with only 10–20 % of events at other local times. About 20 % of the events are accompanied by electron temperature increases only, regardless of local time, and another 5–10 % of noon-sector events and 20–25 % of morning-sector events are accompanied by ion temperature increases. The remaining 15–40 % appear unaccompanied by any appreciable ion or electron heating.

The occurrence probability and morphological characteristics of the ion upflows observed at both EISCAT and ESR exhibit seasonal as well as diurnal and solar cycle variations (Foster et al. 1998). Above 300 km altitude at EISCAT, the occurrence frequency of upflow is greater during the winter months. Compared with the quieter phase of the solar cycle, the upflow during the active phase of the cycle has a larger ion flux, a smaller ion velocity, and its occurrence frequency has a more pronounced nightside maximum (Liu et al. 2001). The predominance of larger-flux events at solar maximum may be attributed to the higher prevailing ambient plasma density, and the smaller velocities in these events to a smaller per-capita amount of free energy available for acceleration and/or a larger energy loss to ion-neutral collisions. Compared with quiet times, the occurrence frequency of ion upflow is significantly larger at all altitudes during disturbed times ($K_P \geq 4$) (Liu et al. 2001). Furthermore, the starting altitude of upflow is lower (200–250 km), and the increase of occurrence frequency with geomagnetic activity is much more pronounced on the dawn side than on the dusk side, resulting in a higher frequency on the dawn side. The increase in frequency with altitude is also stronger.

The observed magnetic activity dependence of ion upflow is consistent with ion acceleration in the F-region and the topside ionosphere receiving important contributions from both $E \times B$-driven ion frictional heating and precipitating soft electron-driven electron heating. The effect of ion frictional heating is expected to increase with K_P and to be stronger on the dusk side and in the winter: this explains the higher occurrence frequency on the dusk side at EISCAT's latitude, and the increase in occurrence frequency with geomagnetic activity at both ESR and EISCAT. The effect of soft electron precipitation is expected to be stronger during disturbed times, particularly in the dusk quadrant, and to play a more dominant role on the dayside where the precipitating electrons tend to be softer: this explains the higher

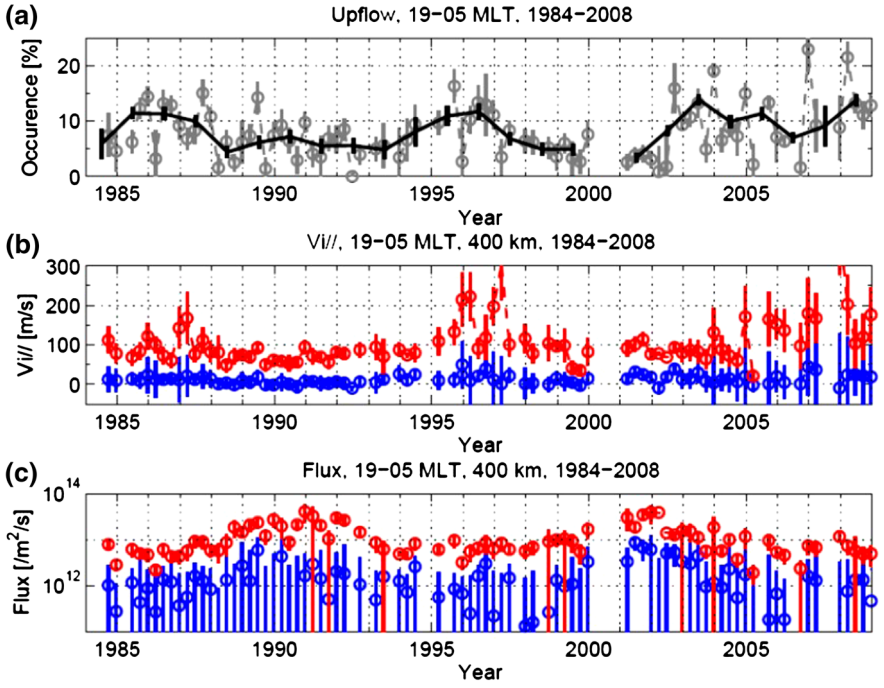

Fig. 3 (**a**) 12- (*black*) and 3-month (*grey*) averages of occurrence frequency of night side (19–05 MLT) ion up-flow at EISCAT starting between 200–550 km from 1984 to 2008; 3-month averages of (**b**) field-aligned ion velocity and (**c**) ion flux at 400 km over all up-flow events (*red*) and data samples (*blue*) From Ogawa et al. (2010)

dayside occurrence frequency at ESR compared with EISCAT at both quiet and disturbed times, and the higher frequency on the dawn side during disturbed times. It also suggests that soft electron-driven electron heating may be more efficient than convection-driven ion heating in driving ion upflow.

The long time coverage of the EISCAT data set makes it extremely valuable for studying the influence of solar activity on ion upflows. Figure 3 shows (a) the 12- (black) and 3-month (grey) averages of the observed occurrence frequency of nightside (19–05 MLT) between 200 and 550 km, and (b) the field-aligned ion velocity and (c) ion flux at 400 km at low (F10.7 $<$ 140) and high (F10.7 $>$ 140) solar flux, respectively, from 1984 to 2008. On average, the upward ion velocity in upflow events was a factor of 2 higher at low solar flux than at high solar flux (F10.7 $>$ 140), when the upward ion flux was a factor of 4 higher. The larger flux at high solar flux (i.e. near solar maximum) is attributed to the stronger solar EUV flux and resulting ionization in the F-region, and the smaller velocity to the higher ion-neutral collision frequency due in turn to the higher exospheric temperature and neutral density in the thermosphere.

Ogawa et al. (2009) found the ion upflow occurrence frequency to increase with both solar wind density (above 30 cm^{-3}) and solar wind velocity (up to 700 km/s), and to peak in value inside the cusp, while the upward ion flux increases with solar wind density and decreases with solar wind velocity. Both IMF B_Y and B_Z are found to affect the upflow occurrence frequency, which increases with increasing magnitude of B_Y and peaks at B_Z ~ -5 nT. The apparent movement of the dayside ion upflow region may be understood

in terms of the influence of solar wind velocity and density and the IMF B_Y and B_Z on the shape, size and location of the upflow region, since the location of the dayside cusp is known to move equatorward with decreasing IMF B_Z or increasing solar wind dynamic pressure.

Ogawa et al. (2010) found the average starting altitude of ion up-flow to track the measured electron density peak and to be typically 100–150 km higher than the latter. The distribution of starting altitude is quite different at low and high solar flux, respectively. At low solar flux, the distribution exhibits a broad peak starting at ~300 km; peaking near 450 km and extending to ~520 km. At high solar flux, the distribution shifted to higher altitude, starting near ~350 km; peaking more sharply near 450 km and extending to at least 540 km. The variation of the starting height with solar activity level can be attributed to the increased atmospheric density and ion-neutral collision frequency at a given altitude near solar maximum: the solar minimum neutral atomic oxygen density at the starting height of 300 km is $\sim 3 \times 10^8$ cm^{-3}, compared with the corresponding (solar maximum) density value of $\sim 3.3 \times 10^8$ cm^{-3} at the (increased, solar-maximum) starting height of ~450 km. This implies that the atmospheric density and ion-neutral collision frequency at the starting upflow altitude are comparable at solar minimum and maximum, respectively.

The DE-2 and the EISCAT/ESR radar observations demonstrate that both soft electron-driven electron heating and convection-driven ion heating play a significant role in auroral ion upflow production. Frictional heating of O^+ ions enhances the ion temperature in the F-region and increases the pre-existing parallel pressure gradient, and the ions respond by flowing to higher altitudes to attain a new equilibrium scale height distribution. Although the increase of the scale height is a transient feature, the upflow can remain if new plasma is horizontally convected into the heating region. Likewise, soft precipitating electrons deposit their energy in the F-region via electron impact ionization of the neutrals and collisional energy transfer with the neutrals, and thereby increase the average thermal electron energy (i.e. electron temperature) and enhance the ambipolar electric field.

The category of suprathermal ion outflows includes ion beams, ion conics, transversely accelerated ions (TAI), and upwelling ions (UWI). The occurrence and morphological characteristics of ion beams and conics in the different altitude regions were the subject of a number of statistical studies using S3-3, DE-1, Viking, Akebono, Freja, Fast and Polar satellite data, including several prior to 1997, which were reviewed in detail by Yau et al. (1997).

Ion beams are upflowing ions (UFI) that have a peak flux along the upward magnetic field direction. They are generally observed above 5000 km altitude, but are occasionally present down to about 2000 km during active aurora. The occurrence probability of both H^+ and O^+ ion beams increases with altitude at both quiet and active times. The increase is most prominent for the lower-energy (<1 keV) ions.

In contrast, ion conics have a peak flux at an angle to the upward magnetic field direction, and are observed down to sounding rocket altitudes (1000 km or below; Yau et al. 1983), and up to several Earth radii and beyond (Hultqvist 1983; Bouhram et al. 2004). At high altitude (above ~10,000 km), the occurrence probability of low-energy conics (<1 keV) decreases with increasing altitude. The motion of an ion conic is typically non-adiabatic as it evolves along the field line.

Transversely accelerated ions (TAI) have peak pitch angles at or close to 90°, and may be regarded as a special case of ion conics. They are regularly present down to about 3000 km (Whalen et al. 1991) on the dayside, and down to 1400–1700 km (Klumpar 1979; André et al. 1998) and to the active-time topside ionosphere above 400 km (Yau et al. 1983; Arnoldy et al. 1992) on the nightside.

Upwelling ions are observed exclusively in the morning sector of the auroral oval and the lower latitudes of the polar cap, and display the effects of both parallel (upward) and

perpendicular energization to energies from one to tens of eV (Pollock et al. 1990). They are the most persistent suprathermal ion outflow feature in the cleft region, and are dominated by O^+ ions. Compared with ion conics with the same perpendicular energy, upwelling ions are more upward moving (have higher upward mean velocity). They often appear as field-aligned ion flows at other local times at higher altitudes in the presence of anti-sunward convection, hence the term "cleft ion fountain".

Both ion beams and ion conics are a common phenomenon, with occurrence frequencies sometimes higher than 50 % above 1 R_E altitude, and are dominated by H^+ and O^+ ions in the 10 eV to a few keV range. UFI's of a few tens of keV energy also occur occasionally. Distributions of UFI may evolve in different ways as they move upward. Ion conics often do not start as TAI distributions heated within a narrow altitude range and then move adiabatically up the geomagnetic field. Statistically (Miyake et al. 1993, 1996; Peterson et al. 1995), the energy of dayside ion conics increases with altitude, from ∼10 eV near 2000 km to ≤100 eV near 9000 km. The cone (apex) angle of ion conics decreases with altitude much more slowly than expected from adiabatic motion. In the so-called "restricted" ion conics, the ion distribution has a well-defined cone angle. However, in the so-called "extended" or "bimodal" conics (Klumpar et al. 1984), the cone angle increases with energy and the lower energy ions have a significant flux along the field line.

The occurrence probability of both H^+ and O^+ upflowing ions is fairly independent of magnetic activity (K_P index). However, the intensity distribution of O^+ UFI exhibits a marked dependence on magnetic activity that is absent in H^+. On DE-1 (Yau et al. 1984), the occurrence probability of intense ($>10^7$ cm^{-2} s^{-1} sr^{-1}) lower-energy (<1 keV) O^+ at active times ($K_P \geq 4-$) is a factor of 3 higher than at quiet times. A similar but smaller increase is also apparent in the occurrence probability of intense ($>10^6$ cm^{-2} s^{-1} sr^{-1}) higher-energy (>1 keV) ions. In contrast, the intensity distribution for H^+ remains fairly unchanged with K_P.

The observed O^+ UFI distributions exhibit significant seasonal and long-term variations, which are attributed to changes in the incident solar EUV flux on the atmosphere in different seasons of the year and at different phases of the 11-year solar cycle. The corresponding variations in the H^+ UFI distributions are much smaller. On DE-1, the probability of the O^+ UFI decreased by about a factor of 2 from near solar maximum in 1981 to the declining phase in 1984. The decrease in probability of intense UFI fluxes was even larger, by about a factor of 3–4. In contrast, there was no discernible change in the H^+ occurrence probability during the same period. Throughout the period, the occurrence probability of O^+ UFI was significantly higher in the summer than in the winter, the frequency of intense events being about a factor of 2 larger. The increase in occurrence probability, intensity, and conic abundance of O^+ UFI in periods of increased solar activity results in a large increase in the overall ion outflow rate.

Peterson et al. (2008) recast the observed ion outflow flux and energy distributions near Polar perigee in dynamic boundary-related coordinates. It was found that for all three ion species (H^+, O^+ and He^+), only a very small fraction (∼2–3 %) of the observed energetic UFI was in the polar cap. However, their presence confirms that not only are energetic ions being transported by prevailing convection electric fields to the high-altitude polar cap, but they are also produced by ion acceleration events in the polar cap ionosphere. In the auroral zone, the flux in the midnight quadrant dominated, and consisted of ∼50 % of the total H^+ and He^+ flux and ∼30 % of the O^+ flux, compared with ∼37 % of O^+ flux in the noon quadrant where most of the flux was on cusp field lines (e.g. Zheng et al. 2005).

Figure 4 shows the net ion outflow rates of both H^+ and O^+, obtained by integrating the DE-1 ion flux measurements over all magnetic local times and all invariant latitudes

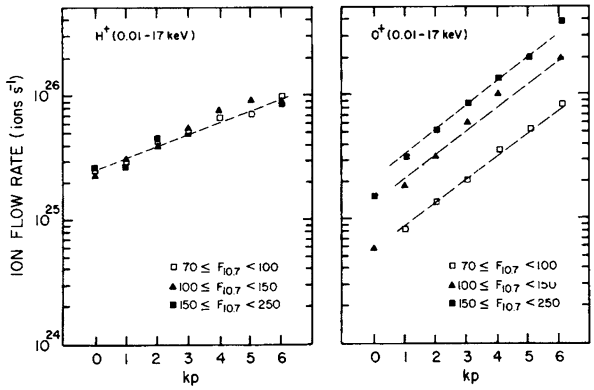

Fig. 4 H^+ and O^+ ion outflow rates at 0.01–17 keV observed at 16,000–24,000 km on DE-1, integrated over all MLT above 56° invariant latitude in both hemispheres as a function of K_P, for different ranges of F10.7. From Yau et al. (1988)

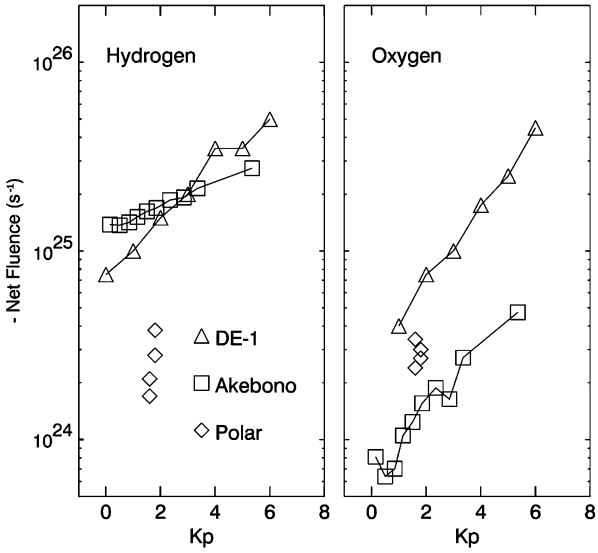

Fig. 5 H^+ and O^+ ion outflow rates near solar minimum as a function of K_P. *Squares* indicate low-energy rates on Akebono below 9000 km; *triangles* show suprathermal energy rates on DE-1 above 16,000 km; *diamonds* show suprathermal energy rates on POLAR below 9000 km. From Cully et al. (2003a)

above 56°, as a function of the magnetic K_P index for three F10.7 ranges (Yau et al. 1988). The O^+ rate increased exponentially with K_P, by a factor of 20 from $K_P = 0$ to 6, and exceeded 3×10^{26} ions s^{-1} at times of high solar and magnetic activity. The rate at low solar activity was about a factor of 4 smaller than that at high activity. In contrast, the H^+ rate was very similar across each of the three F10.7 ranges. In all three F10.7 ranges, the dependence of the O^+ rate on K_P was similar. In comparison, the H^+ rate increased with K_P more moderately, by a factor of 4 from $K_P = 0$ to 6.

Figure 5 compares the observed low-energy ion outflow rates observed on Akebono below 9000 km near solar minimum with the corresponding suprathermal energy rates on Polar at the same altitudes (15 eV–16 keV) and on DE-1 above 16,000 km (10 eV–16 keV), respectively. The rate of low-energy H^+ on Akebono is comparable with the suprathermal energy rate on DE-1 and a factor of 4-10 higher than the suprathermal energy rate on Polar. This indicates that significant acceleration of H^+ occurs above 9000 km in the high-latitude ionosphere. In contrast, the rate of low-energy O^+ below 9000 km is less than the corresponding suprathermal rate above this altitude, which is in turn less than the corresponding suprathermal rate above 16,000 km. This means that a significant fraction of O^+ is accel-

erated below 9,000 km, and that the acceleration continues between 9,000 and 16,000 km. In other words, a significant fraction of low-energy ions at low altitudes in the high-latitude ionosphere, including polar wind ions and auroral ion upflows, are accelerated to suprathermal energies at higher altitudes, where they lose their identity as thermal-energy ions. Thus, it is important to consider both thermal and suprathermal ion outflow in the high- latitude ionosphere as an integrated entity.

Additional suprathermal outflow arises from polar cap arcs of energetic electron precipitation. The difference with the auroral zone comes from the source region: the auroral zone is magnetically connected to the plasmasheet, while the polar cap is connected to the lobes. Therefore, the polar activity is expected to be closely related to the dynamics of distant magnetospheric regions or to the interaction between the solar wind and the magnetosphere, which vary between the different planets. For the Earth, the knowledge of polar cap arcs and of their plasma environment has benefited from flybys over the polar caps at different altitudes by numerous satellites with optical and in-situ instruments.

Polar cap arcs dominantly appear when the interplanetary magnetic field (IMF) is directed northward and during quiet geomagnetic conditions in the magnetosphere. A large variety of shapes, widths, lengths, and motions are reported from ground-based instruments and low-altitude satellites, which possibly suggests different driving mechanisms and different source regions for the electrons. Most studies focus on electrodynamics and in relation to the large-scale convection pattern (see reviews by Zhu et al. 1997; Kullen 2002). It is not yet fully understood whether polar cap arcs occur on open or closed field lines, and thus whether the source region is related to a highly distorted plasmasheet or to the magnetopause and boundary layers (Carlson 2005; Frey 2007). Recent work (Fear et al. 2014) connects arcs as observed by the IMAGE satellite with plasma observations from the Cluster constellation that are characteristic of popluations trapped on closed field lines. This supports the hypothesis that arcs occur on closed field lines.

Outflowing H^+ beams of polar arc source were first detected at low-altitude above the polar cap with characteristics significantly different from both the polar wind (Shelley et al. 1982) and from ionospheric ions escaping from the cusp/cleft ion fountain. Since this early detection, very few references exist in the literature about outflowing ions related to polar cap arcs before the Cluster observations. During periods of northward or weak IMF, Cluster flybys over the polar cap at relatively high altitudes (between 4 and 8 R_E) revealed that accelerated electron beams precipitating into the polar ionosphere were systematically accompanied by outflowing ion beams with a typical shape of inverted V (Nilsson et al. 2006). These observations are also correlated with the presence of convergent electric fields perpendicular to the magnetic field. As in the auroral zone, these characteristics are interpreted as the effect of a U-shape potential structure below the spacecraft, which accelerates ionospheric ions upwards. The simultaneous acceleration of the precipitating electron beams demonstrates that the potential structure must extend to altitudes higher than the spacecraft, whereas the acceleration region is assumed to be confined at the topside of the ionosphere in the auroral zone (Maggiolo et al. 2006; Teste et al. 2007). A case study with a good conjunction between Cluster observations of precipitating electrons and ion outflows at high altitude, and optical observations of an arc by the TIMED spacecraft, confirmed the relationship between polar cap arcs and accelerated ion outflows with typical shape of inverted "V"s (Maggiolo et al. 2012). A statistical study of ion outflows showed that they form elongated and sun-aligned structures with widths typically of the order of 30 km mapped to the ionospheric level. Their temperature is of the order of tens of eVs and they are accelerated to average energies of about 400–500 eV, with highest values up to 1–2 keV (Maggiolo et al. 2011). Periods of northward or weak IMF

are not favorable for low-latitude reconnection processes at the magnetopause. During this period, substorm activity was limited and the auroral and geomagnetic activity in the magnetosphere was quite weak. The only signs of activity in the magnetosphere occurred in the polar cap with the presence of polar arcs. The associated outflowing ion beams represent a plasma source for the magnetosphere in such conditions of weak to northward IMF.

In addition, Teste et al. (2010) showed that these polar cap arc structures were surrounded by upwelling electron beams, accelerated from the ionosphere to low energies typically less than 100 eV. The return downward current carried by these outflowing electron beams was estimated and found to be comparable with the adjacent upward current carried by precipitating particles. This suggests that both upward and downward currents are part of the same current circuit closing through the ionosphere. Finally, during northward IMF periods, the polar cap exhibits successive sheets of outflowing ionospheric ions and electrons, the outflowing ion beams being associated with electron precipitations. These observations reinforce the role of the polar ionosphere as an alternative plasma (ions and electrons) source for the magnetosphere during periods of Northward IMF.

2.2 Low Latitude Ionospheric Plasma

At sub-auroral latitudes, ionospheric outflow slowly saturates closed flux tubes to create the plasmasphere. The plasmasphere is the torus of cold and dense plasma, which encircles the Earth at geomagnetic latitudes less than about 65°, occupying the inner magnetosphere out to a boundary known as the plasmapause (Carpenter 1962; Lemaire and Gringauz 1998; Kotova 2007). There, the density can drop by 1 to 2 orders of magnitude; the boundary is observed to be much more diffuse during prolonged quiet periods. The plasmasphere comprises the corotating region of the magnetosphere and is magnetically coupled to the ionosphere. Magnetic field lines are closed and approximately dipolar, permitting filling of the plasmasphere by plasma escaping from the Earth's ionosphere.

During quiet times the ionospheric plasma at mid-latitudes can expand upward along the magnetic field lines and fill them until the plasma gas pressure is equalized along the entire field line. In establishing the equilibrium between the plasmasphere and the ionosphere, plasma flows both to and from the plasmasphere. A net flow into the plasmasphere is often called "refilling" (Park 1970; Banks et al. 1971; Kotova 2007).

Early models of ionospheric plasma escape (Banks and Holzer 1969; Lemaire and Scherer 1970) predicted that the light ions H^+ and He^+ should flow out into the magnetosphere, while the heavy ions should remain gravitationally bound in the ionosphere and provide much smaller upwelling fluxes. H^+ is thus the principal plasmaspheric ion, while He^+ is the second most abundant species in the plasmasphere, accounting for approximately 5–10 % of the plasmasphere plasma. The ratio between He^+ and H^+ changes with geomagnetic activity, ranging from 3 % to about 50 % (Darrouzet et al. 2009, and references therein).

Heavy ion content in the plasmasphere is generally very low. Grew et al. (2007), by combining all measurements on a field line at $L = 2.5$, were able to solve simultaneous equations for the abundances of H^+, He^+ and heavier ions (taken to be O^+). For the $H^+ : He^+ : O^+$ ratio they found $\sim 82 : 15 : 3$ by number (~ 3 % O^+). An interesting deviation from this norm occurred just outside the plasmasphere, when the inferred O^+ proportion reached ~ 60 %. Dandouras et al. (2005) analysed ion composition measurements from the CIS experiment onboard the Cluster spacecraft (Rème et al. 2001) in the outer plasmasphere, at $L \sim 4$, and observed a quasi-absence of O^+ ions (O^+ less than 4 % by number). However, outside the main plasmasphere, a few low-energy O^+ observations occurred within detached plasma

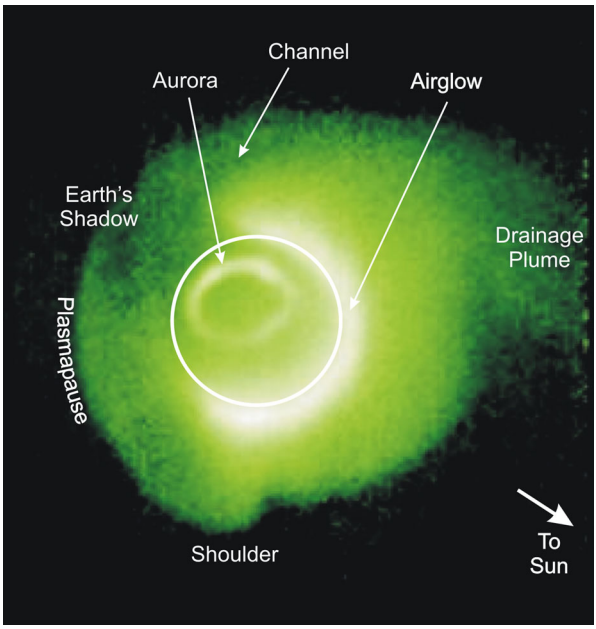

Fig. 6 Plasmasphere image obtained by the Extreme Ultraviolet Imager (EUV) onboard the IMAGE spacecraft, during a magnetic storm. From Sandel et al. (2003)

events, originating from deeper in the plasmasphere and having an outward expansion velocity towards higher L-shells. Chappell (1982) and Roberts et al. (1987), using the retarding potential ion mass spectrometer on board the Dynamics Explorer 1 satellite, also reported heavy ion observations in the region of the plasmasphere just inside the plasmapause. These observations allowed the separation of O^+, O^{++}, N^+ and N^{++} ions, all of which were observed in the plasmasphere.

The He^+ outside Earth's shadow resonantly scatters the solar 30.4 nm radiation, so that the plasmasphere glows (Fig. 6). The plasmaspheric He^+ emission is optically thin, therefore the integrated column density of He^+ along the line of sight through the plasmasphere is directly proportional to the intensity of the emission. The Extreme Ultraviolet Imager (EUV) onboard the IMAGE spacecraft allows for the study of the distribution of cold plasma in Earth's plasmasphere via imaging of the distribution of the He^+ ion through its emission at 30.4 nm (Sandel et al. 2000, 2003).

2.3 Solar Wind Plasma

Solar wind entry to the magnetosphere, due to magnetic reconnection with a southward oriented interplanetary magnetic field and the consequent occurrence of a solar wind driven convection cycle, was first proposed by Dungey (1961). The general concept is now widely accepted, but work is ongoing to develop a detailed understanding of when, where and how magnetopause reconnection proceeds. The recent reviews of Fuselier and Lewis (2011) and Paschmann et al. (2013) summarize our current understanding of this complex phenomena.

Reconnection at the magnetopause current sheet is a rather asymmetric situation, with the magnetic field strengths and orientations, as well as plasma properties differing on either side of the current sheet. As discussed in Hultqvist et al. (1999), early work (Sonnerup 1980) suggested that the magnetic fields either side of the current sheet should have equal components parallel to the reconnection line and that strongest rates of reconnection would occur

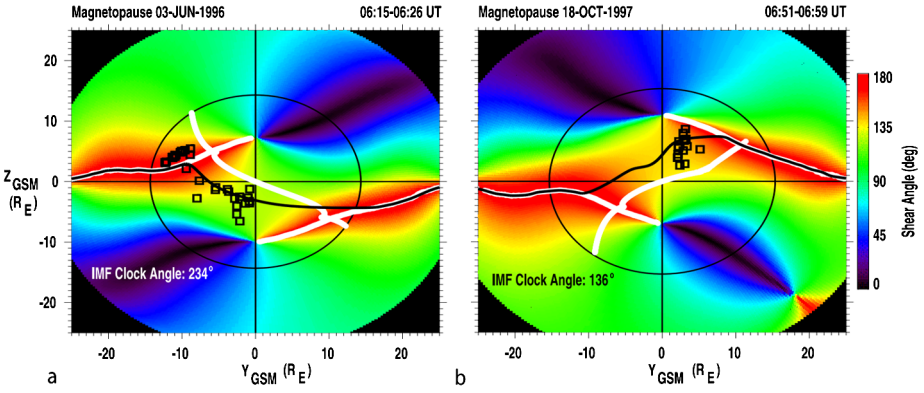

Fig. 7 This figure shows a projection of the magnetopause as seen from the Sun, in GSM coordinates, The *colour* represents the magnetic shear between draped magnetosheath magnetic field and magnetosphere boundary layer magnetic field, for southward interplanetary magnetic fields having significant dusk/dawn components. The *white region* superimposed *on red* shows where antiparallel reconnection would be favoured, while the remaining *white line* shows the locations where component reconnection as formulated in Moore (2002) is favoured. The *black trace* shows the locus of maximum magnetic shear, in the Trattner et al. (2007b) model which includes a treatment of dipole tilt, unlike Moore (2002), and thus shows a corresponding seasonal difference between the *left* and *right hand plots* (for northen hemisphere summer and winter respectively). The *black boxes* show inferred locations of reconnection, determined by analysis of dispersed ion signatures observed in the cusp regions with the Polar spacecraft. Adapted from Trattner et al. (2007a)

for anti-parallel fields. Cowley (1976) argued that the reconnection line forms in an orientation perpendicular to a line along which the magnetic fields, either side of the magnetopause current sheet, have opposite components (those being the "reconnecting components") with arbitrary components parallel to the line. This idea was developed by Cowley and Owen (1989) and, using more realistic magnetic field models, by Cooling et al. (2001) who explored the motion of newly reconnected flux across the magnetopause, and Moore (2002) who focused only on where reconnection is expected to occur. Cooling et al. (2001) introduced an assumption that reconnection can only proceed when the mean current density in the sheet exceeds a minimum level, or equivalently that the magnitude of the difference between the reconnecting magnetic field components exceeds a threshold. A given threshold can be exceeded at smaller shear angles where there are stronger magnetic fields, so we may expect reconnection at lower shear angles near the sub-solar magnetopause. At other locations with weaker reconnecting component fields, higher shear angles are needed, and in some locations the threshold may not met for any shear angle. Moore (2002) required that the reconnecting magnetic field components were equal and opposite. Trattner et al. (2007b) built on this earlier work by combining a magnetospheric magnetic field model with dipole tilt (Tsyganenko 1995) and a model of the draped magnetosheath magnetic field (Cooling et al. 2001) in order to determine both the magnetic shear and the locations most favourable for component reconnection at all points on the magnetopause for given solar wind conditions. Figure 7 illustrates typical predictions of the model showing, for southward IMF with a dominant dawn-dusk component, that the expected outcome is a component reconnection line in the subsolar regions that joins anti-parallel reconnection lines in the flank regions.

Trattner et al. (2007b, 2007a) used POLAR Toroidal Imaging Mass-Angle Spectrograph (TIMAS) observations of ion velocity dispersion observed in the high latitude magnetic cusp regions to infer the lower latitude locations of reconnection X-line from which the ions had travelled. This was done for a range of IMF conditions, and the results were compared with

the predictions of anti-parallel and component reconnection models. It was concluded that both reconnection scenarios appear to occur, depending on IMF conditions. Furthermore, it was shown that the reconnection line occurs where the magnetic shear angle maximizes, giving reconnection X-line locations which may differ from the predictions of Moore (2002) due to seasonal non-zero dipole tilt (as illustrated in Fig. 7) and IMF B_X effects.

The "maximum magnetic shear" model has been tested (Trattner et al. 2012) by comparing the locations of 7 active low latitude reconnection lines directly observed by THEMIS spacecraft, with locations predicted by the model under the corresponding interplanetary magnetic field conditions. The study assumed that flow reversals are the signature of the spacecraft crossing an active reconnection line, rather than the signature of multiple reconnection lines. The model was shown to be very effective when IMF B_Y dominated. However, when the dominant IMF direction was southward or in the B_X direction, the model was less effective.

The Cluster spacecraft have crossed the dayside magnetopause across all latitudes, during more than a decade of operations, and provided observations which can be used to test the predictions of the maximum magnetic shear model. Fuselier et al. (2011) were able to identify 15 cases with clock angles between 105° and 228° (southward B_Z and varying B_Y components) where the antiparallel reconnection X-lines were predicted to lie polewards of the spacecraft and the component reconnection X-lines would lie equatorwards of the spacecraft. Careful analysis of spacecraft observations of ion and electron populations identified as being on newly reconnected field lines revealed whether the reconnection X-line in fact lay polewards or equatorwards of the spacecraft in each case. It was found that the observations were consistent with model predictions in 13 of the cases, while in the other two cases the observed flow direction in the magnetosheath boundary layer (MSBL) differed from the direction in the magnetospheric low latitude boundary layer (LLBL) preventing determination of the direction to the reconnection line. Counter-streaming electrons in the magnetosheath boundary layer were observed during 6 events. These were interpreted as indications of multiple reconnection, occurring perhaps initially at the equatorwards component reconnection line and later at an antiparallel reconnection line poleward of the spacecraft; this situation is not predicted by the maximum magnetic shear model.

Under northward interplanetary magnetic field conditions, as Dungey (1961) noted, magnetic reconnection may occur at high latitudes, poleward of the magnetospheric cusp, between magnetosheath and magnetotail lobe magnetic fields. Ongoing reconnection at a high-latitude site does not create or destroy closed magnetic flux, and thus does not provide an entry route for plasma into the magnetosphere. However, if the interplanetary magnetic field was to undergo reconnection with both the north and south magnetotail lobes, it could, in principle, form a newly closed dayside magnetic field line, containing trapped magnetosheath plasma. The idea that this process might occur under conditions of strongly northward IMF, and the suggestion that it could play a role in the formation of a low latitude boundary layer, was proposed by Song and Russell (1992) as a contribution to understanding why a well-defined structured LLBL occurs under strongly northward IMF.

A study by Twitty (2004) examined 3 years of Cluster high latitude magnetopause crossings tailward of the cusp, during intervals of relatively stable IMF, for evidence of reconnection associated plasma flows. Reversed energy-latitude ion dispersion signatures were used to confirm the interpretation that the observed plasma flows are signatures of reconnection. The survey showed that such flows were seen during ~90 % of the intervals when the IMF had a northward component, and almost never when the IMF had a southward component. The observations are predominantly from the northern hemisphere, and do not discriminate between single and dual-lobe reconnection.

Direct evidence of dual lobe reconnection has been sought by examining the properties of suprathermal electrons in the high latitude magnetosheath boundary layer (MSBL) under northward IMF conditions. Magnetosheath electrons flowing along the magnetic field towards a reconnection site are cooler than magnetosheath plasma returning from the reconnection site, as those electrons have been heated while crossing the magnetopause, reflecting at the ionosphere and heated again when recrossing the magnetopause to return to the magnetosheath boundary layer (Fuselier et al. 1997). A case study by Onsager et al. (2001) of a high latitude magnetopause crossing by the Polar spacecraft found evidence of open field lines connected to the northern hemisphere and others connected to the southern hemisphere. Bi-directional heated electrons in the MSBL were interpreted as evidence of high latitude reconnection in both hemispheres. The study also suggested that reconnection was occurring over a broad local time extent.

Statistical studies, which applied this technique to Cluster high latitude magnetopause crossing data, showed that the geomagnetic dipole tilt is the main influence on which hemisphere is more likely to show lobe reconnection, with the IMF tilt angle being less significant (Lavraud 2005; Lavraud et al. 2006). Observations of bi-directional heated MSBL electrons interpreted as evidence for dual-lobe reconnection were quite common and were shown to occur not only for strictly northward IMF, but across a range of clock angles smaller than 60°, in a sample of 56 magnetopause crossings.

Further work has demonstrated that the dual-lobe reconnection process must usually occur in two steps, which are separated in time. This interpretation reconciles contradictions between models proposed based on observations of bi-directional MSBL heated magnetosheath electron populations at high latitudes, which suggested that they should also be seen at low latitudes in the MSBL, with observations at lower latitudes in which heated MSBL electrons are typically uni-directional and bi-directional electrons are only seen inside the magnetopause current layer in the LLBL, as well as corresponding issues regarding observations of low latitude O^+ ions (Fuselier et al. 1995). Fuselier et al. (2012) revisited Cluster magnetopause observations, and analysed a large dataset covering 2001–2009, which included the high latitude crossings studied by Lavraud et al. (2006) and newer low latitude observations which became available due to the evolving orbit of Cluster. This statistical study confirmed the findings of Lavraud (2005) at high latitudes, while also confirming earlier works showing that the majority of low latitude events show uni-directional heated electrons in the MSBL. Figure 8 illustrates a way to reconcile these observations, in which time elapses between reconnections in the two hemispheres, during which the reconnected field line evolves and convects tailwards before the second reconnection occurs. As Fuselier et al. (2012) point out, since their study was confined to regions within 4 hours magnetic local time of noon, further work is needed to determine how far tailwards the reconnected field line typically convects before a second reconnection occurs.

In companion papers, Øieroset (2005) and Li (2005) presented complementary studies that indicate that magnetosheath plasma trapped by dual lobe reconnection might ultimately contribute to the formation of a cold dense magnetotail plasmasheet. A case study used Cluster observations to demonstrate the existence of a cold dense magnetotail plasmasheet (Øieroset et al. 2005) in association with a long duration interval of northward IMF. Low altitude observations from Defense Meteorological Satellite Program (DMSP) spacecraft demonstrated that the cold, dense plasmasheet was present across the span of the magnetotail from dawn to dusk, not only at the Cluster location. Furthermore, cusp ion dispersion signatures characteristic of high latitude lobe reconnection, poleward of the cusp, were observed by the low altitude FAST spacecraft, confirming lobe reconnection in at least one hemisphere. An MHD global magnetosphere simulation study (Li 2005) illustrated how

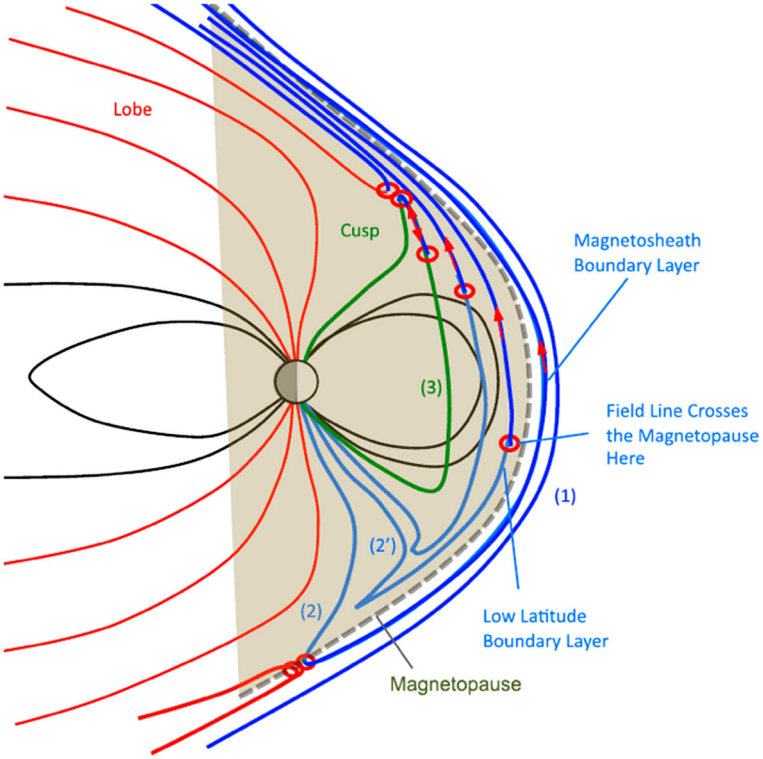

Fig. 8 The interpretation proposed by Fuselier et al. (2012) to explain magnetosheath boundary layer electron signatures at low and high latitudes under northward IMF conditions. A magnetosheath magnetic field line reconnects (in this sketch) poleward of the southern hemisphere cusp, and begins to contract to reduce curvature under the tension force. The part of the field line near the subsolar magnetopause meanwhile convects tailwards; the part of the field line outside the magnetopause carries uni-directional heated magnetosheath electrons travelling northwards. Only after enough time has elapsed for the magnetopause crossing point of the field line to reach quite high latitudes does the field line re-reconnect poleward of the northern hemisphere cusp, producing bidirectional heated magnetosheath electrons in a relatively localized high latitude magnetosheath boundary layer region

dual lobe reconnection might capture magnetosheath plasma and how this plasma may be transported to the magnetotail to be observed by Cluster, in a process similar to that envisaged by Song and Russell (1992).

Solar wind entry on the flanks of the magnetopause has been proposed to occur in the special context of rolled up Kelvin–Helmholtz vortices. This is of particular interest under northward IMF conditions, where it competes with the dual-lobe reconnection entry picture and the diffusive entry picture, as an explanation for the formation for the low latitude boundary layer and possibly the cold dense magnetotail plasmasheet, as described for example in Hultqvist et al. (1999).

Kelvin–Helmholtz waves on the magnetopause boundary have been recognised for many years (e.g., Otto and Fairfield 2000), and clearly represent a way to transfer energy and momentum from the magnetosheath flow to the magnetospheric boundary layer. The Cluster multi-spacecraft mission has enabled their properties to be measured more completely than by earlier missions. Owen et al. (2004) reported Cluster observations consistent with Kelvin–Helmholtz waves on the dawn flank magnetopause, during northward IMF, provid-

ing information on wavelength and propagation direction and noting a steepened leading (tailward) edge. This observation was consistent with predictions by Miura (1990) helping to resolve conflicting conclusions of earlier observational studies using one or two spacecraft datasets. Further studies of the conditions for formation of, and the development of magnetopause Kelvin–Helmholtz waves include Foullon et al. (2008) and Hwang et al. (2011, 2012) which demonstrate that, given suitable IMF conditions, such waves can grow at high latitudes under strong dawnward IMF, and under southern IMF, as well as the more commonly expected low latitude regions under northern IMF.

Hasegawa et al. (2004) examined a dusk flank magnetopause crossing and used multipoint Cluster data to identify specific plasma and magnetic signatures associated with Kelvin–Helmholtz vortices. They further argued that simultaneous observations of plasma at solar wind and magnetospheric energies, on the magnetosphere side of the magnetopause implied that plasma transport had occurred within the vortices, though they were unable to firmly identify the mechanism. Further work to confirm the result and to identify more examples of Kelvin–Helmholtz vortices followed, including studies by Hasegawa et al. (2006), which set out criteria with which to identify such vortices in single spacecraft datasets. The statistics of Hasegawa et al. (2006) and Taylor et al. (2012) show observations usually at low latitudes, and not only tailward but also sunward of the terminator (suggesting that at least sometimes they may develop very rapidly). Events have also been reported on the dusk flank during sourthward IMF conditions (Yan et al. 2014), as previously predicted.

It has been suggested for some time that these magnetopause disturbances are significantly contributing to solar wind plasma entry into the magnetosphere. The entangling of magnetospheric and magnetosheath magnetic field lines does not of itself enable plasma entry; it is necessary to also invoke a process such as magnetic reconnection or a cross-magnetic field diffusion process within the vortices. Nykyri et al. (2006) presented Cluster observations of reconnection inside Kelvin–Helmholtz vortices, but acknowledged that it was not clear that these reconnection events contributed to significant plasma transport into the magnetosphere.

Hasegawa et al. (2009) used simultaneous observations of the equatorial magnetopause about 15:00 MLT by Geotail and downstream about 19:00 MLT by Cluster to examine the formation of the LLBL during a prolonged interval of northward IMF. The Geotail observations show a LLBL for which high latitude reconnection was found to be the most plausible explanation. Cluster observes rolled up vortices and evidence is presented indicating that local reconnection at the edge of a rolled up vortex is seen by one of the spacecraft. However, it is suggested that this is a small scale event (other Cluster spacecraft did not see it) and in the absence of evidence for reconnection seen in relation to other vortices, it was concluded that vortex reconnection could not account for the significant plasma entry near Cluster. Based on data showing a larger plasma density in the LLBL at Cluster ($\sim$3 cm^{-3}) than Geotail ($\sim$2 cm^{-3}), it is argued that LLBL flux tubes must have gained material while convecting between Geotail and Cluster, as a reduced density ($\sim$1 cm^{-3}) might otherwise be expected due to expansion of the flux tubes. It should be noted that this conclusion relies on an assumption that Geotail and Cluster plasma instruments have good relative accuracy. Taylor et al. (2008) draw a similar conclusion from a study with Polar and Double Star TC-1, in a study of an interesting interval which has rolled up vortices, dual-lobe reconnection and a cold dense plasma sheet observed by Double Star TC-2.

Bavassano Cattaneo et al. (2010) performed a detailed examination of very large rolled up Kelvin Helmholtz vortices observed by Cluster during a long lasting interval of northward IMF in the dusk equatorial magnetopause region. The vortices are suggested to have been generated further upstream, due to their large size. Magnetospheric and magnetosheath

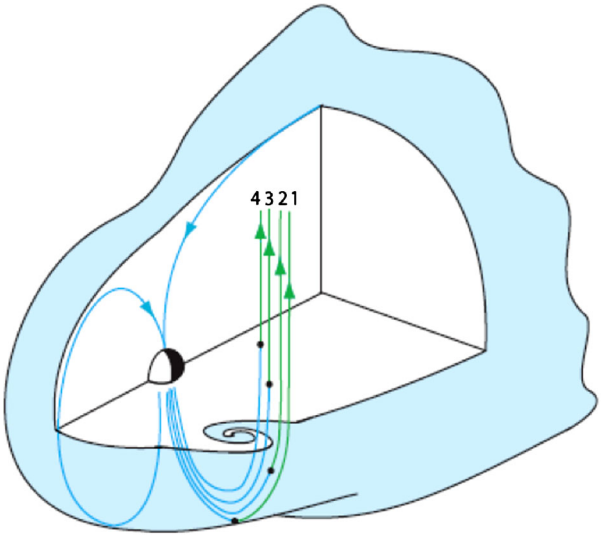

Fig. 9 The scenario described by Bavassano Cattaneo et al. (2010) in which magnetosheath magnetic field lines are reconnected at high latitudes under northward IMF conditions, and then convect tailwards to become entangled in Kelvin–Helmholtz vortices that form from Kelvin–Helmholtz boundary waves that also propagate tailwards along the magnetopause. The *blue parts* of these open field lines are within the magnetosphere while the *green parts* are outside. Near the equatorial plane, field lines 3 and 4 have crossed the magnetopause to become part of the low latitude boundary layer inside the magnetopause while field lines 1 and 2 are contributing to a magnetosheath boundary layer. The crossing point on a given field line effectively moves northwards as the field line moves tailwards

plasma coincide on the magnetosphere side of the magnetopause, similar to the findings of Hasegawa et al. (2004). Electron, proton and O^+ ion distributions observed in a succession of vortices show, in each case, a sequence of differing signatures consistent with crossing back and forward from the magnetosheath to the magnetosphere through a magnetosheath boundary layer (MSBL) and low latitude boundary layer (LLBL) of the kind that is expected for persistent lobe reconnection at high (southern) latitudes. In particular, parallel and antiparallel ion populations carry clear information about the different ages of the reconnected field lines in the inner and outer LLBL and the outer and inner MSBL. A key finding is that field aligned O^+ ions, while prevalent in the magnetotail plasmasheet, could not be found near the magnetopause current sheet, as might be expected for local reconnection allowing transport across the low latitude magnetopause. It is therefore suggested that, for this event at least, the reconnected field lines, while convecting tailwards became embedded in the developing vortices, as illustrated in Fig. 9.

Takagi et al. (2006) and Faganello et al. (2012) proposed that solar wind plasma entry to the magnetosphere can occur through so-called "double mid-latitude reconnection" occurring on the magnetospheric flanks as a consequence of rolling up of Kelvin–Helmholtz vortices. The concept is that there is a limited latitudinal extent over which conditions for vortex formation are favourable, and that magnetic flux that is separated by distances comparable to vortex scales sizes at low latitudes is able to reconnect at mid-latitudes, as shown in Fig. 10. In effect, this is similar to double-lobe (behind the cusp) reconnection, but the along-field distance between reconnection sites is smaller. Faganello et al. (2014) published a case study providing observational evidence for the occurrence of this scenario using THEMIS spacecraft data. There may not yet be a consensus on this scenario, as the same THEMIS

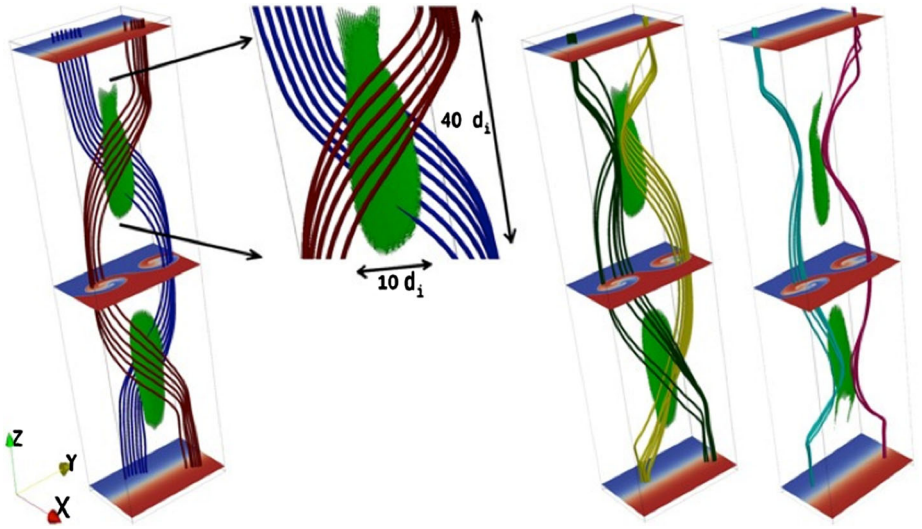

Fig. 10 Illustration from Faganello et al. (2012), of double mid-latitude reconnection associated with Kelvin Helmholtz vortices at the flank magnetopause. On the *left hand side* of the figure, *blue* (magnetospheric) and *red* (magnetosheath) field lines are shown becoming intertwined and twisted due to vortical flows at low latitude that do not occur at higher northerly or southerly latitudes. *Green shapes* show where mid-latitude current sheets form, which may become suspectible to magnetic reconnection. The *right hand pair* of figures show reconnection first at the upper current sheet, producing open field lines (*green* and *yellow*) and then at the lower current sheet producing newly closed pale *blue* field lines carrying a population of captured magnetosheath plasma

data were also used to provide support for an interpretation involving reconnection at low latitudes and sub-vortex scales, according to three-dimensional fully kinetic simulations by Nakamura et al. (2013).

It remains to be firmly demonstrated that reconnection-based processes can fully explain the observed magnetospheric boundary layers, particularly under northward IMF conditions, so it remains relevant to consider the relative effectiveness of other processes that may play a role. Alternative scenarios for plasma transport across the magnetic field at the magnetopause typically invoke a kinetic process that acts on scales smaller than those for which ideal magnetohydrodynamics is applicable.

For example, it has been proposed that cross-magnetic field diffusion may play a role in flank magnetopause plasma entry. Smets et al. (2007) used hybrid simulations to show that diffusion due to finite Larmor radius effects may occur at a tangential discontinuity magnetopause for southward IMF, and that its effectiveness is improved when Kelvin–Helmholtz waves activity occurs. Interestingly, this study predicts observations of "D-shaped" ion distributions, previously considered to be a unique indicator of magnetic reconnection.

When the wavelength of waves at the magnetopause is on the order of the ion gyroradius, the waves can lead to diffusive transport of transport of the magnetosheath ions across the magnetopause (Johnson and Cheng 1997; Chen 1999; Chaston et al. 2008). One of the likely types of waves is large-amplitude kinetic Alfvén waves (KAW). KAWs have been observed on the magnetospheric boundary (Tsurutani et al. 1982; Labelle and Treumann 1988; Anderson and Fuselier 1994). KAWs could result from mode conversion of magnetosheath compressions in the sharp magnetopause gradients at the magnetopause (Lee et al. 1994; Johnson and Cheng 1997, 2001). The mode conversion has been demonstrated with 2D hy-

brid simulations (Lin et al. 2010) and 3D simulations (Lin et al. 2012). Yao et al. (2011) surveyed wave power in the sheath and magnetopause and their results suggest that the wave power associated with transverse KAWs is enhanced along the dawn flank, which would provide enhanced transport. Particles can be heated nonlinearly by KAWs as they diffuse across the magnetopause (Johnson and Cheng 2001; Chaston et al. 2008). The parallel electric field of KAWs can heat electrons in the parallel direction (Hasegawa and Chen 1975; Hasegawa and Mima 1978). When the waves have large amplitudes, they can also heat ions in the perpendicular direction (Johnson and Cheng 2001). Chaston et al. (2008) showed observational evidence of stochastic heating of ions by KAWs as predicted by Johnson and Cheng (2001). The extent to which this source contributes plasma to the magnetosphere remains poorly understood.

In introducing magnetopause sources of plasma, Hultqvist et al. (1999) summarizes the total magnitude of this source with a single number that represents the sum of all above processes: 10^{26} ions/s. This number remains widely accepted today. Refinement of this number, its division amongst contributing processes, and its dependence on solar and magnetospheric conditions all remain open questions.

2.4 Other Sources

The Earth's magnetosphere is rarely considered to have any other sources beyond the solar wind and ionosphere. However, this is not strictly true. Other systems, especially those of the gas giants, can receive significant contributions from their satellites. Production can occur from surface sources, such as sputtering or volcanic activity, or from ionospheric processes on moons with sufficiently dense atmospheres. In a similar fashion, the Earth's moon can act as a third source of magnetospheric plasma.

The Moon crosses the Earth's magnetotail at $r \sim 60\ R_E$ for ~5 days each month. The Moon does not have a significant atmosphere and only has a tenuous exosphere of neutral species. When in the magnetotail lobes, pickup ions can be produced on or above the lunar dayside by several mechanisms (Poppe et al. 2012):

1. photoionization of the neutral exosphere,
2. micrometeoroid bombardment of the surface,
3. photon- and electron-stimulated desorption on the surface, or
4. photo-ionized products of neutrals vented from a localized source in the lunar crust (see Seki 2015).

Lunar pickup ions are heavy ions, including He^+, C^+, O^+, Na^+, K^+, Ar^+, Al^+, and Si^+ (Tanaka et al. 2009; Saito et al. 2010). The Density of pickup ions can be in the order of 0.1 cm^{-3} and is several times higher than the density in the lobes (Harada et al. 2013; Zhou et al. 2013). Two electric fields can accelerate the freshly born ions: the photoelectric field from the existence of a high-energy tail of lunar-surface photoelectrons due to incident solar ultraviolet radiation and the convection electric field in the lobes. The ions can be accelerated to energies from several tens to several hundreds of eV (Poppe et al. 2012). Considering the pickup ions are only produced within the immediate neighborhood of the Moon, their contribution as a source for the Earth's tail plasma sheet is negligible in comparison with the mantle plasma.

3 Transport and Acceleration

3.1 Ionospheric Plasma Transport

Following the Dynamics Explorer 1 (DE-1) mission (1981) and before the Cluster mission, launched in 2000 into a 4×19 R_E elliptical polar orbit, the fate of ionospheric outflow at the nightside equatorial plane was studied using Akebono measurements in LEO (e.g., Cully et al. 2003a, 2003b), Polar measurements in HEO (apogee $\sim$9 R_E) (e.g. Huddleston et al. 2005), and by employing particle trajectory modeling (e.g., Delcourt et al. 1989) to predict where the outflow observed by the spacecraft ended up; the modeling done using the Akebono and Polar measurements both showed the ionosphere to be capable of providing enough low energy plasma to fill the magnetosphere, lending support to an early prediction motivated by DE-1 observations (Chappell et al. 1987).

More recent studies on the occurrence of magnetospheric low energy plasma and its solar or terrestrial origin have drawn on the enhanced observational capabilities provided by the four-satellite Cluster mission and, beginning in 2007, the five-satellite Time History of Events and Macroscale Interactions during Substorms (THEMIS) mission. The Cluster spacecraft orbits allow for sampling of plasma directly above the polar caps and also at larger geocentric distance in the tail lobes and plasma sheet; the instrumentation was also designed to observe the dominant ion species for studying sources and transport and could combat some of the difficulties of observing low energy plasma with the ability to actively control the spacecraft potential (ASPOC). Together, these capabilities enable a cradle-to-grave inquiry into the transport of low energy plasma (O^+ in particular) from the ionosphere into the magnetosphere and near the equatorial plane as well as its energization (e.g., Kistler et al. 2005, 2010b; Liao et al. 2012, 2014). Such observations motivate recent particle trajectory modeling studies (Yau et al. 2012) and are also the subject of multiple global magnetospheric simulations (Lotko 2007; Glocer et al. 2009a, 2009b; Brambles et al. 2011; Yu and Ridley 2013). In the following, we review our current knowledge of ion transport and acceleration based on past and recent measurements.

The transport of low-energy plasma through the magnetosphere is, in its simplest form, a combination of the parallel motion along the field line and the convective $E \times B$ motion perpendicular to the field. Low-energy, in this case, refers to ions for which gradient and curvature drifts are not significant. As has been discussed above, there is essentially always ionospheric outflow at some level, due to the ambipolar electric field, and the fate of that outflow depends on the configuration (i.e. open or closed) and convective motion of the field-line. In the inner magnetosphere, for example, the ions that flow out on magnetic field lines that are corotating are able to accumulate, forming the dense plasmasphere, while ions that flow out at higher L-shells are continually convected towards the magnetopause, and so the density never reaches high levels.

At high latitudes, particularly in the cusp and auroral regions, there is further acceleration of the ions. The outflow in these regions covers a wide range of energies, from eV up to as high as 10 keV. In the case of the cusp, the combination of the parallel motion and $E \times B$ motion leads to what is known as the "velocity filter" effect, or the "tail lobe ion spectrometer" (Horwitz 1986). The $E \times B$ motion of the ions does not depend on energy, while the parallel velocity increases with energy. Thus, as a field line convects over the polar cap and into the lobe, the high energy ions are able to travel further down the tail than lower energy ions. Thus there is a separation of the ions by their velocity. Horwitz (1986) modeled this effect, providing maps that showed how the velocity of the ions entering the plasma sheet increased with distance downtail. Modeling by Delcourt et al. (1992) also showed the energy dependence of the transport paths. Because the process separates ions by velocity, not

energy, lighter species go further down that tail than heavier species of the same energy, and at a particular location, different species with the same velocity, corresponding to different energies, are observed (Chappell et al. 1987). These populations are loosely referred to as "beams" as the flow outward along field lines.

Because O^+ has a higher energy than H^+ for the same velocity, it is easier to observe the O^+ ion beams in the lobes that result from the cusp outflow than the H^+ beams. The H^+ beams are often below the energy threshold of the plasma instruments, and/or below the energy of the positive spacecraft potential in the lobe. Thus, observations supporting the "ion spectro" picture have originated with (Candidi et al. 1982) and continue to come from O^+ ions. Liao et al. (2010) performed a statistical study of the occurrence of these O^+ beams using data from the Cluster/CODIF instrument ($\sim > 40$ eV). They found that the occurrence frequency of the ions increased with geomagnetic activity, although the beams could be observed for all levels of activity. They also found that the spatial distribution depended strongly on IMF B_Y, with O^+ from the northern cusp streaming towards the dawnside lobe when the IMF B_Y is positive, while O^+ from the south stream towards the duskside lobe. Liao et al. (2012) showed a positive correlation between solar activity and O^+ lobe beam observations. Although the beam occurrence frequency decreased with lower solar activity, their trends showed that in the lobes still occurred between 0–25 % of the time approaching solar minimum without accounting for ions below the instrument detection threshold. They noted seasonal as well as an orbital bias: the equatorial magnetosphere between 4 and 15 R_EE was not sampled often due to the Cluster orbit. Still, their results suggested ionospheric outflows contribute to the equatorial plasma content at all levels of solar activity but that this contribution should be greater near solar maximum, as shown in Fig. 11. Liao et al. (2015), compared the phase space density of the individual O^+ lobe beams with the phase space density of the outflowing cusp density and confirmed that the observed beam flux and the increase in energy of the beams down the tail are consistent with the velocity filter effect during quiet times, with no significant acceleration of the O^+ along this path. A small increase due to centripetal acceleration, however, as suggested by Nilsson et al. (2010), is not excluded. However, during active times, more acceleration during the transport is observed.

Because there is also significant cusp and polar cap outflow of H^+, H^+ should also be present in the lobes. However, studies of low-energy H^+ are plagued by electric shielding, as sunlit spacecraft are often charged positively from 10 to 100 V. Several methods have been employed to overcome this difficulty and obtain H^+ measurements. Relaxation sounders, which are antenna that obtain electron densities by emitting waves at characteristic plasma frequencies and observing the resulting plasma resonance (Harvey et al. 1978), do not suffer from electric shielding. These instruments were the first to measure cold, dense plasma in the plasma sheet boundary layer (Etcheto and Saint-Marc 1985). For particle detectors, one method to overcome shielding is to artificially lower the spacecraft potential by emitting positive ions (Moore et al. 1997; Torkar et al. 2008). Despite these efforts, a potential of typically a few Volts remains. During some periods, a spacecraft can be temporarily in eclipse and hence negatively charged, and low-energy ions can reach the onboard detectors (Seki et al. 2003). An alternative is to obtain the total plasma density from wave observations of the plasma frequency and then subtract the hot ion density observed by particle detectors (Sauvaud et al. 2001).

An alternative way to obtain the density is to use the fact that the spacecraft potential depends on the density and can, after calibration, be used to estimate the total density (Lybekk et al. 2012; Haaland et al. 2012). To also estimate the velocity of low-energy ions that can not reach a charged spacecraft, a recently developed technique has been used to analyze Cluster

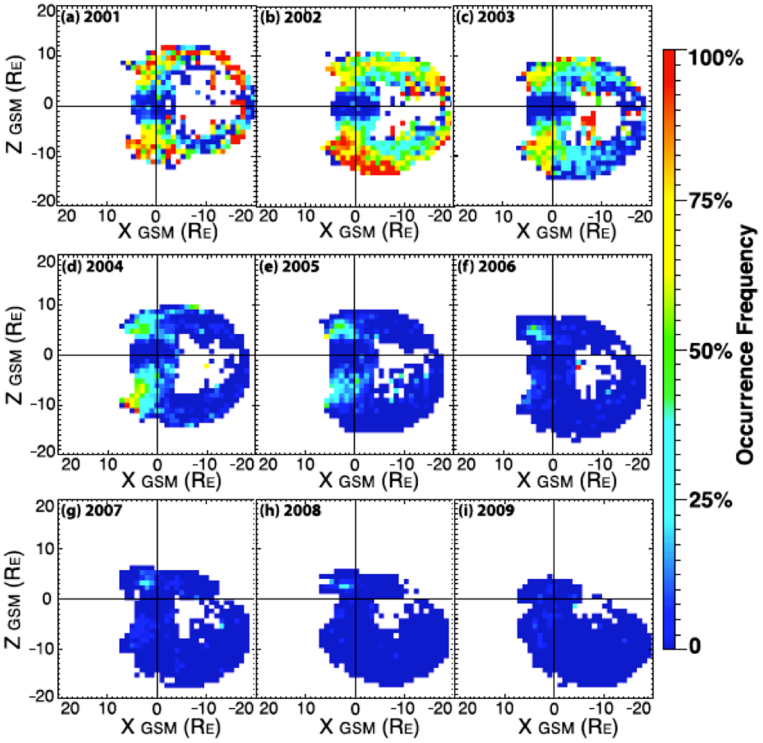

Fig. 11 Streaming O^+ occurrence from Liao et al. (2012). Each frame shows results from a different year and, therefore, different points in the solar cycle and phase of the Cluster II orbit

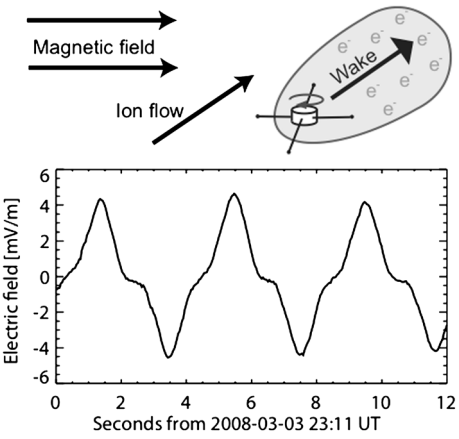

Fig. 12 A diagram illustrating the formation of the electron wake forming about a positively charged spacecraft (*top frame*) and the resulting electric field observed by the spacecraft. From Engwall et al. (2009b)

data. A supersonic flow of positive low-energy ions can create an enhanced wake behind a positively charged spacecraft. Here the ions are diverted by the potential structure and not by the much smaller spacecraft (Engwall et al. 2006, 2009b, 2009a; André and Cully 2012; André et al. 2015). The conditions for the enhanced wake formation sketched in Fig. 12

(top) are that the ion flow energy, $mv^2/2$, exceeds both the thermal energy, kT, and also is lower than the equivalent energy of the spacecraft potential, eV_{SC}:

$$kT < mv^2/2 < eV_{SC} \tag{1}$$

The ion wake will be filled with electrons, whose thermal energy is higher than the ram kinetic energy, in contrast to that of the ions. The negative space charge density can then create a local wake electric field close to the spacecraft. This electric field can be observed with electric field instruments using probes mounted on wire booms.

For a given velocity, lighter ions, such as H^+ will be more affected by the spacecraft and hence create a larger wake. Figure 12 (bottom) shows an example of a wake electric field observation close to the subsolar magnetopause. The non-sinusoidal repetitive pattern is due to the wake and indicates the presence of low-energy ions. Combining observations of the wake electric field with observations of the magnetic field and observations of the geophysical electric field using another method (the drift of keV electrons artificially emitted from the spacecraft) gives the ion velocity. Combing the velocity with the density from the spacecraft potential, the flux of low-energy ions can be determined (Engwall et al. 2009b, 2009a; André et al. 2010).

Using the Cluster dataset and this unique method to obtain low-energy ion fluxes in the night-side ($X_{GSM} < 0$) André et al. (2015) showed the occurrence rate of low-energy ions was 60–70 % in the lobes to out to X_{GSM} of about 15 R_E during all parts of the solar cycle, as indicated in Fig. 13. The ions' very low energy clearly identified them as ionospheric plasma and their high occurrence rate confirmed both their existence and their prominence in the lobes. Their statistics also showed a decrease in the occurrence rate to <20 % on approach to the plasma sheet ($|Z_{GSM}| < 2$ R_E) and they suggested that the low occurrence at small Z_{GSM} distances was due to the low-energy ions being energized above 10 eV upon approach and passage through the plasma sheet. They also noted, however, an observational limitation arising near the plasma sheet due to the detection method requiring both a steady magnetic field and the absence of ambient hot plasma.

A comparison of the statistical distribution of the O^+ beams from CODIF and the H^+ beams from Engwall et al. (2009b) (see Kronberg et al. 2014, Fig. 9) shows that the velocity distributions are very similar, which is again consistent with picture that the ions are distributed in the tail according to their velocity (not energy). However backtracing of the H^+ distributions observed indicated that at least some fraction of the lobe ions come from the polar cap, not from the cusp (Li et al. 2012). It is not surprising that the source of the lobe beams is mixed, as ions clearly flow from both the cusp and polar cap regions.

Geotail also measured beams of ions at higher energies (~keV) 100s of R_E down the magnetotail (Hirahara et al. 1997; Seki et al. 1999). These beams are observed in the plasma mantle, and consist of both ionospheric-source ions (e.g. O^+) as well as solar wind ions (H^+ and He^{++}). These beams were found to be too energetic to be consistent with just the velocity filter effect. Seki et al. (1996, 1998, 1999) investigated the possible transport routes and identified three possible sources: cusp outflow, recirculation of upward flowing ions from the nightside auroral region, and a dayside trapped population that enters the mantle through dayside reconnection. Recent measurements from Cluster (Nilsson et al. 2012, 2013) show that energetic O^+ is further accelerated in the high altitude cusp, and mixes with magnetosheath solar wind. This population moving tailward is likely the source of the deep tail beams.

The ions beams in the lobe move into the plasma sheet when the lobe field lines reconnect. Orsini et al. (1990) showed that the O^+ beams in the lobe accelerate and isotropize as they move into the plasma sheet. Kistler et al. (2010b) showed that during geomagnetic

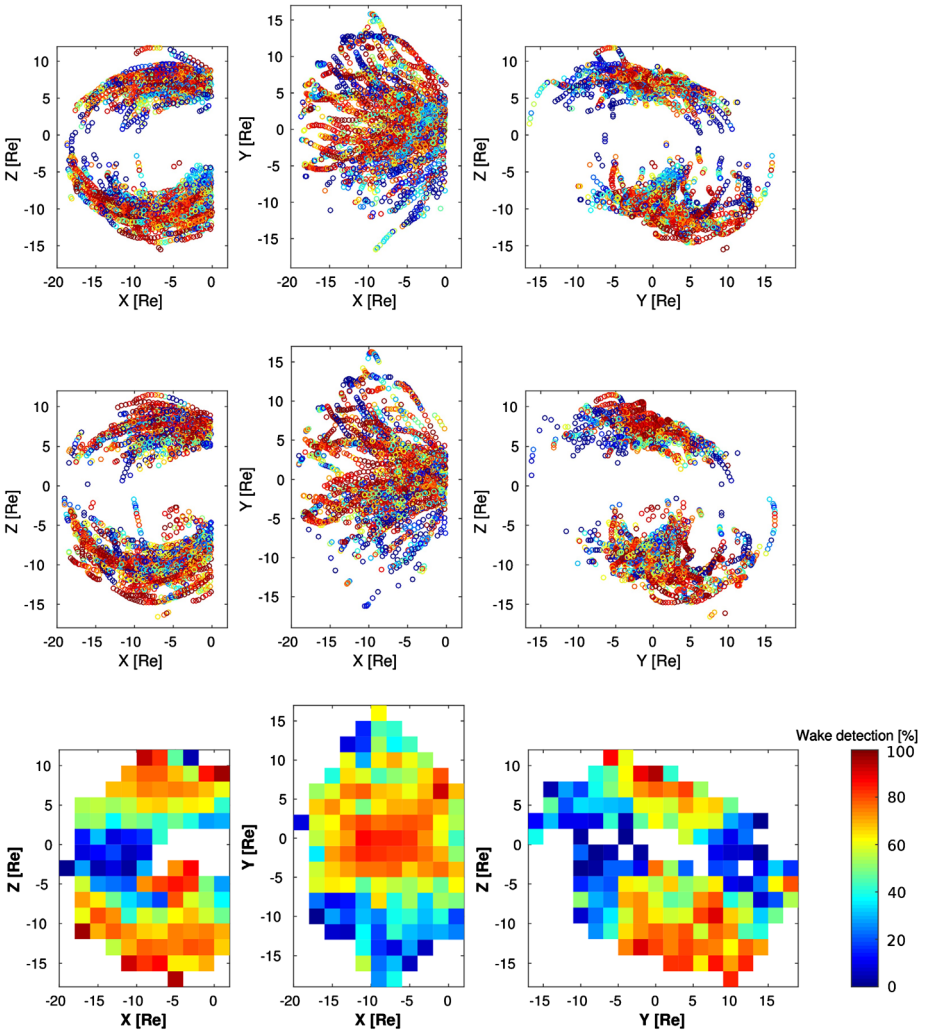

Fig. 13 Occurrence of low-energy ions. Detection of flowing low-energy ions in the GSM X-Z, X-Y, and Y-Z planes: (*top*) Cluster 1 2001–2009; (*middle*) Cluster 3 2001–2010; and (*bottom*) the sum of all data (*top* and *middle*) grouped in bins of 2 R_E by 2 R_E. From André et al. (2015)

storms, the lobe O^+ beams are observed crossing the plasma sheet boundary layer, and into the ∼20 R_E plasma sheet. Once they cross the neutral sheet, the beams become isotropized. Hirahara et al. (1994), using Geotail Low Energy Particle (LEP) data, found that the lobe beams increase in energy as they move into the plasma sheet, due to enhanced $E \times B$ drift. Liao et al. (2015) also found that the beams increase in energy, and that on average, the perpendicular increase is consistent with an enhanced drift speed, due to a relatively constant average electric field, but a decreasing magnetic field towards the c enter of the plasma sheet. There is also an increase in the parallel direction, due to either wave heating, or non-adiabatic acceleration of the O^+. Kistler et al. (2010a), using STEREO/PLASTIC data from the deep tail pass of the STEREO-B spacecraft at 200–300 R_E, found that O^+ is also a con-

stant presence in the deep tail plasma sheet during quiet times indicating that O^+ still has access to the plasma sheet downstream of the distant neutral line.

Liemohn (2005) performed a statistical survey of the <300 eV streaming ions in the nightside lobe and plasma sheet at closer radial distances (~9.5 R_E) using POLAR/TIDE measurements. They found that the cold ion streams were common, occurring >70 % of the time at these distances. They found that the tailward streaming lobe beams became bidirectional beams when they entered the plasma sheet. This shows that in contrast to further down the tail, at these closer radial distances, the field line curvature radius at the center of the plasma sheet is normally not small enough to scatter the ions, so the ions mirror and bounce. During active times, the bi-directional beams were less frequent, indicating that in these cases, the ions did scatter and isotropize.

The bouncing ion populations seen by Polar and other satellites were pursued by Chappell et al. (2008), who noticed a similarity between their persistent occurrence in Polar observations and in a compilation of particle observations from multiple past satellite missions (ATS, ISEE, SCATHA, DE-1). As this population convects inward, it drifts eastward due to the corotation electric field, remaining outside the closed drift paths of the plasmapause. Chappell et al. (2008) named this population the warm plasma cloak, due to its observed features that showed it to be a bi-directional streaming population of warm (~10 eV to few keV) plasma draped over the plasmasphere that was being blown sunwards by convection. This population co-exists with the more energetic ring current. The authors also performed particle trajectory modeling to explain its formation, showing that a polar wind proton that is centrifugally accelerated and crosses the plasma sheet at a smaller geocentric distance would pick up less energy, would not get deflected around dusk by magnetic drifts on earthward approach, and instead flow around the dawnside due to combined convection and co-rotation drifts that transport it towards the dayside magnetopause.

In addition to ions from the lobe, ions can also enter the plasma sheet directly from the nightside aurora region, which can also lead to bidirectional ion beams. Daglis and Axford (1996) suggested that the auroral outflow provides a fast feeding of the inner plasma sheet with O^+ during the substorm expansion phase. This was based on observations of the increase in the O^+ energy density at substorm onset, using AMPTE/CHEM observations (Daglis et al. 1994) at distances close to the AMPTE/CCE apogee, 8.8 R_E. This study showed that the O^+ energy density has a strong correlation with Auroral Envelope (AE) index. AMPTE/CHEM covered the energy range 1 keV to 300 keV, but its sensitivity to O^+ below ~30 keV was very low. Thus, while it could measure the accelerated O^+, it could not verify the auroral source. Gazey et al. (1996) reported an example where the EISCAT radar observed a discrete auroral arc associated with considerable upflow of ionospheric plasma. At the same time, the MICS instrument on the CRRES satellite observed two substorm injections, the second of which was O^+ dominated. MICS also measures energetic ions, from 50–300 keV. They concluded that the auroral outflow could be the source of the O^+, although they found they could not exclude a cleft source. Sauvaud et al. (2004) showed an example where an injection of O^+ from the nightside aurora accounted for 80 % of the O^+ in the mid-tail region during a geomagnetic storm.

Finally, coexisting with these warmer plasma sheet populations are a significant cold population in the equatorial nightside magnetosphere. As in the case with the global ion beams, these ions are difficult to measure because they are often below the lower energy threshold of the plasma instruments, and they are also often below the spacecraft potential, which tends to charge positive when the spacecraft is exposed to sunlight. Seki et al. (2003) used a time period when the Geotail spacecraft was in eclipse at a distance of 9 R_E down the tail, to show that there existed a cold population that had a density (~0.2 cm^{-3}) equal

to the hot population occurring at the same time. Hirahara (2004) used a different technique to find cold ions in the same region. During time periods when Pc5 ULF waves occurred, multiple cold ion species (H^+, He^+, and O^+) otherwise invisible to particle detectors were accelerated into the energy range of the particle instrument. Hirahara (2004) showed that these cold ions were present 40–70 % of the time that the Pc5 waves were observed. These observations confirmed that the cold ions were observed simultaneously with a hot ion component at the inner edge of the plasma sheet, indicating that ionospheric cold plasma could cross the plasma sheet without being significantly energized. These cold ions, with partial densities comparable to the energetic ion component, were observed more frequently during the rising phase of the solar cycle. As a result, the authors suggested that the observed cold ion signatures were due to direct feeding of ionospheric outflow into the plasma sheet that was dependent on solar activity.

Nightside equatorial cold ions were sampled using the ULF wave technique by Lee and Angelopoulos (2014) out to ~13 R_E during predominantly quiet times (observation interval between 2008 and 2013). They used the THEMIS satellites to sample cold ions during intervals of enhanced bulk plasma flows (convection or ULF waves) that accelerated ambient cold ions above the spacecraft potential so they could be detected by the particle instruments carried by the three inner THEMIS spacecraft (low inclination, 1.5 by 13 R_E). They estimated the partial densities and temperatures of the three dominant ion species (H^+, He^+ and O^+) during such flow intervals and showed that all three occurred around 1–20 % of the time on the nightside, but that the heavier ions were more abundant and also warmer than the protons (H^+: few to 10 eV, He^+: 10s eV, O^+: 100s eV), as illustrated in Fig. 14. These nightside equatorial observations support the interpretation by Engwall et al. (2009b) that the outflowing LEP observed with Cluster II were likely energized above the energy needed to form a wake at locations near the plasma sheet. Lee and Angelopoulos (2014) used the heavy ion density ratios and higher temperatures on the nightside to also infer a major ionospheric source of LEP at $L < 13$ R_E. They noticed another trend: the median temperatures of all three species were quite warm (10–100s eV) and traced out a path from pre-midnight through the dawn side, consistent with particles in the warm plasma cloak, with evidence of another path of the nightside warm ions along the dusk side. The dawnside trend implied that the heavy ions, likely to originate from the nightside ionosphere, could make it to the equator, gain moderate energy from injections or waves, and then become part of the cloak, which was discussed but not directly observed by Chappell et al. (2008).

During geomagnetic storms, enhanced convection brings the hot plasma sheet population into the inner magnetosphere. The inward motion to a stronger magnetic field increases the energy of the ions through conservation of the first adiabatic invariant. The first measurements of the ring current population (Krimigis et al. 1985; Gloeckler and Hamilton 1987) showed that during moderately active times, the ionospheric contribution was about equal to the solar wind contribution. Hamilton et al. (1988) showed that during a very large storm, ionospheric O^+ became the dominant contributor to the plasma pressure at the peak of the main phase. Greenspan and Hamilton (2002) performed a statistical study of the O^+/H^+ ratio during storms, using 68 storms that covered the rising phase of solar cycle 22. They found that both Dst and F10.7, a measure of solar EUV, are important and nearly independent predictors of the O^+/H^+ energy density ratio. Thus a large storm, at any time, will have high O^+, while even a small storm at solar maximum can have a high O^+ contribution.

Modeling of ion transport during storm times (e.g., Kistler et al. 1989, 1999; Jordanova et al. 2001, 2003, 2010) have shown that particle drift from the near-earth plasma sheet, with a large convection electric field bringing the ions into the inner magnetosphere, and then a reduced convection electric trapping the ions in the inner magnetosphere, is able to explain

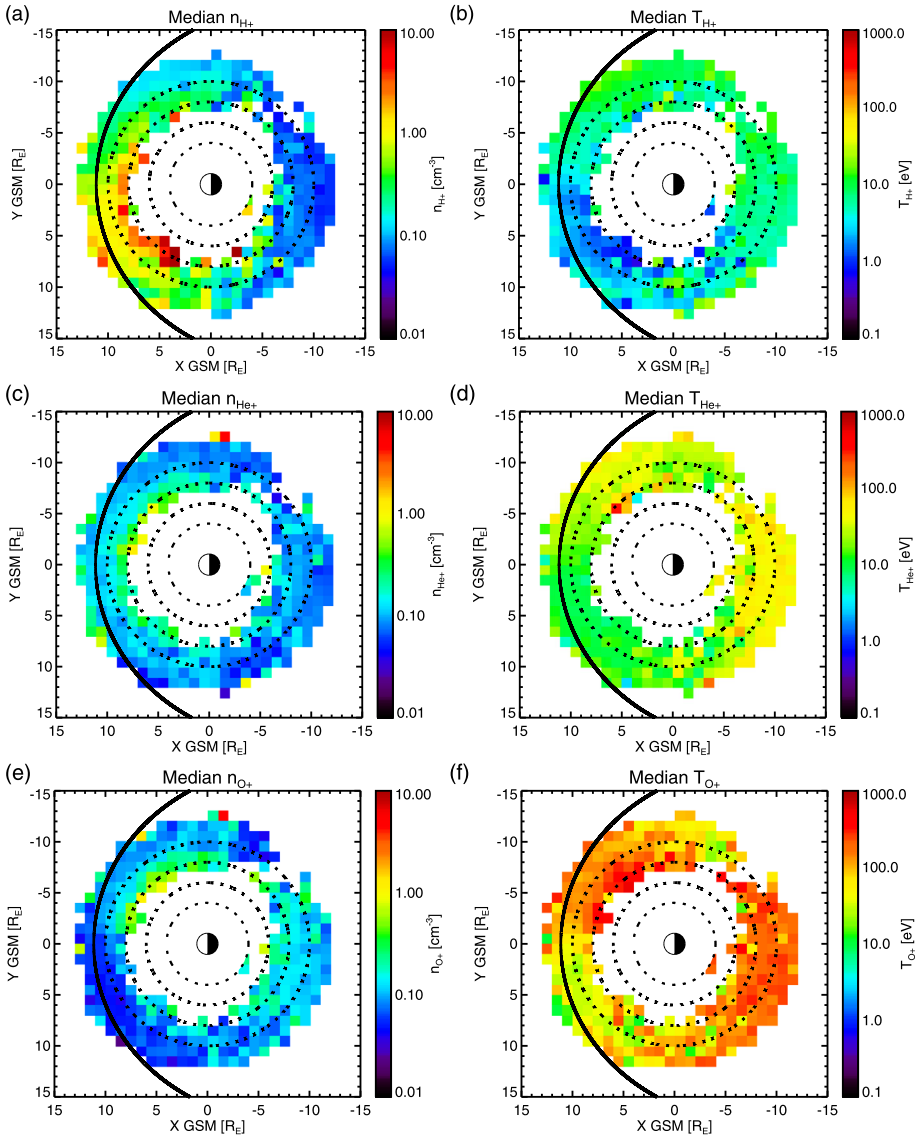

Fig. 14 Global cold ion species properties from Lee and Angelopoulos (2014)

the observed ring current spectra. The complex, non-maxwellian energy spectra observed in the ring current result from the competition between gradient curvature and $E \times B$ drifts in the inner magnetosphere, combined with loss processes along the drift path. An open question, however, is how the O^+ gets accelerated to become the dominant species in the ring current. The observations and possible mechanisms on this question have recently been reviewed by Keika et al. (2013). They address whether this is mainly due to the enhanced O^+ density in the plasma sheet from the increased entry from the lobe and night side aurora, or whether O^+ is also preferentially accelerated in the plasma sheet. As discussed above, it is clear that the O^+ is enhanced in the plasma sheet during storm times, and so that is certainly

part of the answer. The question of whether O^+ is preferentially accelerated in the plasma sheet, and the role of substorms in generating the ring current is reviewed in Sect. 3.4

3.2 Plasmaphere Transport

Much of the most exciting new work concerning transport of plasmaspheric material concerns investigation of the plasmapause, or the outer boundary of the plasmasphere. The position of the plasmapause is determined by the interplay between the corotation and the convection electric fields. The magnetospheric convection electric field, controlled by the solar wind conditions and the level of geomagnetic activity, is a key factor in all existing theories for the formation of the plasmapause (Pierrard et al. 2008, and references therein).

The configuration and dynamics of the plasmapause are highly sensitive to geomagnetic disturbances. During extended periods of relatively quiet geomagnetic conditions the plasmasphere expands and the plasmapause can become diffuse, with a gradual fall-off of plasma density. Inversely, during increasing magnetospheric activity, the plasmasphere gets compressed and the plasmapause is eroded. Plasmaspheric ions can then be peeled off and escape toward the outer magnetosphere. Observations and modelling efforts have demonstrated that, for instance, plasma tongues can be wrapped around the plasmasphere, shoulders can be formed, or that plasma irregularities can be detached from the main body of the plasmasphere and form plumes (Lemaire 2001; Goldstein 2003; Sandel et al. 2003; Dandouras et al. 2005; Pierrard et al. 2008).

The plasmaspheric plumes are especially relevant because they constitute a cold plasma outflow mechanism, from the plasmasphere to the outer magnetosphere. They are associated with active periods, and during these periods they contribute typically $\sim 2 \times 10^{26}$ ions/s to the magnetospheric populations (Borovsky and Denton 2008). Recent studies have also demonstrated that plumes may affect dayside merging conditions (e.g., Walsh et al. 2014), discussed further in Sect. 4. The remote sensing observations of the plasmasphere by the IMAGE spacecraft and the in situ observations obtained by the Cluster constellation provide some novel views of this region.

Figure 15 gives an example of a plasmaspheric plume development during a magnetic substorm on the June 10, 2001, following a steady increase of the K_P activity index in the two preceding days. The plasmapause formation is simulated (Pierrard and Cabrera 2005), based on the instability mechanism for the plasmapause formation (Lemaire 2000, 2001; Pierrard and Lemaire 2004) and depending on the time history of the values of K_P. The development of a plume is clearly visible in the dusk LT sector at 7 UT. Figure 15(b) shows the EUV/IMAGE observation at 07:00 UT. A plume is indeed observed in the same LT sector, as predicted by the simulations.

Another way to observe large scale plume dynamics is to observe their connection with the ionosphere. For cold plasmas originating in the ionosphere and outer plasmasphere, $E \times B$ drift redistribution keeps both low altitude (F region O^+) and high altitude (topside H^+) ions on the same flux tube as they are convected from the plasmasphere boundary layer (PBL) to higher latitude field lines. Incoherent scatter radar observations reveal plumes of ionospheric storm enhanced density (SED; primarily O^+) extending from the dusk sector PBL to the vicinity of the noontime cusp (Foster 1993). These radar observations of SED have been projected into the equatorial plane by Su et al. (2001) and compared with geosynchronous orbit observations of a sunward-streaming plume of plasmaspheric material. That study concluded that the eroded plasmaspheric/ionospheric material is extended along the magnetic field and that SED is an ionospheric signature of the erosion of the outer plasmasphere.

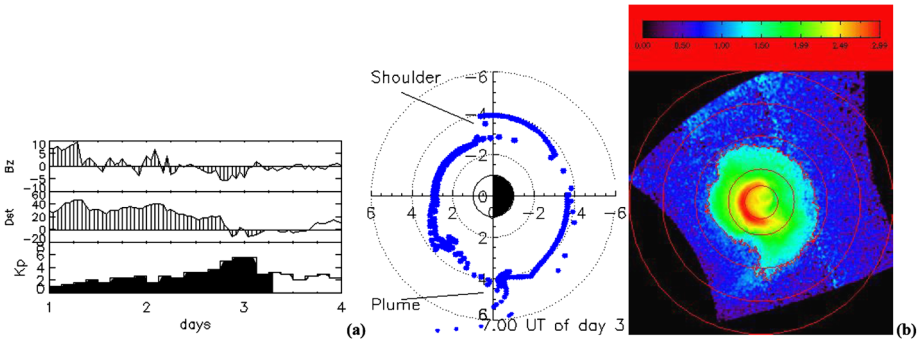

Fig. 15 Plasmaspheric plume development on the June 10, 2001, 07:00 UT. The center frame shows simulation results from Pierrard and Cabrera (2005), based on the instability mechanism (Lemaire 2000, 2001), the E5D electric field model (McIlwain 1986) and the value of K_P. The plasmapause in the geomagnetic equatorial plane corresponds to the *blue line*. The indexes B_Z, D_{ST} and K_P, observed during the previous and following days, are shown in the *left frame*. The *dotted circles* correspond to $L = 1, 2, 4$ and 6. The *right frame* shows EUV observations for this event projected in the geomagnetic equatorial plane. The *red line* corresponds to 40 % of the maximum intensity of the image and permits one to visualize the plasmapause. The *red circles* correspond to $L = 1, 2, 4, 6$ and 8. From Pierrard and Cabrera (2005)

In conjunction with radar observations, the spatial-temporal evolution of the plasmasphere/ionosphere plume can be measured through observations of Total Electron Content (TEC) from ground-based Global Positioning Satellite (GPS) receivers. The satellites of the GPS constellation are in 12-hr circular orbits (∼20,000 km altitude) with orbital inclination ∼55°. The GPS satellites have apogee near 20,000 km ($L \sim 4$) and the integrated total electron content (TEC), determined from analysis of their transmissions, is the combined contribution of the ionosphere and the overlying plasmasphere. An example of an SED plume originating from the duskside ionosphere and traversing poleward, illustrated by GPS TEC, is shown in Fig. 16. The narrow band of elevated TEC extending antisunward from the cusp across polar latitudes to the nightside auroral oval reveals how these plumes earned their other common title: the polar tongue of ionization (TOI) (Foster 2005; Thomas et al. 2013).

These GPS TEC observations have enabled new studies that further connect SED plumes with the plasmasphere. Figure 17 shows the plasmasphere erosion plume on October 8, 2013 (GPS TEC mapped to GSM equatorial plane) and the intersecting orbits of Van Allen Probes RBSP-A and Themis E_{SC}. The Van Allen Probes satellites, with their 5.5 R_E apogee, were well positioned to observe the plume in-situ, and found good agreement with the TEC maps. Additionally, it was found that the plume was oxygen rich: the O^+/H^+ density ratio increased threefold within the plume (Foster et al. 2014a).

An analysis of the April 11, 2001 event by Foster (2004) indicates that at F-region heights a plume of storm enhanced density stretched continuously from the ionospheric projection of the dusk plasmapause to the dayside cusp. Separate calculations using observations from the Millstone Hill radar, DMSP overflights, and ground-based GPS total electron content (TEC) indicate that the Storm Enhanced Density (SED) plume carried a flux of $>10^{26}$ ions/s into the cusp ionosphere during the peak of the event. At magnetospheric heights, they calculated that the associated plasmasphere drainage plume transported a flux of $>10^{27}$ ions/s to the dayside magnetopause. For comparison, Elphic et al. (1997) have estimated the flux of plasmaspheric ions, which are injected into the magnetotail and convected up and over the polar cap during strong disturbances, to be $\sim 10^{26}$ ions/s.

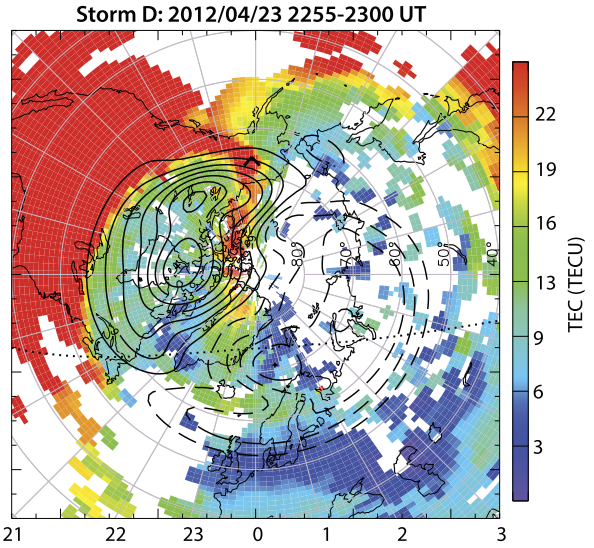

Fig. 16 An example of an SED plume traversing from the duskside ionosphere over the pole (*colored contours*). Units are total electron content unit (TECU), where 1 TECU $= 10^{16}$ e/m^2. *Black solid/dashed lines* are contours of electric potential as observed via radar. From Zou et al. (2014)

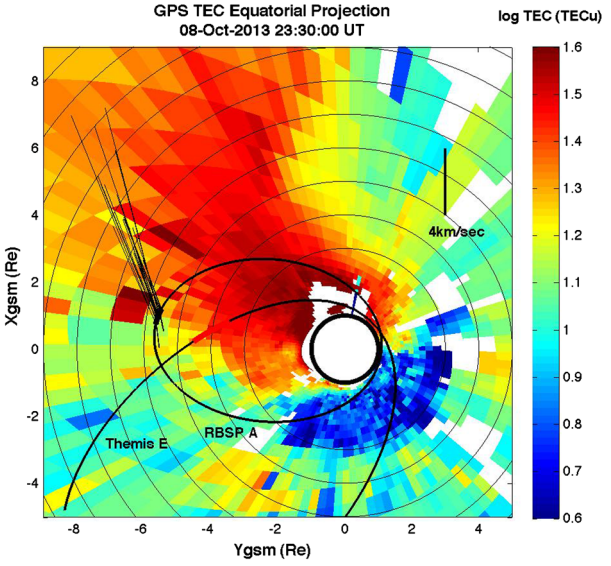

Fig. 17 Plasmasphere erosion plume on October 8, 2013 (GPS TEC mapped to GSM equatorial plane with the sun at the *top*). Orbits of the Van Allen Probes RBSP-A and Themis E are shown. 10 km/s sunward velocity (*vectors* shown) was observed along the outer portion of the plume. From Foster et al. (2014a)

Foster et al. (2014b) investigated geospace cold plasma redistribution combining GPS TEC and incoherent scatter radar ionospheric observations with in situ data in the outer plasmasphere from the Van Allen Probes spacecraft and in the topside ionospheric heights with DMSP. For a moderately disturbed event, they estimate the total fluence of eroded ionospheric/plasmaspheric ions carried antisunward at polar latitudes in the TOI channel to be $\sim 5 \times 10^{25}$ ions/s. A similar calculation of the ion fluence in the SED/erosion plume that carries the eroded plasmasphere material toward the cusp found the sunward fluence across a 5 degree span latitude to be $\sim 7 \times 10^{25}$ ions/s, which compares well with the 5×10^{25} ions/s antisunward fluence observed at that time in the TOI.

Using ground-based TEC maps and measurements from the THEMIS spacecraft, Walsh et al. (2014) investigated simultaneous, magnetically interconnected ionosphere—magnetosphere observations of the plasmaspheric plume and its involvement in unsteady magnetic reconnection. The observations show the full circulation pattern of the plasmaspheric plume and validate the connection between signatures of variability in the dense plume and reconnection at the magnetopause as measured in-situ and through TEC measurements in the ionosphere. The location of THEMIS at the reconnecting magnetopause mapped to the point in the ionosphere, where the TOI is formed, and enhancements in TEC stream tailward over the pole on open field lines. That study confirmed that the formation of the TOI in the ionosphere is spatially linked to the presence of the plume and reconnection at the magnetopause. The dense plasma on newly opened magnetic field lines convected tailward over the pole as observed in the motion of TOI patches in the ionosphere and in-situ at the magnetopause. Foster et al. (2014a) observed such plume/TOI plasma at 5.5 R_E in the midnight sector and its role in substorm injection and particle acceleration to energetic (∼100 keV) and highly relativistic (∼5 MeV) energies. These multi-instrument observational studies demonstrate the extent of plasmaspheric recirculation through the magnetosphere and the effect it has on global dynamics.

Are plasmaspheric plumes the only mode for plasmaspheric material release to the magnetosphere? As indicated above, plasmaspheric plumes are associated with active periods and with fluctuations of the convective large-scale electric field, governed by solar wind conditions. In 1992, however, an additional way for plasmaspheric material release to the magnetosphere was proposed: the existence of a plasmaspheric wind, steadily transporting cold plasmaspheric plasma outwards across the geomagnetic field lines, even during prolonged periods of quiet geomagnetic conditions (Lemaire and Schunk 1992). This wind is expected to be a slow radial flow pattern, providing a continual loss of plasma from the plasmasphere, for all local times and for $L > \sim 2$. It is thus similar, but on a completely different scale, to that of the subsonic expansion of the equatorial solar corona.

The existence of this wind has been proposed on a theoretical basis: it is considered to be the result of plasma interchange motion driven by an imbalance between gravitational, centrifugal, and pressure gradient forces (André and Lemaire 2006; Pierrard et al. 2009). Such a radial plasma transport implies that the plasma streamlines are not closed, and therefore the cold plasma elements slowly drift outward from the inner plasmasphere to the plasmapause, along wound up spiral drift paths. Figure 18 shows the displacements of the plasma elements (the blue × symbols) from their initial positions, i.e. the black dots initially aligned along the dipole magnetic field lines, which are represented by the solid lines. The innermost arc of blue × symbols was thus initially along the innermost magnetic field solid line shown in Fig. 18 (see Pierrard et al. 2009). As shown in this figure, this outward radial transport effect is strongest at the geomagnetic equator.

Indirect evidence suggesting the presence of a plasmaspheric wind has been provided from the plasma refilling timing. Following the erosion of the plasmasphere after a severe geomagnetic storm, the plasma refilling time at $L > 3$ can be 4 days or even as long as 8 days (Park 1970; Banks et al. 1971; Kotova 2007; Obana et al. 2010). Considering a simple refilling scenario, with an ionization flux varying with time as the equatorial density increases, Lemaire and Schunk (1992) estimated the equatorial densities in drifting and refilling flux tubes and noted that a flux tube located at $R = 4$ R_E would take only 2.5 days to completely refill and reach a state of diffusive equilibrium. This refilling timing difference, between calculated and observed times, suggests a continuous plasma leak from the plasmasphere, even during quiet conditions, consistent with the plasmaspheric wind. Evidence for such a continuous plasma leak, outside the plasmapause, has been also provided by global EUV

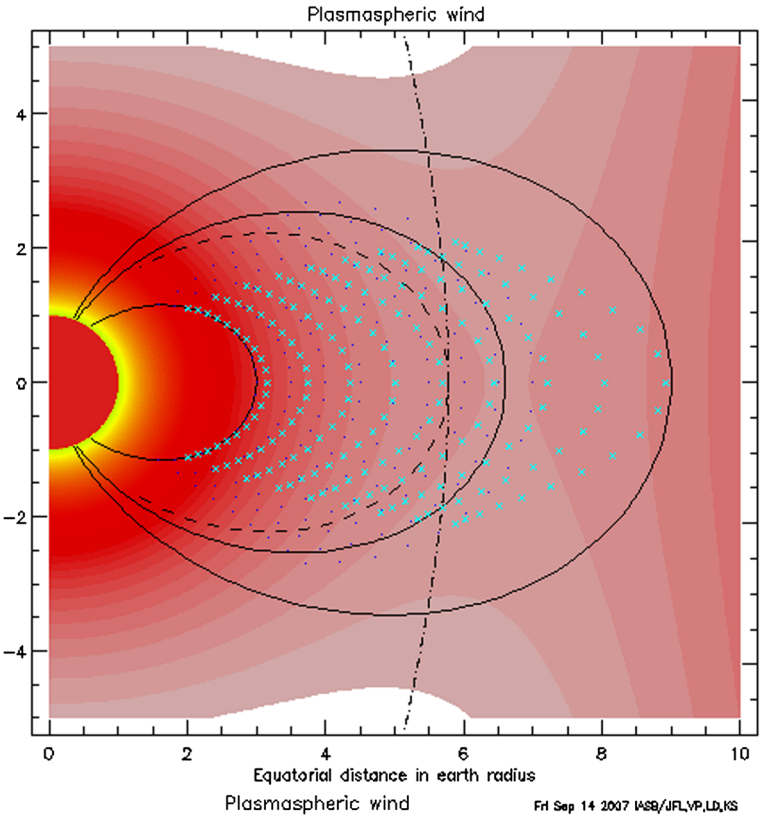

Fig. 18 Plasmaspheric wind formation simulation, as the result from a plasma interchange motion driven by an imbalance between gravitational, centrifugal and pressure gradient forces. It shows the displacements of the plasma elements (the *blue* × symbols) from their initial positions, i.e. the *black dots* initially aligned along the dipole magnetic field lines which are represented by the *solid lines* (Pierrard et al. 2009). Courtesy of Joseph F. Lemaire, Nicolas André and Viviane Pierrard, from a numerical simulation available at http://plasmasphere.aeronomie.be/plasmaspherewindsimulation.html

imaging of the plasmasphere (Yoshikawa 2003). Indirect evidence for the plasmaspheric wind has been also provided from the smooth density transitions from the plasmasphere to the subauroral region, observed during quiet conditions and at various magnetic local times (Tu et al. 2007).

Experimental direct evidence for the plasmaspheric wind has been provided recently (Dandouras 2013) based on the analysis of the ion distribution functions, acquired in the outer plasmasphere by the Cluster Ion Spectrometry (CIS) experiment onboard the Cluster spacecraft. As shown in the example presented in Fig. 19, the ion distribution functions obtained close to the magnetic equator reveal an imbalance between the outward and inward moving ions, both for H^+ and for He^+ ions, corresponding to a net outward flow. This outflow has been observed during all quiet or moderately active magnetospheric conditions events analysed, in all MLT sectors, and is consistent with the plasmaspheric wind proposed on a theoretical basis by Lemaire and Schunk (1992). Calculations show that the observed radial outflow corresponds to a 5×10^{26} ions/s plasma loss rate from the plasmasphere, which at the same time constitutes a cold plasma supply to the outer magnetosphere.

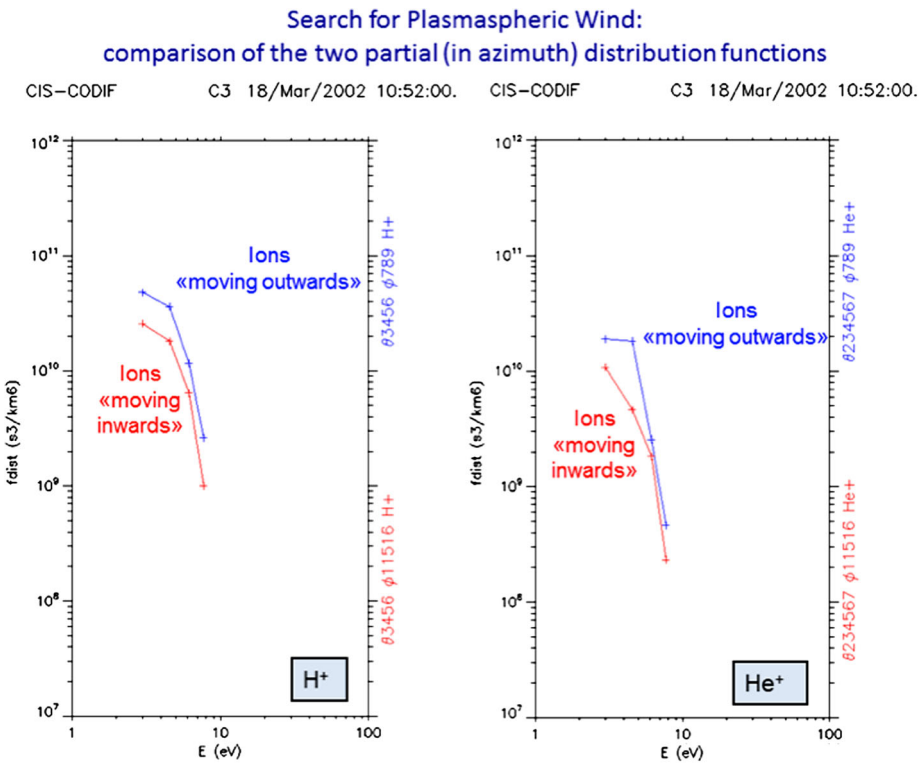

Fig. 19 Partial distribution functions in the outer plasmasphere and close to the magnetic equator, corresponding to ions flowing radially outwards (*blue plots*) and to ions flowing radially inwards (*red plots*). *Left panel* is for H^+ ions and *right panel* is for He^+ ions. Ordinate axis is in phase space density units (ions s^3 km^{-6}). The systematic imbalance between the outwards and inwards propagating ions reveals a net outward flow. From Dandouras (2013)

These plasmaspheric transport mechanisms, i.e., plumes (localised plasma releases, mainly during active periods) and the plasmaspheric wind (continuous outflow, even during prolonged periods of quiet geomagnetic conditions), appear to contribute strongly to other magnetospheric regions. The solar wind source is of the order of 10^{27} ions/s and the high-latitude ionospheric source is of the order of 10^{26} ions/s, varying by a factor of ∼3, as a function of the activity level and particularly dependent on the IMF orientation (Moore 2005; Haaland et al. 2009; Li et al. 2012). It appears thus that plasmaspheric recirculation constitutes a substantial plasma source for the outer magnetosphere and cusp, and it is comparable to the other sources as the solar wind and the high-latitude ionosphere.

3.3 Solar Plasma Transport

Particles originating from the solar wind can enter the open field line region of the magnetosphere (the lobes) through upward flow out of the cusp or via reconnection just tailward of the cusp. The plasma entering the lobes is called the mantle plasma. The mantle plasma is magnetosheath-like with reduced density and velocity. The mantle plasma is relatively much denser and colder than the plasma sheet plasma and with substantial tailward field-aligned bulk flow. The mantle plasma spreads across the full width of the lobes and reaches the

plasma sheet via $E \times B$ drift under the influence of the dawn-to-dusk magnetospheric electric field (Pilipp and Morfill 1978). Conversely, as the solar wind gains access to dayside and terminator regions of the magnetosphere at low latitudes, it forms the Low Latitude Boundary Layer (LLBL). This is a region of northward, closed magnetic flux just inside the magnetopause on the dawn and dusk sides of the magnetotail (Fairfield 1979; Slavin et al. 1985; Kaymaz et al. 1994). Understanding the transport of mantle and LLBL plasma to the plasma sheet and inner magnetosphere is critical for determining the influence of the solar plasma source on magnetospheric dynamics.

Indication of the existence of the mantle plasma was first reported by Hones et al. (1972) and was later confirmed and termed "plasma mantle" by Rosenbauer et al. (1975). The mantle plasma can be seen in the near-Earth region (Haerendel and Paschmann 1975; Taguchi et al. 2001), at the lunar distance (Hardy et al. 1975; Wang et al. 2014), and in the distant tail (Gosling et al. 1984; Slavin et al. 1985; Maezawa and Hori 1998). The plasma mantle is confined to high latitudes closer to the Earth, but spreads to lower latitudes farther down stream as the mantle plasma $E \times B$ drifts down to the plasma sheet (Slavin et al. 1985; Siscoe and Kaymaz 1999).

Two main sources have been suggested for the mantle plasma. For the cusp source, plasma enters the cusp first and then mirror back to nightside high latitude tail. For the magnetopause source, plasma can enter the lobe through open field lines at any downtail location of the magnetopause. From the MHD point of view (Siscoe and Sanchez 1987; Siscoe et al. 2001) mantle plasma can be described as a slow-mode expansion fan of the plasma from the magnetosheath entering through merging lines along the magnetopause. The mantle source is often found to be mixed with plasma from the ionosphere (Seki et al. 1996).

As the mantle plasma flows tailward along the magnetic field lines, it $E \times B$ drifts toward the equator, thus providing particles into the tail plasma sheet (Speiser 1968; Sckopke et al. 1976). The mantle plasma at low latitudes is often found to be adjacent to the plasma sheet and is often mixed with plasma from the plasma sheet boundary layer (PSBL) and plasma sheet (Akinrimisi et al. 1989; Maezawa and Hori 1998). The particle supply depends on the spatial distribution of the mantle plasma. Pilipp and Morfill (1978) theoretically predicted the cross-magnetosphere and down-tail profiles for the mantle plasma resulting from the parallel and perpendicular transport of particles coming from either the cusp or magnetopause source. The model predicted quite different cross-tail profiles corresponding to the source. With the magnetopause source, density, temperature, and bulk velocity are the highest at the magnetopause and decrease with increasing distance away from the magnetopause, while with the cusp source there are almost no cross-tail variations at large downtail distances.

Once the mantle particles reach low-latitudes and become incorporated into the plasma sheet through tail reconnection, they are either transported Earthward in Bursty Bulk Flows (BBFs) (Baumjohann et al. 1990; Angelopoulos et al. 1992) or lost to flow down the tail where they will eventually join the solar wind. Therefore, the location of the reconnection X-lines, from which the earthward and tailward flows emanate, regulates the transport and fate of mantle plasma. At substorm onset, these X-lines form closer to the Earth, $X \sim -20$ to 30 R_E, and they are termed the "near-Earth neutral line" (NENL) (Nagai 2005; Imber et al. 2011). In fact, the frequent observations of flux ropes in this region with diameters of several Earth radii suggests the simultaneous existence of multiple X-lines near the time of onset (Slavin et al. 2003), complicating mantle transport. Observations in the distant magnetotail have shown the persistent presence of a "distant neutral line" (DNL) at $\sim X = -120$ to -140 R_E (Zwickl et al. 1984; Slavin et al. 1985). Earthward of the DNL,

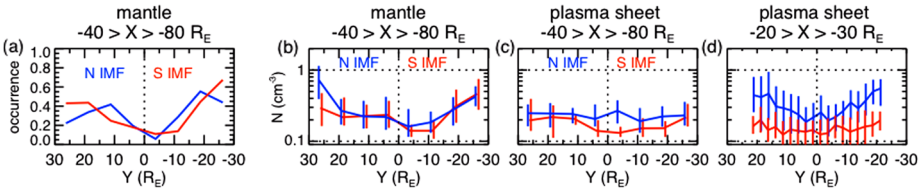

Fig. 20 The occurrence rates (**a**) and density (**b**) for the mantle plasma observed by ARTEMIS. The ion number density for the plasma sheet at $X < -40\,R_E$ observed by ARTEMIS (**c**) and at $X > -30\,R_E$ observed by Geotail (**d**). The *blue* (*red*) *curves* show the profiles corresponding to the 4-hr averaged IMF $B_Z > 0$ (<0). The *curves* indicate median values and *vertical lines* indicate the 25 % and 75 % quartiles. Adapted from Wang et al. (2014)

the plasma sheet flow is sunward except during the expansion phase of substorms when fast flows carry flux ropes, also called plasmoids, tailward. It is unclear whether the DNL is a single stable reconnection X-line or the statistical aggregation of the tailward retreating NENLs from successive substorms (Slavin et al. 1987). Plasma mantle particles reaching the plasma sheet beyond the DNL are all lost down the tail at all times.

The mantle occurrence rate is higher and mantle thickness (the distance from the magnetopause) is larger during southward IMF than northward IMF (Paschmann et al. 1976; Sckopke et al. 1976). The mantle plasma at the lunar distance (60 R_E) has been studied using the instruments on the surface of the moon (Hardy et al. 1975, 1976, 1979). Their results showed that mantle plasma can appear at all Y, but with lower occurrence rate at smaller $|Y|$. The occurrence has a strong dawn-dusk asymmetry depending on the IMF B_Y direction (Hardy et al. 1975; Gosling et al. 1984).

Figure 20 shows the occurrence rates and plasma density for the mantle plasma as a function of Y under north and southward IMF in the magnetotail from $X = -40$ to $-80\,R_E$, observed by the two ARTEMIS spacecraft from August 2010 to December 2012 (Wang et al. 2014). Both the occurrence rates and densities are highest near the flanks and decrease with decreasing $|Y|$, suggesting that the particle supply to the plasma sheet becomes smaller at smaller $|Y|$. There are no significant differences in these cross-tail profiles between north and south IMF conditions, suggesting that the particle supply is independent of the IMF B_Z direction. Figures 20(c) and 20(d) show the plasma sheet density in the tail ($-40 > X > -80\,R_E$) and in the near-Earth tail ($-20 > X > -30\,R_E$) respectively. The magnitude of the plasma sheet density is slightly less than the mantle density during southward IMF. However, during northward IMF the density in the tail at smaller $|Y|$ and in the near-Earth tail is substantially higher than during south IMF. The comparisons suggest that during southward IMF the mantle plasma supply is likely important to the plasma sheet, while during northward IMF cross-tail transport may be needed to bring particles from the flanks toward midnight.

The plasma sheet gradually becomes colder and denser as northward IMF proceeds (Terasawa et al. 1997; Øieroset 2005; Wing et al. 2005, 2006; Wang et al. 2010). The cold-dense plasma is often a mixture of one cool and one warm population (Wang et al. 2012). The cool population can be seen extending from the flanks to midnight during prolonged northward IMF. Both the particle supplies from the low-latitude boundary layer (LLBL) and plasma mantles are strongest near the flanks, thus insufficient to account for the increase of cool particles deep inside the magnetosphere. Therefore, there are likely cross-tail transport processes allowing the cold particles to have access from the flanks to midnight. The gradual increase of cool population during northward IMF suggests that the cross-tail transport is a slow process.

Analysis of transport paths shows that $E \times B$ drift delivers particles toward the earth and the flanks, and thus cannot bring the flank source particles across the tail to midnight (Wang et al. 2007, 2009). Magnetic drift can bring particles from the dawn flank into the midnight plasma sheet (Spence and Kivelson 1993; Wang 2004), however, magnetic drift is too small to move cold particles into the plasma sheet from the dawn flank. Despite that, large-scale $E \times B$ drift transport particles mainly earthward and toward the flanks when closer to the Earth (due to shielding of the convection $E \times B$ field), the plasma sheet flow is constantly fluctuating in both its magnitude and direction even during quiet times (Angelopoulos et al. 1993). The magnitudes of flow fluctuation are significantly larger than the average flow speed. Ionospheric velocity measurements inferred from the SuperDARN radar also suggest that even under steady driven conditions, there are significant ionospheric velocity fluctuations (Bristow 2008). The convection velocity fluctuations are also observed in the lobes by Cluster (Förster et al. 2007).

The flow fluctuation can result in diffusive particle transport if the particle number density has a spatial gradient. It has been proposed (Terasawa et al. 1997; Antonova 2005; Borovsky 2003; Weygand 2005) that diffusion may transport cold particles from the flanks deep into the plasma sheet. The diffusion coefficient associated with flow fluctuations in the plasma sheet has been estimated (Borovsky et al. 1997, 1998; Ovchinnikov et al. 2000; Nagata et al. 2007; Stepanova et al. 2011).

Efficiency of diffusive transport of particles depends on both the distributions of the diffusion coefficients and particle spatial gradients. To evaluate whether diffusion is capable of bringing particles across the tail within the typical observed time scale, (Wang et al. 2010) estimated diffusion coefficients associated with turbulent flows from Geotail observations. They performed a simulation of density evolution due to diffusive and drift transport of particles with the sources at the flanks. In the simulation, the flank sources, drift velocities, and diffusion coefficient are IMF and time-dependent and are established using Geotail data. The simulation results show that diffusive transport due to turbulence can move cold particles from the flank to the midnight meridian during northward IMF to form cold dense plasma sheet with density increase rates consistent with the statistical Geotail results.

However, using the THEMIS observations, Stepanova et al. (2011) showed that diffusion coefficients decrease quickly with decreasing distances from the Earth. This suggests that diffusive transport may become too weak to account for the formation of cold-dense plasma sheet in the near-Earth region ($r < \sim 15\ \mathrm{R}_E$). It has been suggested that interchange motion may be another transport mechanism (Johnson and Wing 2009). The reconnection within a rolled-up K–H vortex should create cold-dense plasma with relatively lower- entropy (i.e., the entropy parameter, $PV^{5/3}$, where P is plasma pressure and V is flux tube volume per unit magnetic flux) than the surrounding hot plasma sheet plasma. This can lead to interchange instability that transports the cold plasma inward. Wang et al. (2014) used the Rice Convection Model (RCM) to simulate the evolution of colder, denser, and lower-entropy ions and electrons that are presumably created locally along the flanks by the Kelvin–Helmholtz vortices and subsequent reconnection. The RCM simulation quantitatively reproduces many prominent features of the formation of cold-dense plasma sheet simultaneously observed by five THEMIS probes near and away from the flank, indicating that interchange motion is a plausible inward transport mechanism for cold particles in the near-Earth plasma sheet.

3.4 Substorm Acceleration

A notable feature of the expansion phase of substorms in the inner terrestrial magnetosphere is the relaxation of magnetic field lines from a stretched configuration to a more dipolar one.

During such events, a variety of in situ measurements reveal that heavy ions (O^+) may be subjected to prominent energization up to the hundred of keV range (Ipavich et al. 1984; Möbius et al. 1986; Nosé et al. 2000). In a number of instances, this effect seems to depend upon mass-to-charge ratio since no similar energization is noticeable for protons. As an example, the observations of energetic neutral atoms reported by Mitchell et al. (2003) show evidence of energetic O^+ injections in conjunction with auroral break-ups, but no significant change in the energetic proton flux. Some energization process thus appears to be at work during such events that preferentially affects O^+ as compared to H^+. A possible mechanism to explain this mass selective ion energization is an impulsive energization under the effect of the electric field, induced by the magnetic field line relaxation.

Indeed, as magnetic field lines rapidly evolve from tail-like to dipole-like configurations, the electric field induced by the magnetic transition is responsible for a convection surge that rapidly injects particles into the inner magnetosphere (Mauk 1986). If the time scale of this reconfiguration is large compared to the gyroperiod of the particles, their magnetic moment (first adiabatic invariant) is conserved and the adiabatic (guiding center) approximation is valid. In contrast, if the time scale of the reconfiguration is comparable to (or smaller than) the particle gyroperiod, the magnetic field varies significantly within a cyclotron turn, the guiding center approximation is not valid, and the particle magnetic moment may not be conserved during transport. This temporal nonadiabaticity (i.e., due to explicit time variations of the magnetic field) differs from spatial nonadiabaticity (i.e., due to field variations on the length scale of the particle Larmor radius like in the magnetotail current sheet) and it may actually occur in regions of the magnetotail where the ion motion would otherwise be adiabatic (i.e., $\kappa > 3$, where κ is the adiabaticity parameter defined as the square root of the minimum curvature radius-to-maximum Larmor radius ratio). In the inner terrestrial magnetosphere, dipolarization of the magnetic fied lines typically occurs on a time scale of a few minutes, which is on the order of the cyclotron period of O^+ in this region of space. Accordingly, while protons may be transported in an adiabatic manner and experience betatron or Fermi-type energization, heavy ions may experience prominent nonadiabatic energization during such events (see Seki et al. 2015, for more detailed discussion of these processes).

Unlike the energy gain due to the large-scale convection electric field that is constrained by the magnitude of the cross-polar cap potential drop, there is no well defined limit for the energization that can be achieved from the induced electric field (Heikkila and Pellinen 1977; Pellinen and Heikkila 1978). As a matter of fact, single-particle trajectory calculations in model reconfigurations of the magnetic field lines reveal that O^+ energization up to the 100 keV range may readily be achieved in the inner magnetosphere (Delcourt et al. 1990). Since this energization occurs in a nonadiabatic manner and goes together with prominent enhancement of the magnetic moment, it radically changes the long-term behavior of the particles. This is illustrated in Fig. 21, from Delcourt (2002), which shows model O^+ trajectories in two distinct cases; steady state (top panels) and assuming a one-minute dipolarization of the field lines at some point during transport (bottom panels). In this figure, the test O^+ ion is considered to originate from the nightside auroral zone and it can be seen that, in steady state, this ion intercepts the mid-tail where it is subjected to magnetic moment scattering upon crossing of the field reversal. As a result, the O^+ subsequently bounces back and forth between high-altitude mirror points, while drifting westward. This ion is ultimately lost into the dusk magnetopause, the net energy gain realized being of the order of 20 keV. In the bottom panels of Fig. 21, a drastically different behavior can be seen as a result of substorm dipolarization. The magnetic field line reconfiguration is here assumed to occur 40 minutes after ejection of the test O^+ from the topside ionosphere and it is apparent that, as a result of this reconfiguration, the ion is rapidly transported from the mid-tail down

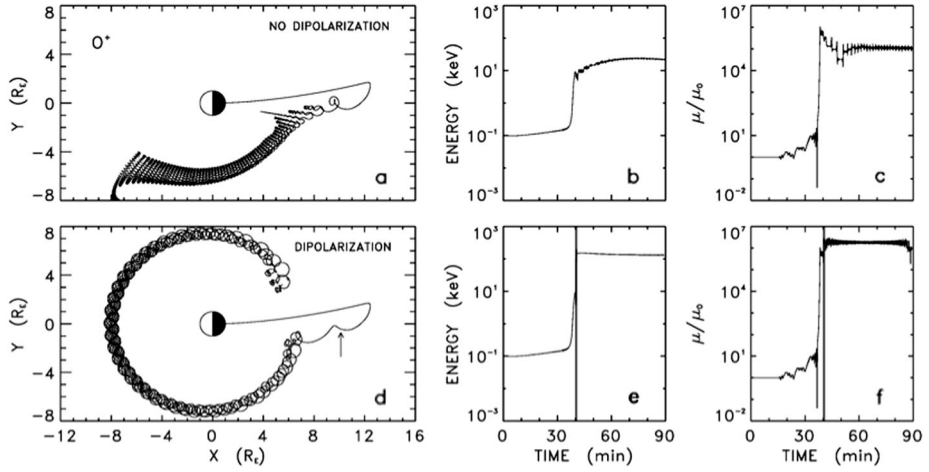

Fig. 21 Trajectories of test O^+ launched from the nightside auroral zone (0000 MLT) with an initial energy of 100 eV and considering either (*top panels*) steady state or (*bottom panels*) 1-min dipolarization during transport. *Left panels* show the trajectory projection in the X-Y plane, whereas center and *right panels* show the kinetic energy and magnetic moment (normalized to the initial value) versus time, respectively. In the *bottom panels*, dipolarization occurs after 40-min time-of-flight (*shaded area* in (**e**) and (**f**)). The *arrow* in (**d**) indicates the O^+ position at the dipolarization onset. From Delcourt (2002)

to the geosynchronous vicinity. During this convection surge, the O^+ experiences a prominent energization that exceeds 100 keV. The nonadiabatic character of this energization is apparent from the rightmost panel that shows further magnetic moment enhancement on the time scale of the dipolarization. Given this large post-dipolarization energy realized, the O^+ motion subsequently is dominated by gradient drift around the planet and, instead of being lost at the magnetopause (top panels), it rapidly encircles the Earth with a drift period of about 50 minutes. It is clearly apparent from Fig. 21 that a short-lived convection surge with prominent nonadiabatic energization is an efficient process to populate the outer ring current with heavy ions of ionospheric origin.

However, a more recent statistical analysis of all the substorm events from 10 years of Geotail data (Ono et al. 2009) indicated that while the greater enhancement of O^+ over H^+ was observed over the energy range 9–36 keV, at higher energies the picture was more mixed. Some events showed the O^+ spectrum becoming harder than H^+, as had been reported before, but other events showed the H^+ spectrum becoming harder than O^+. To explain the new observations, Ono et al. (2009) have suggested that the acceleration is due to the magnetic field fluctuations during the dipolarization, not due to the dipolarization itself. They found that the biggest increases did not occur when the time scales of the dipolarization and the gyrofrequencies were matched. Instead, it was found that the most significant acceleration occurred when the power in the shorter time scale fluctuations was close to the ion gyrofrequencies. In some cases, this power favored the O^+, but in other cases it favored the H^+. Nosé et al. (2014) examined magnetic fluctuations that occurred during dipolarization for 7 events inside geosynchronous orbit. They modeled the ion acceleration in the electromagnetic fields, and found that the O^+ was accelerated in the energy 0.5–5 keV by these fluctuations, while the H^+ was not significantly affected, consistent with the observations. In light of the Delcourt (2002) work, and these recent simulations, it seems likely that both the dipolarization itself, and the smaller scale fluctuations associated with it play a role in the ion acceleration.

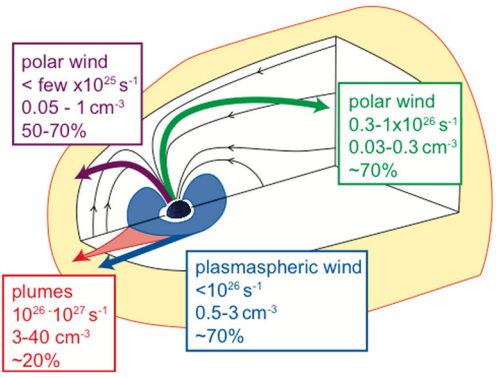

Fig. 22 Estimations of low energy particle densities from André and Cully (2012)

4 Consequences

The immediate and inescapable consequence of the various sources of plasma in the terrestrial system is mass and energy loading of different regions of the magnetosphere, chronicled in detail by Hultqvist et al. (1999). Since the book's release, subsequent work has been driven by a growing awareness of the magnitude of the ionospheric source of light and heavy ions and the potential effects this population has on a vast number of magnetospheric regions. Low-energy ions of ionospheric origin with energies below tens of eV dominate most of the volume of the terrestrial magnetosphere at least 50–70 % of the time. Orders of magnitude estimates for low-energy ion density, outflow and the percentage of time these ions dominate the density are given in Fig. 22 (André and Cully 2012). The nightside outflow is often dominated by low-energy ions. The H^+ outflow is estimated to be about 10^{26} ions/s (Engwall et al. 2009a), which is larger than the previously observed energetic outflow at high altitudes, and consistent with observations at low altitudes (Peterson et al. 2008). On the dayside, the outflow of low-energy ions is very variable. When plasmaspheric plumes are not present, the outflow is typically a few times 10^{26} ions/s, while in plumes (occurring about 20 % of the time) the outflow can be up to 10^{27} ions/s. New results show that low-energy ions can dominate 50–70 % of the time just inside the magnetopause, even when there are no plasmaspheric plumes (André and Cully 2012). The large amount of low-energy plasma detected puts strong limits on heating and acceleration mechanisms. The low-energy plasma will also lower the Alfvén velocity and the dayside reconnection rate, and will also change the micro-physics of the reconnection separatrix region (André et al. 2010). Indeed, a recent review is dedicated to the role of heavy ion outflow in global dynamics (Kronberg et al. 2014). These effects create a new paradigm in which solar wind control of magnetospheric dynamics must compete with internal feedback from ionospheric mass.

A clear example of this is the potential of the plasmasphere population to affect dayside reconnection rates. Borovsky and Steinberg (2006), as part of a larger study of magnetospheric preconditioning before Corotating Interacting Region (CIR) driven storms, initially suggested the possibility of magnetopause mass loading via plasmaspheric plumes. Borovsky and Denton (2008) provided empirical evidence of this effect by examining the AU, AL, and Polar Cap Index (PCI) activity indices. They found that, for a given solar wind electric field ($-vB_Z$), all three indices were statistically lower during periods when a plume was observed at geosynchronous locations versus periods when no plume was observed. Subsequently, this effect was shown to manifest in global, resistive MHD models (Borovsky et al. 2008). Reconnection electric field about the magnetopause was calculated using the

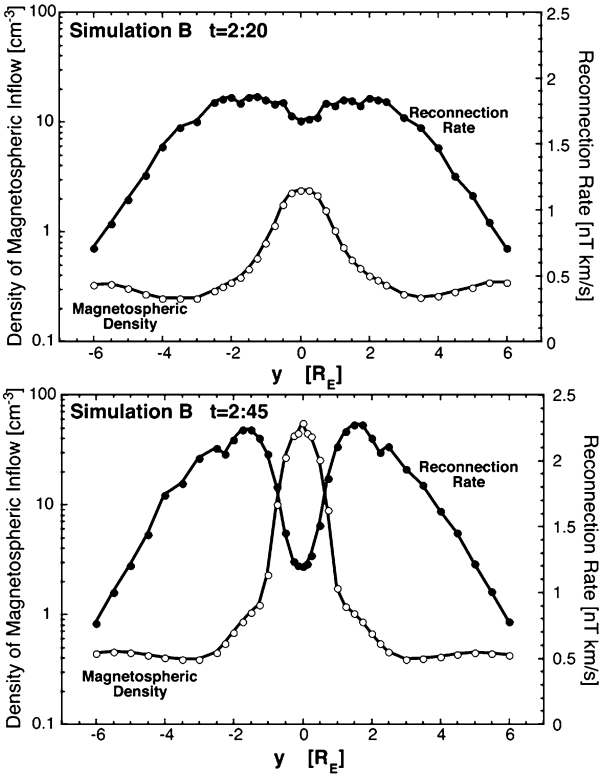

Fig. 23 Reconnection rate and magnetospheric density about the dayside magnetopause before a plasmaspheric plume arrives at the subsolar point (*top frame*) and after (*bottom frame*). From Borovsky and Denton (2008)

formula derived by Cassak and Shay (2007). Figure 23 shows the reconnection electric field (black dotted line) and density along the magnetopause (white dotted line) as a function of distance along the dayside magnetopause, both before (top frame) and after (bottom frame) plume arrival. Once the plume arrives, the local reconnection rate drops dramatically, yielding an overall reduced reconnection rate. Early THEMIS observations used a combination of techniques to obtain cold plasma densities near the magnetopause (McFadden et al. 2008), establishing plume presence in the region. Further observational work has connected in-situ observations of plume arrival at the magnetopause with the onset of bursty reconnection (Walsh et al. 2014). This connection still requires further investigation; indeed, it has been suggested that any plasmasphere impact on the magnetopause would be local and that the magnetosphere shape would adjust to compensate for the mass loading effect (Lopez et al. 2010).

Because the plasmasphere dominates the mass content of the inner magnetosphere, it therefore plays an essential role in governing the radiation belt dynamics (Horne and Thorne 1998; Thorne 2010; Chen et al. 2012). During prolonged geomagnetically quiet periods the plasmapause coincides mostly with the outer edge of the outer radiation belt of energetic electrons (>2 MeV). However, during higher geomagnetic activity time periods, the plasmapause is located closer to the inner boundary of the outer radiation belt (Darrouzet et al. 2013).

The inclusion of the high-latitude ionospheric plasma source in global models has resulted in a set of surprising large-scale effects (recently reviewed in detail by Wiltberger 2015). Initially, global fluid models relied on simple inner boundary conditions (i.e., uni-

form mass density) to passively include this source (e.g., Winglee 1998; Walker et al. 2003; Zhang et al. 2007). Though simple, this outflow specification can form time and space dependent outflows into the magnetosphere (Welling and Liemohn 2014) and dominate the central plasma sheet (Welling and Ridley 2010). Winglee (2002) found that if a heavy ion component was included in a simple, passive outflow source, the modeled cross polar cap potential was reduced significantly compared to an identical simulation that used an all-hydrogen inner boundary. Similar results were obtained when more realistic outflow specifications were applied. Glocer et al. (2009a, 2009b) and Welling et al. (2011), using a first-principles-based outflow model to drive heavy and light ion, polar-wind-like outflow in global MHD, found a similar reduction in CPCP. Brambles et al. (2010) used an empirical formula (Strangeway et al. 2005) that drove outflow of O^+ as a function of joule heating and AC Poynting flux calculated by the Lyon–Fedder–Mobarry model. It was found that the CPCP reduction was produced if the outflow was slow and dense. Though each study provides a unique hypothesis as to why such an effect manifests, not one has been verified to date (Welling and Zaharia 2012).

Other global simulations continue to show that global dynamics dependend on ionospheric outflow. Because the ring current can be fed significant mass from ionospheric sources (Welling and Ridley 2010; Welling et al. 2011), magnetospheric shape appears beholden to the strength of the ionospheric source (Brambles et al. 2010; Garcia et al. 2010). The source location, density, and outflow velocity all appear to be factors in driving this affect (Garcia et al. 2010). Yu and Ridley (2013) noted that as heavy ion outflow populations arrive at the plasma sheet, they can affect the location of reconnection. More dramatically, heavy ion populations that arrive near the magnetic X-line can alter reconnection rates enough to trigger a magnetospheric substorm (Wiltberger et al. 2010; Winglee and Harnett 2011). When causal outflow (i.e., outflow that is a function of magnetospheric dynamics) is employed for periods of strong driving, outflow-triggered substorms can drive additional heavy ion outflows, triggering further substorms (Brambles et al. 2011, 2013; Ouellette et al. 2013). These periodic substorms resemble global sawteeth oscillations (Huang 2003; Henderson 2004), a mode of magnetospheric activity previously unachievable with ideal MHD. A statistical investigation of the O^+/H^+ ratio during sawteeth, substorm, and non-substorm storm periods by Liao et al. (2014) suggests that heavy ion outflow plays a role in sawteeth triggering, but that high O^+ concentrations are neither a necessary or sufficient condition. All of these studies support the view that ionospheric outflow is an integral part in magnetosphere-ionosphere coupling.

5 Losses

5.1 Charge Exchange

In the inner magnetosphere, charge exchange of ions with the neutral hydrogen geocorona is a slow but persistent loss process. The charge exchange cross sections depend on species and energy, so the effects of charge exchange can be clearly identified by the associated composition changes. Kistler et al. (1998) showed an example from the FAST satellite in which the composition of the plasma sheet population changed from a hydrogen dominated population to a helium dominated population as the spacecraft moved into the inner magnetosphere. Comparison with simulations showed that this was expected because of the shorter charge exchange lifetime of H^+ at these energies (1–10 keV). Hamilton et al. (1988) examined the role of charge exchange in explaining the two-phase decay that is often observed

for very large storms. They found that the fast initial decay is consistent with the charge exchange lifetime of the energetic (75–100 keV) O^+ that dominated the main phase ring current. Many examples comparing modeled ring current spectra with observations (e.g. Kistler et al. 1989, 1999; Jordanova et al. 1996, 2001) have shown the importance of charge exchange in explaining the composition changes in the energy ranges where the ion drifts are slow and go deep into the inner magnetosphere.

5.2 Advective Loss

At times of enhanced convection, the outflow of ring current ions on open drift paths to the dayside magnetopause dictates the decay of ring current (Takahashi et al. 1990; Ebihara and Ejiri 1998; Liemohn et al. 1999) and the dawn-dusk component of the solar wind electric field is the parameter that sets up the time scale for ion loss. Also, the energy of the particle along with the timescale of recovery of the cross polar cap potential controls the amount of plasma trapped on the closed field lines (Takahashi et al. 1990).

Due to the long duration of a geomagnetic storm, the particles that are injected on the nightside are able to drift completely through the inner magnetosphere. This energy and convection dependent drift can move the energetic particles from the nightside to the magnetopause in only few hours. The dayside outflow usually takes place during the main and early recovery phase of a storm (Takahashi et al. 1990; Liemohn et al. 1999, 2001; Kozyra 2002), when the ring current is highly asymmetric and most of its energy is flowing along open drift paths (Liemohn et al. 2001; Kozyra 2002). The formation of the symmetric ring current is inhibited by these losses from convection to the dayside magnetopause (Liemohn et al. 1999).

Observations of energetic O^+ ions in the magnetosheath and upstream of the bow shock during times of elevated convection confirms not only the loss of ring current ions to the magnetopause (Möbius et al. 1986; Christon et al. 2000; Zong et al. 2001; Posner 2002), but it is estimated that the loss rate of O^+ ions to the magnetopause can be as high as 6.1×10^{23} ions/s (Zong et al. 2001).

Based on in-situ observations by Geotail/EPIC, Keika (2005) estimate that a minimum of 23 % of the total ring current fast decay is due to dayside ion outflow, even in the case of a sudden northward turning of the interplanetary magnetic field, which causes a sudden decrease in the convection electric field. However, increased convection will push particles closer to the Earth where charge exchange processes can contribute to the rapid decay of the ring current (Ilie et al. 2013). The spatial configuration of the open drift paths and how deep the particles penetrate into the inner magnetosphere determines whether charge exchange makes a significant contribution to the ring current losses as the ions drift through the inner magnetosphere to the dayside magnetopause region.

An example of a high convection event is presented in Fig. 24, from Kozyra and Liemohn (2003), clearly showing that the ion outflow losses dominate the main phase of the storm, while the charge exchange processes contribute significantly to the ring current decay during the recovery phase. The convection strength controls this loss process, i.e. increasing convection will increase the outflow loss and vice versa.

Particles of the same energy but with different pitch angle may follow different drift paths due to MLT-asymmetry of the magnetospheric electric field (Roederer and Schulz 1971) or magnetic field (Roederer 1967; Roederer et al. 1973), which is the so-called drift shell splitting. For high-energy ions dominated by magnetic drift, magnetic drift shell splitting is important. For example, Takahashi et al. (1997) showed that in a realistic magnetic field configuration (compressed on the dayside and stretched on the nightside) for particles of the

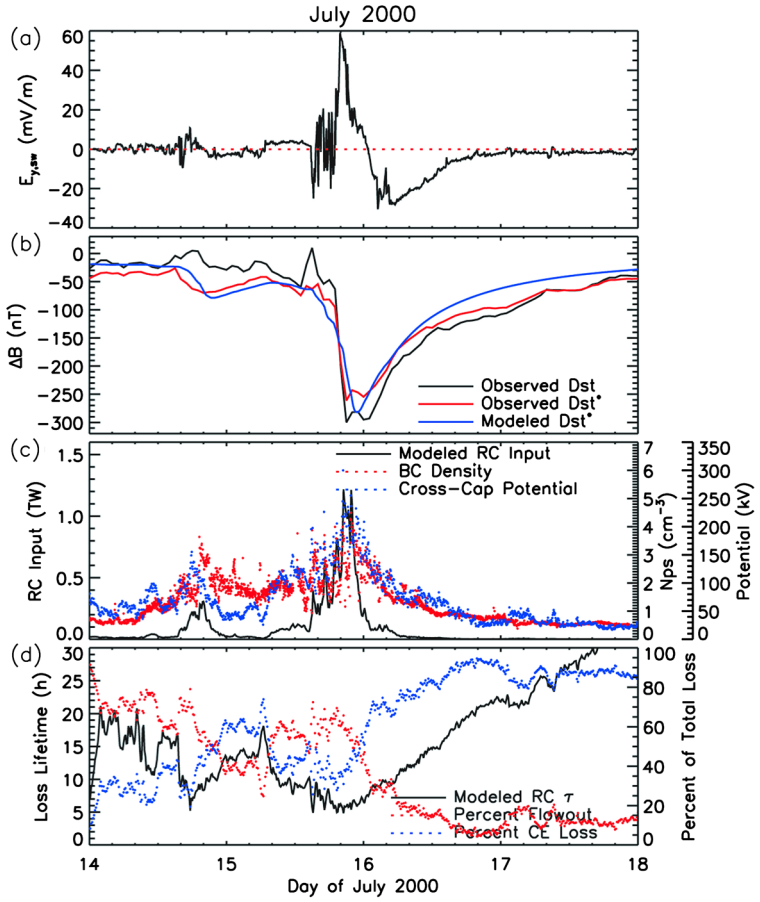

Fig. 24 Simulation results for the July 14, 2000 magnetic storm. *Top panel*: eastward component of the solar wind electric field (Ey, sw (mV/m)). *Second panel*: modeled Dsts nT (*blue line*), the observed Dst (*black line*) and observed Dsts (*red line*). *Third panel*: energy input through the nightside outer boundary ($L = 6.75$) of the model (*black line*), plasma density at geosynchronous orbit (*red dotted line*) and the cross polar cap potential (*blue dotted line*). *Bottom panel*: the globally-averaged loss lifetime for the ring current is presented in the *bottom panel* (*black line*) along with percentage of loss due to charge exchange (*blue dotted line*) and flow-out (*red dotted line*). From Kozyra and Liemohn (2003)

same energy at $r = r_0$ at noon, 90° ions come from $r < r_0$ at the midnight MLT while 30° ions come from $r > r_0$.

Given this magnetic drift shell splitting, 90° ions from the nightside at larger r are more likely to hit the duskside magnetopause than are ions of other pitch-angles. These particles are lost to the magnetopause and thus cannot complete the drift circle and return back to the nightside. As a result, there are relatively fewer ions near 90° than ions of other pitch-angles in the post-midnight sector. This process is known as magnetopause shadowing. Magnetopause shadowing produces butterfly pitch angle distributions (PADs) with negative anisotropy (more particles in the parallel than perpendicular directions) in the post-midnight sector (Sibeck et al. 1987; Fritz et al. 2003). Figure 25 shows the statistical spatial distributions of the pitch-angle anisotropy for 10, 20, 45, and 100 keV ions observed by THEMIS (Wang et al. 2012). It can be seen for ions above ~40 keV, anisotropy is negative is the

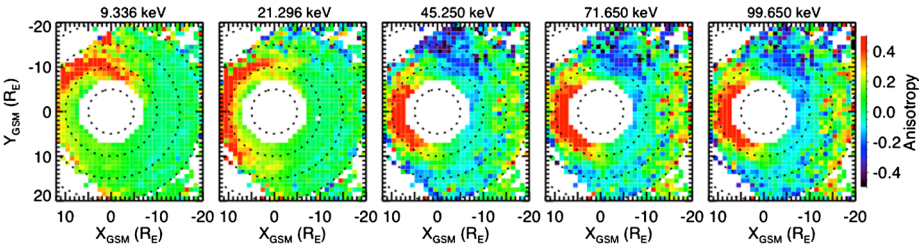

Fig. 25 Equatorial distributions of the ion pitch-angle anisotropy for different energies for $-5 > D_{ST} > -20$ nT. Anisotropy $= 0$ indicates an isotropic distribution. Anisotropy >0 (<0) indicates higher particle fluxes in the perpendicular (*parallel*) direction. Adapted from Wang et al. (2012)

post-midnight MLTs at $r \sim 10$–$15\ R_E$. The shape of pitch-angle distribution in the negative anisotropy region is dominantly a butterfly distribution. Thus the magnetopause shadowing is an important loss mechanism for high-energy ions with near 90° pitch-angle.

Opposite of magnetopause loss is plasma exhaust downtail, which has an estimated loss rate of 10^{28-29} ions/s (Hultqvist et al. 1999). Tailward flow is frequently punctuated by transients, such as plasmoids resulting from magnetospheric substorm events (see the recent reviews of McPherron 2015 and Eastwood and Kiehas 2015). New observations of these flows in the deep tail (Opitz et al. 2014) has been afforded by the Solar Terrestrial Relations Observatory (STEREO). During January through May of 2007, STEREO Ahead (STA) was 200–800 R_E upstream of the Earth and observing the undisturbed solar wind flow. Simultaneously, STEREO Behind (STB) was 200–800 R_E down stream of the Earth, passing in and out of the magnetotail. The Solar Electron Proton Telescopes (SEPT, Luhmann et al. 2007) on both STA and STB observed 110–2200 keV ion enhancements corresponding to corotating interacting region (CIR) events. During periods when STB was in the tail, the ion fluxes were both of higher magnitude and more anti-sunward aligned, indicating an additional magnetospheric source. Additionally, the enhanced STB-observed fluxes were impulsive in nature and correlated with increases in the Auroral Electrojet (AE) index, indicating a substorm source. These new observations confirm previous observations of escaping energetic magnetosphere populations and ties them to substorm activity.

5.3 Atmospheric Precipitation

Particles with a pitch angle contained in the so-called atmospheric loss-cone (i.e. with their mirror points located below the topside ionosphere) precipitate into the atmosphere and are lost from the magnetosphere. It is generally accepted that wave-particle interaction processes develop during magnetospheric transport and cause a persistent pitch-angle scattering into the loss cone. Electron cyclotron waves are known to cause pitch-angle scattering, but recent works show that whistler-mode chorus waves could play a dominant role (Ni et al. 2011a, 2011b). Plasmasheet particles are continuously lost during their transport from their injection in the tail on the night side until the plasmasheet inner edge and then until they reach the dayside. Diffuse aurorae develop at the ionospheric footprint of their magnetic field lines and form two belts permanently surrounding the magnetic North and South poles. The polar boundary of the auroral oval corresponds to the field-aligned mapping of the injection region in the distant tail on the night side and of the exit region near the magnetopause on the dayside. The equatorward boundary corresponds to the mapping the plasmasheet inner edge.

Discrete and intense auroral arcs appear at smaller scale inside the auroral oval mainly during disturbed magnetic conditions (see Frey 2007, for a review). They are brighter than diffuse aurorae and can be observed from the ground with different sizes, and shapes and fast motions. As diffuse aurorae, they are also caused by precipitating plasmasheet particles, but usually with higher energies. Acceleration processes develop under various conditions, during transient events in the plasmasheet, or depending on solar-wind magnetosphere interactions, or due to wave-particle interaction processes. As noticed quite some time ago by Akasofu (1964), the appearance of discrete auroral arcs is often related to disturbed conditions, as during substorms, impulsive events of great magnitude, responsible for global changes in the magnetosphere: magnetic reconfiguration, particle acceleration, electric current and field enhancements.

Resonant pitch angle scattering also has the potential to remove resonant ions on timescales of under one hour. This timescale is therefore much shorter than the loss rate associated with collisional processes (Feldstein et al. 1994). The wave particle interaction mechanism is primarily important during the main phase of the storm (Gonzalez et al. 1989), possibly contributing to the geomagnetic trapping and acceleration of ionospheric ions that are injected during the main phase of a storm. Nevertheless, due to their localized nature (Jordanova et al. 1998), their contribution to the decay of the ring current is small relative to outflow, charge exchange and Coulomb collision losses.

Coulomb collisions between charged particles can also cause losses from the magnetosphere. While energy degradation from hot to cold particles occurs during these interactions (e.g., Fok et al. 1995; Jordanova et al. 1999; Liemohn et al. 2000) and in fact the energy deposition from this process is the cause of stable auroral red arcs (Kozyra et al. 1997), the primary contribution to mass loss from Coulomb collisions is via pitch angle scattering. Several studies have shown that this term is smaller than scattering due to wave-particle interactions and much smaller than either dayside flow out or charge exchange (e.g., Fok et al. 1993; Kozyra et al. 1998; Jordanova et al. 1998; Liemohn et al. 1997, 1999).

6 Open Questions

A great deal of work has been performed since the release of the Hultqvist et al. (1999) book. However, a great deal of questions remain unanswered. The balance of the contribution of solar and ionospheric plasma to the magnetosphere has shifted to the ionospheric source, especially in light of the expanded observations of the cold, "invisible" source. However, this topic is far from settled. The contribution of solar plasma is still only tenuously understood, especially as it is often difficult to separate from ionosphere populations. The magnitude of the flank-entering solar source is still undetermined, with further research required to determine what mechanisms efficiently allow mass entry into the magnetosphere.

Our understanding of the plasmasphere has also drastically transformed from a passive population to a critical reservoir of cold ions that has far-reaching implications. Further research into the effectiveness of the plasmaspheric wind in supplying cold ions to the outer magnetosphere is ongoing, as is work to determine the importance of plume material recirculating into other regions. The possibility of this material affecting solar-magnetosphere coupling by altering reconnection rates is also only tenuously understood.

Finally, with the advent of global models that better capture the different ionospheric sources of plasma, the self-consistent effects of all plasma sources on global dynamics are being rapidly explored. Recent work demonstrates that ionospheric outflow may regulate many global features, such as the development of substorms and sawteeth oscilla-

tions. A plethora of studies to scrutinize these potential relationships and demonstrate—or refute—their existence remain to be performed.

Conflict of interest The authors declare that they have no conflict of interests. This work did not include human or animal subjects.

References

T. Abe, B.A. Whalen, A.W. Yau, S. Watanabe, E. Sagawa, K.I. Oyama, Altitude profile of the polar wind velocity and its relationship to ionospheric conditions. Geophys. Res. Lett. **20**(24), 2825–2828 (1993a). doi:10.1029/93GL02837

T. Abe, B.A. Whalen, A.W. Yau, R.E. Horita, S. Watanabe, E. Sagawa, EXOS D (Akebono) suprathermal mass spectrometer observations of the polar wind. J. Geophys. Res. **98**(A7), 11191 (1993b). doi:10.1029/92JA01971

T. Abe, S. Watanabe, B.A. Whalen, A.W. Yau, E. Sagawa, Observations of polar wind and thermal ion outflow by Akebono/SMS. J. Geomagn. Geoelectr. **48**(3), 319–325 (1996). doi:10.5636/jgg.48.319. https://www.jstage.jst.go.jp/article/jgg1949/48/3/48_3_319/_article

T. Abe, Long-term variation of the polar wind velocity and its implication for the ion acceleration process: Akebono/suprathermal ion mass spectrometer observations. J. Geophys. Res. **109**(A9), 09305 (2004). doi:10.1029/2003JA010223

S.-I. Akasofu, The development of the auroral substorm. Planet. Space Sci. **12**(4), 273–282 (1964). doi:10.1016/0032-0633(64)90151-5. http://www.sciencedirect.com/science/article/pii/0032063364901515

J. Akinrimisi, S. Orsini, M. Candidi, H. Balsiger, *Ion Dynamics in the Plasma Mantle* (1989). http://www.researchgate.net/publication/234190759_Ion_dynamics_in_the_plasma_mantle

B.J. Anderson, S.A. Fuselier, Response of thermal ions to electromagnetic ion cyclotron waves. J. Geophys. Res. **99**(A10), 19413 (1994). doi:10.1029/94JA01235

M. André, C.M. Cully, Low-energy ions: a previously hidden solar system particle population. Geophys. Res. Lett. **39**(3) (2012). doi:10.1029/2011GL050242

M. André, K. Li, A.I. Eriksson, Outflow of low-energy ions and the solar cycle. J. Geophys. Res. Space Phys. (2015). doi:10.1002/2014JA020714

M. André, A. Vaivads, Y.V. Khotyaintsev, T. Laitinen, H. Nilsson, G. Stenberg, A. Fazakerley, J.G. Trotignon, Magnetic reconnection and cold plasma at the magnetopause. Geophys. Res. Lett. **37**(22) (2010). doi:10.1029/2010GL044611

M. André, P. Norqvist, L. Andersson, L. Eliasson, A.I. Eriksson, L. Blomberg, R.E. Erlandson, J. Waldemark, Ion energization mechanisms at 1700 km in the auroral region. J. Geophys. Res. **103**(A3), 4199 (1998). doi:10.1029/97JA00855. http://adsabs.harvard.edu/abs/1998JGR...103.4199A

N. André, J.F. Lemaire, Convective instabilities in the plasmasphere. J. Atmos. Sol.-Terr. Phys. **68**(2), 213–227 (2006). doi:10.1016/j.jastp.2005.10.013. http://www.sciencedirect.com/science/article/pii/S1364682605002932

V. Angelopoulos, W. Baumjohann, C.F. Kennel, F.V. Coroniti, M.G. Kivelson, R. Pellat, R.J. Walker, H. Lühr, G. Paschmann, Bursty bulk flows in the inner central plasma sheet. J. Geophys. Res. **97**(A4), 4027 (1992). doi:10.1029/91JA02701

V. Angelopoulos, C.F. Kennel, F.V. Coroniti, R. Pellat, H.E. Spence, M.G. Kivelson, R.J. Walker, W. Baumjohann, W.C. Feldman, J.T. Gosling, C.T. Russell, Characteristics of ion flow in the quiet state of the inner plasma sheet. Geophys. Res. Lett. **20**(16), 1711–1714 (1993). doi:10.1029/93GL00847

E.E. Antonova, The structure of the magnetospheric boundary layers and the magnetospheric turbulence. Planet. Space Sci. **53**, 161–168 (2005). doi:10.1016/j.pss.2004.09.041. http://www.sciencedirect.com/science/article/pii/S0032063304001813

R.L. Arnoldy, K.A. Lynch, P.M. Kintner, J. Vago, S. Chesney, T.E. Moore, C.J. Pollock, Bursts of transverse ion acceleration at rocket altitudes. Geophys. Res. Lett. **19**(4), 413–416 (1992). doi:10.1029/92GL00091

P.M. Banks, T.E. Holzer, High-latitude plasma transport: the polar wind. J. Geophys. Res. **74**(26), 6317–6332 (1969). doi:10.1029/JA074i026p06317

P.M. Banks, A.F. Nagy, W.I. Axford, Dynamical behavior of thermal protons in the mid-latitude ionosphere and magnetosphere. Planet. Space Sci. **19**(9), 1053–1067 (1971). doi:10.1016/0032-0633(71)90104-8. http://www.sciencedirect.com/science/article/pii/0032063371901048

W. Baumjohann, G. Paschmann, H. Lühr, Characteristics of high-speed ion flows in the plasma sheet. J. Geophys. Res. **95**(A4), 3801 (1990). doi:10.1029/JA095iA04p03801

M.B. Bavassano Cattaneo, M.F. Marcucci, Y.V. Bogdanova, H. Rème, I. Dandouras, L.M. Kistler, E. Lucek, Global reconnection topology as inferred from plasma observations inside Kelvin–Helmholtz vortices. Ann. Geophys. **28**(4), 893–906 (2010). doi:10.5194/angeo-28-893-2010. http://www.ann-geophys.net/28/893/2010/angeo-28-893-2010.html

J. Borovsky, M.F. Thomsen, R.C. Elphic, The driving of the plasma sheet by the solar wind. J. Geophys. Res. **103**(A8), 17617–17639 (1998)

J.E. Borovsky, MHD turbulence in the Earth's plasma sheet: dynamics, dissipation, and driving. J. Geophys. Res. **108**(A7), 1284 (2003). doi:10.1029/2002JA009625

J.E. Borovsky, M.H. Denton, A statistical look at plasmaspheric drainage plumes. J. Geophys. Res. **113**(A9), 09221 (2008). doi:10.1029/2007JA012994

J.E. Borovsky, J.T. Steinberg, The "calm before the storm" in CIR/magnetosphere interactions: occurrence statistics, solar wind statistics, and magnetospheric preconditioning. J. Geophys. Res. **111**(A7), 7–10 (2006). doi:10.1029/2005JA011397

J.E. Borovsky, R.C. Elphic, H.O. Funsten, M.F. Thomsen, *The Earth's Plasma Sheet as a Laboratory for Flow Turbulence in High-β MHD* (Cambridge University Press, Cambridge, 1997). doi:10.1017/S0022377896005259. http://journals.cambridge.org/abstract_S0022377896005259

J.E. Borovsky, M. Hesse, J. Birn, M.M. Kuznetsova, What determines the reconnection rate at the dayside magnetosphere? J. Geophys. Res. **113**(A7), 07210 (2008). doi:10.1029/2007JA012645

M. Bouhram, B. Klecker, W. Miyake, H. Rème, J.-A. Sauvaud, M. Malingre, L. Kistler, A. Blăgău, On the altitude dependence of transversely heated O⁺ distributions in the cusp/cleft. Ann. Geophys. **22**(5), 1787–1798 (2004). doi:10.5194/angeo-22-1787-2004. http://www.ann-geophys.net/22/1787/2004/angeo-22-1787-2004.html

O.J. Brambles, W. Lotko, P.a. Damiano, B. Zhang, M. Wiltberger, J. Lyon, Effects of causally driven cusp O+ outflow on the storm time magnetosphere-ionosphere system using a multifluid global simulation. J. Geophys. Res. **115**, 1–4 (2010). doi:10.1029/2010JA015469

O.J. Brambles, W. Lotko, B. Zhang, M. Wiltberger, J. Lyon, R.J. Strangeway, Magnetosphere sawtooth oscillations induced by ionospheric outflow. Science **332**(6034), 1183–1186 (2011). doi:10.1126/science.1202869

O.J. Brambles, W. Lotko, B. Zhang, J. Ouellette, J. Lyon, M. Wiltberger, The effects of ionospheric outflow on ICME and SIR driven sawtooth-events. J. Geophys. Res. Space Phys. **118**(10), 6026–6041 (2013). doi:10.1002/jgra.50522

W. Bristow, Statistics of velocity fluctuations observed by SuperDARN under steady interplanetary magnetic field conditions. J. Geophys. Res. Space Phys. **113**(A11), 11202 (2008). doi:10.1029/2008JA013203

M. Candidi, S. Orsini, V. Formisano, The properties of ionospheric O/+/ ions as observed in the magnetotail boundary layer and northern plasma lobe. J. Geophys. Res. **87**, 9097–9106 (1982)

H.C. Carlson, Accelerated polar rain electrons as the source of Sun-aligned arcs in the polar cap during northward interplanetary magnetic field conditions. J. Geophys. Res. **110**(A5), 05302 (2005). doi:10.1029/2004JA010669

D.L. Carpenter, Electron-density variations in the magnetosphere deduced from whistler data. J. Geophys. Res. **67**(9), 3345–3360 (1962). doi:10.1029/JZ067i009p03345

P.A. Cassak, M.A. Shay, Scaling of asymmetric magnetic reconnection: general theory and collisional simulations. Phys. Plasmas **14**(10), 102114 (2007). doi:10.1063/1.2795630. http://scitation.aip.org/content/aip/journal/pop/14/10/10.1063/1.2795630

C.R. Chappell, Initial observations of thermal plasma composition and energetics from dynamics explorer-1. Geophys. Res. Lett. **9**(9), 929–932 (1982). doi:10.1029/GL009i009p00929

C.R. Chappell, The role of the ionosphere in providing plasma to the terrestrial magnetosphere—an historical overview. Space Sci. Rev. (2015, submitted)

C.R. Chappell, T.E. Moore, J.H. Waite, The ionosphere as a fully adequate source of plasma for the Earth's magnetosphere. J. Geophys. Res. **92**(A6), 5896 (1987). doi:10.1029/JA092iA06p05896

C.R. Chappell, M.M. Huddleston, T.E. Moore, B.L. Giles, D.C. Delcourt, Observations of the warm plasma cloak and an explanation of its formation in the magnetosphere. J. Geophys. Res. **113**(A9), 09206 (2008). doi:10.1029/2007JA012945

C. Chaston, J. Bonnell, J.P. McFadden, C.W. Carlson, C. Cully, O. Le Contel, A. Roux, H.U. Auster, K.H. Glassmeier, V. Angelopoulos, C.T. Russell, Turbulent heating and cross-field transport near the magnetopause from THEMIS. Geophys. Res. Lett. **35**(17), L17S08 (2008). doi:10.1029/2008GL033601

L. Chen, Theory of plasma transport induced by low-frequency hydromagnetic waves. J. Geophys. Res. **104**(A2), 2421 (1999). doi:10.1029/1998JA900051

L. Chen, W. Li, J. Bortnik, R.M. Thorne, Amplification of whistler-mode hiss inside the plasmasphere. Geophys. Res. Lett. **39**(8) (2012). doi:10.1029/2012GL051488

S.P. Christon, M.I. Desai, T.E. Eastman, G. Gloeckler, S. Kokubun, A.T.Y. Lui, R.W. McEntire, E.C. Roelof, D.J. Williams, Low-charge-state heavy ions upstream of Earth's bow shock and sunward flux of ionospheric O+1, N+1, and O+2 ions: Geotail observations. Geophys. Res. Lett. **27**(16), 2433–2436 (2000). doi:10.1029/2000GL000039

B.M.A. Cooling, C.J. Owen, S.J. Schwartz, Role of the magnetosheath flow in determining the motion of open flux tubes. J. Geophys. Res. **106**(A9), 18763 (2001). doi:10.1029/2000JA000455

S.W.H. Cowley, Comments on the merging of non-antiparallel magnetic fields. J. Geophys. Res. **81**, 3455–3458 (1976)

S.W.H. Cowley, C.J. Owen, A simple illustrative model of open flux tube motion over the dayside magnetopause. Planet. Space Sci. **37**(11), 1461–1475 (1989). doi:10.1016/0032-0633(89)90116-5. http://www.sciencedirect.com/science/article/pii/0032063389901165

C.M. Cully, E. Donovan, A.W. Yau, G.G. Arkos, Akebono/Suprathermal mass spectrometer observations of low-energy ion outflow: dependence on magnetic activity and solar wind conditions. J. Geophys. Res. **108**(A2), 1093 (2003a). doi:10.1029/2001JA009200

C.M. Cully, E.F. Donovan, A.W. Yau, H.J. Opgenoorth, Supply of thermal ionospheric ions to the central plasma sheet. J. Geophys. Res. **108**(A2), 1092 (2003b). doi:10.1029/2002JA009457

I.A. Daglis, W.I. Axford, Fast ionospheric response to enhanced activity in geospace: ion feeding of the inner magnetotail. J. Geophys. Res. **101**(A), 5047–5066 (1996)

L.A. Daglis, S. Livi, E.T. Sarris, B. Wilken, Energy density of ionospheric and solar wind origin ions in the near-Earth magnetotail during substorms. J. Geophys. Res. **99**, 5691–5703 (1994)

I. Dandouras, Detection of a plasmaspheric wind in the Earth's magnetosphere by the Cluster spacecraft. Ann. Geophys. **31**(7), 1143–1153 (2013). doi:10.5194/angeo-31-1143-2013. http://www.ann-geophys.net/31/1143/2013/angeo-31-1143-2013.html

I. Dandouras, V. Pierrard, J. Goldstein, C. Vallat, G.K. Parks, H. Rème, C. Gouillart, F. Sevestre, M. Mccarthy, L.M. Kistler, B. Klecker, A. Korth, P. Bavassano-Cattaneo, M.B. Escoubet, A. Masson, No TitleMultipoint observations of ionic structures in the plasmasphere by CLUSTER'CIS and comparisons with IMAGE-EUV observations and with model simulations, in *Inner Magnetosphere Interactions: New Perspectives from Imaging*, ed. by J. Burch, M. Schulz, H. Spence (Am. Geophys. Union, Washington, 2005). doi:10.1029/159GM03

F. Darrouzet, V. Pierrard, S. Benck, G. Lointier, J. Cabrera, K. Borremans, N.Y. Ganushkina, J.D. Keyser, Links between the plasmapause and the radiation belt boundaries as observed by the instruments CIS, RAPID, and WHISPER onboard Cluster. J. Geophys. Res. Space Phys. **118**(7), 4176–4188 (2013). doi:10.1002/jgra.50239

F. Darrouzet, D.L. Gallagher, N. André, D.L. Carpenter, I. Dandouras, P.M. Décréau, J.D. Keyser, R.E. Denton, J.C. Foster, J. Goldstein, M.B. Moldwin, B.W. Reinisch, B.R. Sandel, J. Tu, Plasmaspheric density structures and dynamics: properties observed by the CLUSTER and IMAGE missions, in *The Earth's Plasmasphere*, ed. by F. Darrouzet, J. De Keyser, V. Pierrard (Springer, New York, 2009), pp. 55–106. 978-1-4419-1322-7. doi:10.1007/978-1-4419-1323-4. http://link.springer.com/10.1007/978-1-4419-1323-4

D.C. Delcourt, J.A. Sauvaud, A. Pedersen, Dynamics of single-particle orbits during substorm expansion phase. J. Geophys. Res. **95**(A12), 20853 (1990). doi:10.1029/JA095iA12p20853

D.C. Delcourt, C.R. Chappell, T.E. Moore, J.H. Waite, A three-dimensional numerical model of ionospheric plasma in the magnetosphere. J. Geophys. Res. **94**(A9), 11893 (1989). doi:10.1029/JA094iA09p11893. http://adsabs.harvard.edu/abs/1989JGR....9411893D

D.C. Delcourt, T.E. Moore, J.A. Sauvaud, C.R. Chappell, Nonadiabatic transport features in the outer cusp region. J. Geophys. Res. **97**, 16833 (1992)

D.C. Delcourt, Particle acceleration by inductive electric fields in the inner magnetosphere. J. Atmos. Sol.-Terr. Phys. **64**(5-6), 551–559 (2002). doi:10.1016/S1364-6826(02)00012-3. http://www.sciencedirect.com/science/article/pii/S1364682602000123

E. Drakou, A.W. Yau, T. Abe, Ion temperature measurements from the Akebono suprathermal mass spectrometer: application to the polar wind. J. Geophys. Res. **102**(A8), 17523 (1997). doi:10.1029/97JA00099

J.W. Dungey, The steady state of the Chapman–Ferraro problem in two dimensions. J. Geophys. Res. **66**(4), 1043–1047 (1961). doi:10.1029/JZ066i004p01043. http://adsabs.harvard.edu/abs/1961JGR....66.1043D

J.P. Eastwood, S.A. Kiehas, in *Magnetotails in the Solar System*, ed. by A. Keiling, C.M. Jackman, P. Delmare (Wiley, Hoboken, 2015), pp. 269–287. Chap. 16

Y. Ebihara, M. Ejiri, Modeling of solar wind control of the ring current buildup: a case study of the magnetic storms in April 1997. Geophys. Res. Lett. **25**(20), 3751–3754 (1998). doi:10.1029/1998GL900006

R.C. Elphic, M.F. Thomsen, J.E. Borovsky, The fate of the outer plasmasphere. Geophys. Res. Lett. **24**(4), 365–368 (1997). doi:10.1029/97GL00141

E. Engwall, A.I. Eriksson, M. André, I. Dandouras, G. Paschmann, J. Quinn, K. Torkar, Low-energy (order 10 eV) ion flow in the magnetotail lobes inferred from spacecraft wake observations. Geophys. Res. Lett. **33**(6), 06110 (2006). doi:10.1029/2005GL025179

E. Engwall, A.I. Eriksson, C.M. Cully, M. André, R. Torbert, H. Vaith, *Earth's Ionospheric Outflow Dominated by Hidden Cold Plasma* (2009a). doi:10.1038/ngeo387. http://dx.doi.org/10.1038/ngeo387

E. Engwall, A.I. Eriksson, C.M. Cully, M. André, P.A. Puhl-Quinn, H. Vaith, R. Torbert, Survey of cold ionospheric outflows in the magnetotail. Ann. Geophys. **27**(8), 3185–3201 (2009b). doi:10.5194/angeo-27-3185-2009. http://www.ann-geophys.net/27/3185/2009/

J. Etcheto, A. Saint-Marc, Anomalously high plasma densities in the plasma sheet boundary layer. J. Geophys. Res. **90**(A6), 5338 (1985). doi:10.1029/JA090iA06p05338

M. Faganello, F. Califano, F. Pegoraro, T. Andreussi, S. Benkadda, Magnetic reconnection and Kelvin–Helmholtz instabilities at the Earth's magnetopause. Plasma Phys. Control. Fusion **54**(12), 124037 (2012). doi:10.1088/0741-3335/54/12/124037. http://stacks.iop.org/0741-3335/54/i=12/a=124037

M. Faganello, F. Califano, F. Pegoraro, A. Retinò, Kelvin–Helmholtz vortices and double mid-latitude reconnection at the Earth's magnetopause: comparison between observations and simulations. Europhys. Lett. **107**(1), 19001 (2014). doi:10.1209/0295-5075/107/19001. http://stacks.iop.org/0295-5075/107/i=1/a=19001

D.H. Fairfield, On the average configuration of the geomagnetic tail. J. Geophys. Res. **84**(A5), 1950 (1979). doi:10.1029/JA084iA05p01950

R.C. Fear, S.E. Milan, R. Maggiolo, A.N. Fazakerley, I. Dandouras, S.B. Mende, Direct observation of closed magnetic flux trapped in the high-latitude magnetosphere. Science **346**(6216), 1506–1510 (2014). doi:10.1126/science.1257377. http://www.sciencemag.org/content/346/6216/1506.short

Y.I. Feldstein, A.E. Levitin, S.A. Golyshev, L.A. Dremukhina, U.B. Vestchezerova, T.E. Valchuk, A. Grafe, Ring current and auroral electrojets in connection with interplanetary medium parameters during magnetic storm. Ann. Geophys. **12**(7), 602–611 (1994). doi:10.1007/s00585-994-0602-6. http://www.ann-geophys.net/12/602/1994/

M.-C. Fok, J.U. Kozyra, A.F. Nagy, C.E. Rasmussen, G.V. Khazanov, Decay of equatorial ring current ions and associated aeronomical consequences. J. Geophys. Res. **98**(A11), 19381 (1993). doi:10.1029/93JA01848

M.-C. Fok, P.D. Craven, T.E. Moore, P.G. Richards, Ring current-plasmasphere coupling through Coulomb collisions, in *Cross-Scale Coupling in Space Plasmas*, ed. by J.L. Horwitz, N. Singh, J.L. Burch (Am. Geophys. Union, Washington, 1995). doi:10.1029/GM093p0161

M. Förster, G. Paschmann, S.E. Haaland, J.M. Quinn, R.B. Torbert, H. Vaith, C.A. Kletzing, High-latitude plasma convection from Cluster EDI: variances and solar wind correlations. Ann. Geophys. **25**(7), 1691–1707 (2007). https://hal.archives-ouvertes.fr/hal-00318357/

C. Foster, M. Lester, J.A. Davies, A statistical study of diurnal, seasonal and solar cycle variations of F-region and topside auroral upflows observed by EISCAT between 1984 and 1996. Ann. Geophys. **16**(10), 1144–1158 (1998). doi:10.1007/s00585-998-1144-0. http://www.ann-geophys.net/16/1144/1998/

J.C. Foster, Stormtime observations of the flux of plasmaspheric ions to the dayside cusp/magnetopause. Geophys. Res. Lett. **31**(8), 08809 (2004). doi:10.1029/2004GL020082

J.C. Foster, Multiradar observations of the polar tongue of ionization. J. Geophys. Res. **110**(A9), 9–31 (2005). doi:10.1029/2004JA010928

J.C. Foster, P.J. Erickson, D.N. Baker, S.G. Claudepierre, C.A. Kletzing, W. Kurth, G.D. Reeves, S.A. Thaller, H.E. Spence, Y.Y. Shprits, J.R. Wygant, Prompt energization of relativistic and highly relativistic electrons during a substorm interval: Van Allen Probes observations. Geophys. Res. Lett. **41**(1), 20–25 (2014a). doi:10.1002/2013GL058438

J.C. Foster, P.J. Erickson, A.J. Coster, S. Thaller, J. Tao, J.R. Wygant, J.W. Bonnell, Storm time observations of plasmasphere erosion flux in the magnetosphere and ionosphere. Geophys. Res. Lett. **41**(3), 762–768 (2014b). doi:10.1002/2013GL059124

J.C. Foster, Storm time plasma transport at middle and high latitudes. J. Geophys. Res. **98**(A2), 1675 (1993). doi:10.1029/92JA02032

C. Foullon, C.J. Farrugia, A.N. Fazakerley, C.J. Owen, F.T. Gratton, R.B. Torbert, Evolution of Kelvin–Helmholtz activity on the dusk flank magnetopause. J. Geophys. Res. **113**(A11), 11203 (2008). doi:10.1029/2008JA013175

H.U. Frey, Localized aurora beyond the auroral oval. Rev. Geophys. **45**(1), 1003 (2007). doi:10.1029/2005RG000174

T.A. Fritz, M. Alothman, J. Bhattacharjya, D.L. Matthews, J. Chen, Butterfly pitch-angle distributions observed by ISEE-1. Planet. Space Sci. **51**(3), 205–219 (2003). doi:10.1016/S0032-0633(02)00202-7. http://www.sciencedirect.com/science/article/pii/S0032063302002027

S.A. Fuselier, W.S. Lewis, Properties of near-Earth magnetic reconnection from in-situ observations. Space Sci. Rev. **160**(1-4), 95–121 (2011). doi:10.1007/s11214-011-9820-x. http://link.springer.com/10.1007/s11214-011-9820-x

S.A. Fuselier, B.J. Anderson, T.G. Onsager, Particle signatures of magnetic topology at the magnetopause: AMPTE/CCE observations. J. Geophys. Res. **100**(A7), 11805 (1995). doi:10.1029/94JA02811
S.A. Fuselier, B.J. Anderson, T.G. Onsager, Electron and ion signatures of field line topology at the low-shear magnetopause. J. Geophys. Res. **102**(A3), 4847 (1997). doi:10.1029/96JA03635
S.A. Fuselier, K.J. Trattner, S.M. Petrinec, Antiparallel and component reconnection at the dayside magnetopause. J. Geophys. Res. **116**(A10), 10227 (2011). doi:10.1029/2011JA016888
S.A. Fuselier, K.J. Trattner, S.M. Petrinec, B. Lavraud, Dayside magnetic topology at the Earth's magnetopause for northward IMF. J. Geophys. Res. **117**(A8), 08235 (2012). doi:10.1029/2012JA017852
K.S. Garcia, V.G. Merkin, W.J. Hughes, Effects of nightside O+ outflow on magnetospheric dynamics: results of multifluid MHD modeling. J. Geophys. Res. **115**(May), 1–9 (2010). doi:10.1029/2010JA015730
N.G.J. Gazey, M. Lockwood, M. Grande, C.H. Perry, P.N. Smith, S. Coles, A.D. Aylward, R.J. Bunting, H. Opgenoorth, B. Wilken, EISCAT/CRRES observations: nightside ionospheric ion outflow and oxygen-rich substorm injections. Ann. Geophys. **14**(1), 1032–1043 (1996)
A. Glocer, G. Tóth, T. Gombosi, D. Welling, Modeling ionospheric outflows and their impact on the magnetosphere, initial results. J. Geophys. Res. **114**(A5), 1–16 (2009a). doi:10.1029/2009JA014053
a. Glocer, G. Tóth, Y. Ma, T. Gombosi, J.-C. Zhang, L.M. Kistler, Multifluid block-adaptive-tree solar wind roe-type upwind scheme: magnetospheric composition and dynamics during geomagnetic storms initial results. J. Geophys. Res. **114**(A12), 12203 (2009b). doi:10.1029/2009JA014418
G. Gloeckler, D.C. Hamilton, AMPTE ion composition results. Phys. Scr. T **18**, 73–84 (1987)
J. Goldstein, Control of plasmaspheric dynamics by both convection and sub-auroral polarization stream. Geophys. Res. Lett. **30**(24), 2243 (2003). doi:10.1029/2003GL018390
W.D. Gonzalez, B.T. Tsurutani, A.L.C. Gonzalez, E.J. Smith, F. Tang, S.-I. Akasofu, Solar wind-magnetosphere coupling during intense magnetic storms (1978–1979). J. Geophys. Res. **94**(A7), 8835 (1989). doi:10.1029/JA094iA07p08835
J.T. Gosling, D.N. Baker, S.J. Bame, E.W. Hones, D.J. McComas, R.D. Zwickl, J.A. Slavin, E.J. Smith, B.T. Tsurutani, Plasma entry into the distant tail lobes: ISEE-3. Geophys. Res. Lett. **11**(10), 1078–1081 (1984). doi:10.1029/GL011i010p01078
M.E. Greenspan, D.C. Hamilton, Relative contributions of H+ and O+ to the ring current energy near magnetic storm maximum. J. Geophys. Res. Space Phys. **107**(A), 1043 (2002)
R.S. Grew, F.W. Menk, M.A. Clilverd, B.R. Sandel, Mass and electron densities in the inner magnetosphere during a prolonged disturbed interval. Geophys. Res. Lett. **34**(2), 02108 (2007). doi:10.1029/2006GL028254
S. Haaland, B. Lybekk, K. Svenes, A. Pedersen, M. Förster, H. Vaith, R. Torbert, Plasma transport in the magnetotail lobes. Ann. Geophys. **27**(9), 3577–3590 (2009). doi:10.5194/angeo-27-3577-2009. http://www.ann-geophys.net/27/3577/2009/angeo-27-3577-2009.html
S. Haaland, A. Eriksson, E. Engwall, B. Lybekk, H. Nilsson, A. Pedersen, K. Svenes, M. André, M. Förster, K. Li, C. Johnsen, N. Østgaard, Estimating the capture and loss of cold plasma from ionospheric outflow. J. Geophys. Res. **117**(A7), 07311 (2012). doi:10.1029/2012JA017679
G. Haerendel, G. Paschmann, Entry of solar wind plasma into the magnetosphere, in *Physics of the Hot Plasma in the Magnetosphere*, ed. by B. Hultqvist, L. Stenflo (Springer, New York, 1975), pp. 23–43. doi:10.1007/978-1-4613-4437-7_2
D.C. Hamilton, G. Gloeckler, F.M. Ipavich, W. Stüdemann, B. Wilken, G. Kremser, Ring current development during the great geomagnetic storm of February 1986. J. Geophys. Res. **93**(A12), 14343 (1988). doi:10.1029/JA093iA12p14343
Y. Harada, S. Machida, J.S. Halekas, A.R. Poppe, J.P. McFadden, ARTEMIS observations of lunar dayside plasma in the terrestrial magnetotail lobe. J. Geophys. Res. Space Phys. **118**(6), 3042–3054 (2013). doi:10.1002/jgra.50296
D.A. Hardy, J.W. Freeman, H.K. Hills, Plasma observations in the magnetotail, in *Magnetospheric Particles and Fields*, ed. by B.M. McCormac, Hingham, Mass., USA (1976), p. 89
D.A. Hardy, H.K. Hills, J.W. Freeman, A new plasma regime in the distant geomagnetic tail. Geophys. Res. Lett. **2**(5), 169–172 (1975). doi:10.1029/GL002i005p00169
D.A. Hardy, H.K. Hills, J.W. Freeman, Occurrence of the lobe plasma at lunar distance. J. Geophys. Res. **84**(A1), 72 (1979). doi:10.1029/JA084iA01p00072
C. Harvey, J. Etcheto, Y. Javel, R. Manning, M. Petit, The ISEE electron density experiment. IEEE Trans. Geosci. Electron. **16**(3), 231–238 (1978). doi:10.1109/TGE.1978.294553. http://ieeexplore.ieee.org/lpdocs/epic03/wrapper.htm?arnumber=4071924
A. Hasegawa, L. Chen, Kinetic process of plasma heating due to Alfvén wave excitation. Phys. Rev. Lett. **35**(6), 370–373 (1975). doi:10.1103/PhysRevLett.35.370. http://link.aps.org/doi/10.1103/PhysRevLett.35.370
A. Hasegawa, K. Mima, Anomalous transport produced by kinetic Alfvén wave turbulence. J. Geophys. Res. **83**(A3), 1117 (1978). doi:10.1029/JA083iA03p01117

H. Hasegawa, M. Fujimoto, T.-D. Phan, H. Rème, A. Balogh, M.W. Dunlop, C. Hashimoto, R. Tandokoro, Transport of solar wind into Earth's magnetosphere through rolled-up Kelvin–Helmholtz vortices. Nature **430**(7001), 755–758 (2004). doi:10.1038/nature02799. http://dx.doi.org/10.1038/nature02799

H. Hasegawa, M. Fujimoto, K. Takagi, Y. Saito, T. Mukai, H. Rème, Single-spacecraft detection of rolled-up Kelvin–Helmholtz vortices at the flank magnetopause. J. Geophys. Res. **111**(A9), 09203 (2006). doi:10.1029/2006JA011728

H. Hasegawa, A. Retinò, A. Vaivads, Y. Khotyaintsev, M. André, T.K.M. Nakamura, W.-L. Teh, B.U.O. Sonnerup, S.J. Schwartz, Y. Seki, M. Fujimoto, Y. Saito, H. Rème, P. Canu, Kelvin–Helmholtz waves at the Earth's magnetopause: multiscale development and associated reconnection. J. Geophys. Res. **114**(A12), 12207 (2009). doi:10.1029/2009JA014042. http://adsabs.harvard.edu/abs/2009JGRA..11412207H

R.A. Heelis, J.D. Winningham, M. Sugiura, N.C. Maynard, Particle acceleration parallel and perpendicular to the magnetic field observed by DE-2. J. Geophys. Res. **89**(A6), 3893 (1984). doi:10.1029/JA089iA06p03893

W.J. Heikkila, R.J. Pellinen, Localized induced electric field within the magnetotail. J. Geophys. Res. **82**(10), 1610–1614 (1977). doi:10.1029/JA082i010p01610

M.G. Henderson, The may 2–3, 1986 CDAW-9C interval: a sawtooth event. Geophys. Res. Lett. **31**(11), 11804 (2004). doi:10.1029/2004GL019941

M. Hirahara, Periodic emergence of multicomposition cold ions modulated by geomagnetic field line oscillations in the near-Earth magnetosphere. J. Geophys. Res. **109**(A3), 03211 (2004). doi:10.1029/2003JA010141

M. Hirahara, M. Nakamura, T. Terasawa, T. Mukai, Y. Saito, T. Yamamoto, A. Nishida, S. Machida, S. Kokubun, Acceleration and heating of cold ion beams in the plasma sheet boundary layer observed with GEOTAIL. Geophys. Res. Lett. **21**, 3003–3006 (1994) (ISSN 0094-8276)

M. Hirahara, T. Terasawa, T. Mukai, M. Hoshino, Y. Saito, S. Machida, T. Yamamoto, S. Kokubun, Cold ion streams consisting of double proton populations and singly charged oxygen observed at the distant magnetopause by Geotail: a case study. J. Geophys. Res. **102**(A), 2359–2372 (1997)

E.W. Hones, J.R. Asbridge, S.J. Bame, M.D. Montgomery, S. Singer, S.-I. Akasofu, Measurements of magnetotail plasma flow made with Vela 4B. J. Geophys. Res. **77**(28), 5503–5522 (1972). doi:10.1029/JA077i028p05503

R.B. Horne, R.M. Thorne, Potential waves for relativistic electron scattering and stochastic acceleration during magnetic storms. Geophys. Res. Lett. **25**(15), 3011–3014 (1998). doi:10.1029/98GL01002

J.L. Horwitz, The tail lobe ion spectrometer. J. Geophys. Res. **91**, 5689–5699 (1986)

C.-S. Huang, Periodic magnetospheric substorms and their relationship with solar wind variations. J. Geophys. Res. **108**(A6), 1255 (2003). doi:10.1029/2002JA009704

M.M. Huddleston, C.R. Chappell, D.C. Delcourt, T.E. Moore, B.L. Giles, M.O. Chandler, An examination of the process and magnitude of ionospheric plasma supply to the magnetosphere. J. Geophys. Res. Space Phys. **110** (2005). doi:10.1029/2004JA010401

B. Hultqvist, On the origin of the hot ions in the disturbed dayside magnetosphere. Planet. Space Sci. **31**(2), 173–184 (1983). doi:10.1016/0032-0633(83)90052-1. http://www.sciencedirect.com/science/article/pii/0032063383900521

B. Hultqvist, M. Øieroset, G. Paschmann, R.A. Treumann (eds.), *Magnetospheric Plasma Sources and Losses*. Space Sciences Series of ISSI, vol. 6 (Springer, Dordrecht, 1999). 978-94-010-5918-3. doi:10.1007/978-94-011-4477-3. http://www.springerlink.com/index/10.1007/978-94-011-4477-3

K.-J. Hwang, M.M. Kuznetsova, F. Sahraoui, M.L. Goldstein, E. Lee, G.K. Parks, Kelvin–Helmholtz waves under southward interplanetary magnetic field. J. Geophys. Res. **116**(A8), 08210 (2011). doi:10.1029/2011JA016596

K.-J. Hwang, M.L. Goldstein, M.M. Kuznetsova, Y. Wang, A.F. Viñas, D.G. Sibeck, The first in situ observation of Kelvin–Helmholtz waves at high-latitude magnetopause during strongly dawnward interplanetary magnetic field conditions. J. Geophys. Res. **117**(A8), 08233 (2012). doi:10.1029/2011JA017256

R. Ilie, R.M. Skoug, H.O. Funsten, M.W. Liemohn, J.J. Bailey, M. Gruntman, The impact of geocoronal density on ring current development. J. Atmos. Sol.-Terr. Phys. **99**, 92–103 (2013). doi:10.1016/j.jastp.2012.03.010. http://www.sciencedirect.com/science/article/pii/S1364682612000946

S.M. Imber, J.A. Slavin, H.U. Auster, V. Angelopoulos, A THEMIS survey of flux ropes and traveling compression regions: location of the near-Earth reconnection site during solar minimum. J. Geophys. Res. **116**(A2), 02201 (2011). doi:10.1029/2010JA016026

F.M. Ipavich, A.B. Galvin, G. Gloeckler, D. Hovestadt, B. Klecker, M. Scholer, Energetic (>100 keV) O+ ions in the plasma sheet. Geophys. Res. Lett. **11**(5), 504–507 (1984). doi:10.1029/GL011i005p00504

J.R. Johnson, C.Z. Cheng, Kinetic Alfvén waves and plasma transport at the magnetopause. Geophys. Res. Lett. **24**(11), 1423–1426 (1997). doi:10.1029/97GL01333

J.R. Johnson, C.Z. Cheng, Stochastic ion heating at the magnetopause due to kinetic Alfvén waves. Geophys. Res. Lett. **28**(23), 4421–4424 (2001). doi:10.1029/2001GL013509
J.R. Johnson, S. Wing, Northward interplanetary magnetic field plasma sheet entropies. J. Geophys. Res. Space Phys. **114** (2009). doi:10.1029/2008JA014017
V.K. Jordanova, L.M. Kistler, J.U. Kozyra, G.V. Khazanov, A.F. Nagy, Collisional losses of ring current ions. J. Geophys. Res. **101**(A1), 111 (1996). doi:10.1029/95JA02000
V.K. Jordanova, C.J. Farrugia, J.M. Quinn, R.M. Thorne, K.E. Ogilvie, R.P. Lepping, G. Lu, A.J. Lazarus, M.F. Thomsen, R.D. Belian, Effect of wave-particle interactions on ring current evolution for January 10-11, 1997: initial results. Geophys. Res. Lett. **25**(15), 2971–2974 (1998). doi:10.1029/98GL00649
V.K. Jordanova, R.B. Torbert, R.M. Thorne, H.L. Collin, J.L. Roeder, J.C. Foster, Ring current activity during the early B z < 0 phase of the January 1997 magnetic cloud. J. Geophys. Res. **104**(A11), 24895 (1999). doi:10.1029/1999JA900339
V.K. Jordanova, L.M. Kistler, C.J. Farrugia, R.B. Torbert, Effects of inner magnetospheric convection on ring current dynamics: March 10–12, 1998. J. Geophys. Res. **106**(A), 29705–29720 (2001)
V.K. Jordanova, L.M. Kistler, M.F. Thomsen, C.G. Mouikis, Effects of plasma sheet variability on the fast initial ring current decay. Geophys. Res. Lett. **30**(6), 41–44 (2003)
V.K. Jordanova, R.M. Thorne, W. Li, Y. Miyoshi, Excitation of whistler mode chorus from global ring current simulations. J. Geophys. Res. **115**, 1–10 (2010). doi:10.1029/2009JA014810
Z. Kaymaz, G.L. Siscoe, N.A. Tsyganenko, R.P. Lepping, Magnetotail views at 33 R E : IMP 8 magnetometer observations. J. Geophys. Res. **99**(A5), 8705 (1994). doi:10.1029/93JA03564
K. Keika, Outflow of energetic ions from the magnetosphere and its contribution to the decay of the storm time ring current. J. Geophys. Res. **110**(A9), 09210 (2005). doi:10.1029/2004JA010970
K. Keika, L.M. Kistler, P.C. Brandt, Energization of O+ ions in the Earth's inner magnetosphere and the effects on ring current buildup: a review of previous observations and possible mechanisms. J. Geophys. Res. Space Phys. **118**(7), 4441–4464 (2013)
L.M. Kistler, F.M. Ipavich, D.C. Hamilton, G. Gloeckler, B. Wilken, Energy spectra of the major ion species in the ring current during geomagnetic storms. J. Geophys. Res. **94**, 3579–3599 (1989)
L.M. Kistler, E. Möbius, D.M. Klumpar, M.A. Popecki, L. Tang, V. Jordanova, B. Klecker, W.K. Peterson, E.G. Shelley, D. Hovestadt, M. Temerin, R.E. Ergun, J.P. McFadden, C.W. Carlson, F.S. Mozer, R.C. Elphic, R.J. Strangeway, C.A. Cattell, R.F. Pfaff, FAST/TEAMS observations of charge exchange signatures in ions mirroring at low altitudes. Geophys. Res. Lett. **25**(1), 2085–2088 (1998)
L.M. Kistler, B. Klecker, V.K. Jordanova, E. Möbius, M.A. Popecki, D. Patel, J.A. Sauvaud, H. Rème, A.M. Di Lellis, A. Korth, M. McCarthy, R. Cerulli, M.B. Bavassano-Cattaneo, L. Eliasson, C.W. Carlson, G.K. Parks, G. Paschmann, W. Baumjohann, G. Haerendel, Testing electric field models using ring current ion energy spectra from the Equator-S ion composition (ESIC) instrument. Ann. Geophys. **17**(1), 1611–1621 (1999)
L.M. Kistler, C. Mouikis, E. Möbius, B. Klecker, J.A. Sauvaud, H. Réme, A. Korth, M.F. Marcucci, R. Lundin, G.K. Parks, A. Balogh, Contribution of nonadiabatic ions to the cross-tail current in an O+ dominated thin current sheet. J. Geophys. Res. Space Phys. **110**(A6), 06213 (2005). doi:10.1029/2004JA010653
L.M. Kistler, C.G. Mouikis, B. Klecker, I. Dandouras, Cusp as a source for oxygen in the plasma sheet during geomagnetic storms. J. Geophys. Res. **115**(A3), 03209 (2010a). doi:10.1029/2009JA014838
L.M. Kistler, a.B. Galvin, M.a. Popecki, K.D.C. Simunac, C. Farrugia, E. Moebius, M.a. Lee, L.M. Blush, P. Bochsler, P. Wurz, B. Klecker, R.F. Wimmer-Schweingruber, A. Opitz, J.-a. Sauvaud, B. Thompson, C.T. Russell, Escape of O+ through the distant tail plasma sheet. Geophys. Res. Lett. **37**(21) (2010b). doi:10.1029/2010GL045075
D.M. Klumpar, Transversely accelerated ions: an ionospheric source of hot magnetospheric ions. J. Geophys. Res. **84**(A8), 4229 (1979). doi:10.1029/JA084iA08p04229
D.M. Klumpar, W.K. Peterson, E.G. Shelley, Direct evidence for two-stage (bimodal) acceleration of ionospheric ions. J. Geophys. Res. **89**(A12), 10779 (1984). doi:10.1029/JA089iA12p10779
G.A. Kotova, The Earth's plasmasphere: state of studies (a review). Geomagn. Aeron. **47**(4), 409–422 (2007). doi:10.1134/S0016793207040019. http://link.springer.com/10.1134/S0016793207040019
J.U. Kozyra, Multistep Dst development and ring current composition changes during the 4–6 June 1991 magnetic storm. J. Geophys. Res. **107**(A8), 1224 (2002). doi:10.1029/2001JA000023
J.U. Kozyra, A.F. Nagy, D.W. Slater, High-altitude energy source(s) for stable auroral red arcs. Rev. Geophys. **35**(2), 155 (1997). doi:10.1029/96RG03194
J.U. Kozyra, M.-C. Fok, E.R. Sanchez, D.S. Evans, D.C. Hamilton, A.F. Nagy, The role of precipitation losses in producing the rapid early recovery phase of the Great Magnetic Storm of February 1986. J. Geophys. Res. **103**(A4), 6801 (1998). doi:10.1029/97JA03330
J.U. Kozyra, M.W. Liemohn, Ring current energy input and decay, in *Magnetospheric Imaging—the Image Prime Mission*, ed. by J.L. Burch (Springer, Berlin, 2003), pp. 105–131. doi:10.1007/978-94-010-0027-7_6

S.M. Krimigis, R.W. McEntire, T.A. Potemra, G. Gloeckler, F.L. Scarf, E.G. Shelley, A synthesis of ring current spectra and energy densities measured with AMPTE/CCE. Geophys. Res. Lett. **12**, 329–332 (1985). Magnetic storm of September 4, 1984 (ISSN 0094-8276)

E.A. Kronberg, M. Ashour-Abdalla, I. Dandouras, D.C. Delcourt, E.E. Grigorenko, L.M. Kistler, I.V. Kuzichev, J. Liao, R. Maggiolo, H.V. Malova, K.G. Orlova, V. Peroomian, D.R. Shklyar, Y.Y. Shprits, D.T. Welling, L.M. Zelenyi, Circulation of heavy ions and their dynamical effects in the magnetosphere: recent observations and models. Space Sci. Rev. **184**(1-4), 173–235 (2014). doi:10.1007/s11214-014-0104-0. http://link.springer.com/10.1007/s11214-014-0104-0

A. Kullen, Solar wind dependence of the occurrence and motion of polar auroral arcs: a statistical study. J. Geophys. Res. **107**(A11), 1362 (2002). doi:10.1029/2002JA009245

J. Labelle, R.A. Treumann, Plasma waves at the dayside magnetopause. Space Sci. Rev. **47**(1–2) (1988). doi:10.1007/BF00223240. http://link.springer.com/10.1007/BF00223240

B. Lavraud, Characteristics of the magnetosheath electron boundary layer under northward interplanetary magnetic field: implications for high-latitude reconnection. J. Geophys. Res. **110**(A6), 06209 (2005). doi:10.1029/2004JA010808

B. Lavraud, M.F. Thomsen, B. Lefebvre, S.J. Schwartz, K. Seki, T.D. Phan, Y.L. Wang, A. Fazakerley, H. Rème, A. Balogh, Evidence for newly closed magnetosheath field lines at the dayside magnetopause under northward IMF. J. Geophys. Res. **111**(A5), 05211 (2006). doi:10.1029/2005JA011266

J.H. Lee, V. Angelopoulos, On the presence and properties of cold ions near Earth's equatorial magnetosphere. J. Geophys. Res. Space Phys. **119**(3), 1749–1770 (2014). doi:10.1002/2013JA019305

L.C. Lee, J.R. Johnson, Z.W. Ma, Kinetic Alfvén waves as a source of plasma transport at the dayside magnetopause. J. Geophys. Res. **99**(A9), 17405 (1994). doi:10.1029/94JA01095

J. Lemaire, M. Scherer, Model of the polar ion-exosphere. Planet. Space Sci. **18**(1), 103–120 (1970). doi:10.1016/0032-0633(70)90070-X. http://www.sciencedirect.com/science/article/pii/003206337090070X

J. Lemaire, R.W. Schunk, Plasmaspheric wind. J. Atmos. Terr. Phys. **54**(3-4), 467–477 (1992). doi:10.1016/0021-9169(92)90026-H. http://www.sciencedirect.com/science/article/pii/002191699290026H

J.F. Lemaire, K.I. Gringauz, *The Earth's Plasmasphere* (Cambridge University Press, Cambridge, 1998), p. 376. 0521675553. http://books.google.com/books?hl=en&lr=&id=xdnWRdPEvdQC&pgis=1

J.F. Lemaire, The formation plasmaspheric tails. Phys. Chem. Earth, Part C, Sol.-Terr. Planet. Sci. **25**(1-2), 9–17 (2000). doi:10.1016/S1464-1917(99)00026-4. http://www.sciencedirect.com/science/article/pii/S1464191799000264

J.F. Lemaire, The formation of the light-ion trough and peeling off the plasmasphere. J. Atmos. Sol.-Terr. Phys. **63**(11), 1285–1291 (2001). doi:10.1016/S1364-6826(00)00232-7. http://www.sciencedirect.com/science/article/pii/S1364682600002327

K. Li, S. Haaland, A. Eriksson, M. André, E. Engwall, Y. Wei, E.A. Kronberg, M. Fränz, P.W. Daly, H. Zhao, Q.Y. Ren, On the ionospheric source region of cold ion outflow. Geophys. Res. Lett. **39**(18) (2012). doi:10.1029/2012GL053297

W. Li, Plasma sheet formation during long period of northward IMF. Geophys. Res. Lett. **32**(12), L12S08 (2005). doi:10.1029/2004GL021524

J. Liao, L.M. Kistler, C.G. Mouikis, B. Klecker, I. Dandouras, J.-C. Zhang, Statistical study of O+ transport from the cusp to the lobes with Cluster CODIF data. J. Geophys. Res. **115**, 1–15 (2010). doi:10.1029/2010JA015613

J. Liao, L.M. Kistler, C.G. Mouikis, B. Klecker, I. Dandouras, Solar cycle dependence of the cusp O+ access to the near-Earth magnetotail. J. Geophys. Res. **117**(A10), 10220 (2012). doi:10.1029/2012JA017819

J. Liao, X. Cai, L.M. Kistler, C.R. Clauer, C.G. Mouikis, B. Klecker, I. Dandouras, The relationship between sawtooth events and O+ in the plasma sheet. J. Geophys. Res. Space Phys. **119**(3), 1572–1586 (2014). doi:10.1002/2013JA019084

J. Liao, L.M. Kistler, C.G. Mouikis, B. Klecker, I. Dandouras, Acceleration of O+ from the cusp to the plasma sheet. J. Geophys. Res. Space Phys. (2015)

M.W. Liemohn, Occurrence statistics of cold, streaming ions in the near-Earth magnetotail: survey of polar-TIDE observations. J. Geophys. Res. **110**(A7), 07211 (2005). doi:10.1029/2004JA010801

M.W. Liemohn, G.V. Khazanov, J.U. Kozyra, Guided plasmaspheric hiss interactions with superthermal electrons: 1. Resonance curves and timescales. J. Geophys. Res. **102**(A6), 11619 (1997). doi:10.1029/97JA00825

M.W. Liemohn, J.U. Kozyra, V.K. Jordanova, G.V. Khazanov, M.F. Thomsen, T.E. Cayton, Analysis of early phase ring current recovery mechanisms during geomagnetic storms. Geophys. Res. Lett. **26**(18), 2845–2848 (1999). doi:10.1029/1999GL900611

M.W. Liemohn, J.U. Kozyra, P.G. Richards, G.V. Khazanov, M.J. Buonsanto, V.K. Jordanova, Ring current heating of the thermal electrons at solar maximum. J. Geophys. Res. **105**(A12), 27767 (2000). doi:10.1029/2000JA000088

M.W. Liemohn, J.U. Kozyra, M.F. Thomsen, J.L. Roeder, G. Lu, J.E. Borovsky, T.E. Cayton, Dominant role of the asymmetric ring current in producing the stormtime Dst*. J. Geophys. Res. **106**(A6), 10883 (2001). doi:10.1029/2000JA000326

Y. Lin, J.R. Johnson, X.Y. Wang, Hybrid simulation of mode conversion at the magnetopause. J. Geophys. Res. **115**(A4), 04208 (2010). doi:10.1029/2009JA014524

Y. Lin, J.R. Johnson, X. Wang, Three-dimensional mode conversion associated with kinetic Alfvén waves. Phys. Rev. Lett. **109**(12), 125003 (2012). doi:10.1103/PhysRevLett.109.125003. http://link.aps.org/doi/10.1103/PhysRevLett.109.125003

H. Liu, S.-Y. Ma, K. Schlegel, Diurnal, seasonal, and geomagnetic variations of large field-aligned ion upflows in the high-latitude ionospheric F region. J. Geophys. Res. **106**(A11), 24651 (2001). doi:10.1029/2001JA900047

R.E. Lopez, R. Bruntz, E.J. Mitchell, M. Wiltberger, J.G. Lyon, V.G. Merkin, Role of magnetosheath force balance in regulating the dayside reconnection potential. J. Geophys. Res. **115**(A12), 12216 (2010). doi:10.1029/2009JA014597

W. Lotko, The magnetosphere–ionosphere system from the perspective of plasma circulation: a tutorial. J. Atmos. Sol.-Terr. Phys. **69**(3), 191–211 (2007). doi:10.1016/j.jastp.2006.08.011. http://www.sciencedirect.com/science/article/pii/S1364682606002604

J.G. Luhmann, D.W. Curtis, P. Schroeder, J. McCauley, R.P. Lin, D.E. Larson, S.D. Bale, J.-A. Sauvaud, C. Aoustin, R.A. Mewaldt, A.C. Cummings, E.C. Stone, A.J. Davis, W.R. Cook, B. Kecman, M.E. Wiedenbeck, T. von Rosenvinge, M.H. Acuna, L.S. Reichenthal, S. Shuman, K.A. Wortman, D.V. Reames, R. Mueller-Mellin, H. Kunow, G.M. Mason, P. Walpole, A. Korth, T.R. Sanderson, C.T. Russell, J.T. Gosling, STEREO IMPACT investigation goals, measurements, and data products overview. Space Sci. Rev. **136**(1-4), 117–184 (2007). doi:10.1007/s11214-007-9170-x. http://adsabs.harvard.edu/abs/2008SSRv..136..117L

B. Lybekk, A. Pedersen, S. Haaland, K. Svenes, A.N. Fazakerley, A. Masson, M.G.G.T. Taylor, J.-G. Trotignon, Solar cycle variations of the Cluster spacecraft potential and its use for electron density estimations. J. Geophys. Res. Space Phys. **117**(A1) (2012). doi:10.1029/2011JA016969

K. Maezawa, T. Hori, The distant magnetotail: its structure, IMF dependence, and thermal properties, in *New Perspectives on the Earth's Magnetotail*, ed. by A. Nishida, D.N. Baker, S.W.H. Cowley (Am. Geophys. Union, Washington, 1998). doi:10.1029/GM105p0001

R. Maggiolo, J.A. Sauvaud, D. Fontaine, A. Teste, E. Grigorenko, A. Balogh, A. Fazakerley, G. Paschmann, D. Delcourt, H. Rème, A multi-satellite study of accelerated ionospheric ion beams above the polar cap. Ann. Geophys. **24**(6), 1665–1684 (2006). doi:10.5194/angeo-24-1665-2006. http://www.ann-geophys.net/24/1665/2006/angeo-24-1665-2006.html

R. Maggiolo, M. Echim, J. De Keyser, D. Fontaine, C. Jacquey, I. Dandouras, Polar cap ion beams during periods of northward IMF: Cluster statistical results. Ann. Geophys. **29**(5), 771–787 (2011). doi:10.5194/angeo-29-771-2011. http://www.ann-geophys.net/29/771/2011/angeo-29-771-2011.html

R. Maggiolo, M. Echim, C. Simon Wedlund, Y. Zhang, D. Fontaine, G. Lointier, J.-G. Trotignon, Polar cap arcs from the magnetosphere to the ionosphere: kinetic modelling and observations by Cluster and TIMED. Ann. Geophys. **30**(2), 283–302 (2012). doi:10.5194/angeo-30-283-2012. http://www.ann-geophys.net/30/283/2012/angeo-30-283-2012.html

B.H. Mauk, Quantitative modeling of the "convection surge" mechanism of ion acceleration. J. Geophys. Res. **91**(A12), 13423 (1986). doi:10.1029/JA091iA12p13423

J.P. McFadden, C.W. Carlson, D. Larson, J. Bonnell, F.S. Mozer, V. Angelopoulos, K.-H. Glassmeier, U. Auster, Structure of plasmaspheric plumes and their participation in magnetopause reconnection: first results from THEMIS. Geophys. Res. Lett. **35**(17), L17S10 (2008). doi:10.1029/2008GL033677

C.E. McIlwain, A Kp dependent equatorial electric field model. Adv. Space Res. **6**(3), 187–197 (1986). doi:10.1016/0273-1177(86)90331-5. http://www.sciencedirect.com/science/article/pii/0273117786903315

R.L. McPherron, Earth's magnetotail, in *Magnetotails in the Solar System*, ed. by A. Keiling, C.M. Jackman, P. Delmare (Wiley, Hoboken, 2015), pp. 61–84. Chap. 3

D.G. Mitchell, P. C:son Brandt, E.C. Roelof, D.C. Hamilton, K.C. Retterer, S. Mende, Global imaging of O+ from IMAGE/HENA. Space Sci. Rev. **109**(1-4), 63–75 (2003). doi:10.1023/B:SPAC.0000007513.55076.00. http://link.springer.com/10.1023/B:SPAC.0000007513.55076.00

A. Miura, Kelvin–Helmholtz instability for supersonic shear flow at the magnetospheric boundary. Geophys. Res. Lett. **17**(6), 749–752 (1990). doi:10.1029/GL017i006p00749

W. Miyake, T. Mukai, N. Kaya, On the evolution of ion conics along the field line from EXOS D observations. J. Geophys. Res. **98**(A7), 11127 (1993). doi:10.1029/92JA00716

W. Miyake, T. Mukai, N. Kaya, On the origins of the upward shift of elevated (bimodal) ion conics in velocity space. J. Geophys. Res. **101**(A12), 26961 (1996). doi:10.1029/96JA02601

E. Möbius, D. Hovestadt, B. Klecker, M. Scholer, F.M. Ipavich, C.W. Carlson, R.P. Lin, A burst of energetic O+ ions during an upstream particle event. Geophys. Res. Lett. **13**(13), 1372–1375 (1986). doi:10.1029/GL013i013p01372

T.E. Moore, The dayside reconnection X line. J. Geophys. Res. **107**(A10), 1332 (2002). doi:10.1029/2002JA009381

T.E. Moore, Plasma sheet and (nonstorm) ring current formation from solar and polar wind sources. J. Geophys. Res. **110**(A2), 02210 (2005). doi:10.1029/2004JA010563

T.E. Moore, C.R. Chappell, M.O. Chandler, P.D. Craven, B.L. Giles, C.J. Pollock, J.L. Burch, D.T. Young, J.H. Waite, J.E. Nordholt, M.F. Thomsen, D.J. McComas, J.J. Berthelier, W.S. Williamson, R. Robson, F.S. Mozer, High-altitude observations of the polar wind. Science **277**(5324), 349–351 (1997). doi:10.1126/science.277.5324.349. http://www.sciencemag.org/cgi/doi/10.1126/science.277.5324.349

T.E. Moore, W.K. Peterson, C.T. Russell, M.O. Chandler, M.R. Collier, H.L. Collin, P.D. Craven, R. Fitzenreiter, B.L. Giles, C.J. Pollock, Ionospheric mass ejection in response to a CME. Geophys. Res. Lett. **26**(15), 2339–2342 (1999). doi:10.1029/1999GL900456

T. Nagai, Solar wind control of the radial distance of the magnetic reconnection site in the magnetotail. J. Geophys. Res. **110**(A9), 09208 (2005). doi:10.1029/2005JA011207

D. Nagata, S. Machida, S. Ohtani, Y. Saito, T. Mukai, Solar wind control of plasma number density in the near-Earth plasma sheet. J. Geophys. Res. Space Phys. **112**(A9), 09204 (2007). doi:10.1029/2007JA012284

T.K.M. Nakamura, W. Daughton, H. Karimabadi, S. Eriksson, Three-dimensional dynamics of vortex-induced reconnection and comparison with THEMIS observations. J. Geophys. Res. Space Phys. **118**(9), 5742–5757 (2013). doi:10.1002/jgra.50547

B. Ni, R.M. Thorne, R.B. Horne, N.P. Meredith, Y.Y. Shprits, L. Chen, W. Li, Resonant scattering of plasma sheet electrons leading to diffuse auroral precipitation: 1. Evaluation for electrostatic electron cyclotron harmonic waves. J. Geophys. Res. **116**(A4), 04218 (2011a). doi:10.1029/2010JA016232

B. Ni, R.M. Thorne, N.P. Meredith, R.B. Horne, Y.Y. Shprits, Resonant scattering of plasma sheet electrons leading to diffuse auroral precipitation: 2. Evaluation for whistler mode chorus waves. J. Geophys. Res. **116**(A4), 04219 (2011b). doi:10.1029/2010JA016233

H. Nilsson, M. Waara, S. Arvelius, O. Marghitu, M. Bouhram, Y. Hobara, M. Yamauchi, R. Lundin, H. Rème, J.-A. Sauvaud, I. Dandouras, A. Balogh, L.M. Kistler, B. Klecker, C.W. Carlson, M.B. Bavassano-Cattaneo, A. Korth, Characteristics of high altitude oxygen ion energization and outflow as observed by Cluster: a statistical study. Ann. Geophys. **24**(3), 1099–1112 (2006). doi:10.5194/angeo-24-1099-2006. http://www.ann-geophys.net/24/1099/2006/angeo-24-1099-2006.html

H. Nilsson, E. Engwall, A. Eriksson, P.A. Puhl-Quinn, S. Arvelius, Centrifugal acceleration in the magnetotail lobes. Ann. Geophys. **28**(2), 569–576 (2010). doi:10.5194/angeo-28-569-2010. http://www.ann-geophys.net/28/569/2010/angeo-28-569-2010.html

H. Nilsson, I.A. Barghouthi, R. Slapak, A.I. Eriksson, M. André, Hot and cold ion outflow: spatial distribution of ion heating. J. Geophys. Res. **117**(A11), 11201 (2012)

H. Nilsson, I.A. Barghouthi, R. Slapak, A.I. Eriksson, M. André, Hot and cold ion outflow: observations and implications for numerical models. J. Geophys. Res. Space Phys. **118**(1), 105–117 (2013)

M. Nosé, A.T.Y. Lui, S. Ohtani, B.H. Mauk, R.W. McEntire, D.J. Williams, T. Mukai, K. Yumoto, Acceleration of oxygen ions of ionospheric origin in the near-Earth magnetotail during substorms. J. Geophys. Res. **105**(A4), 7669 (2000). doi:10.1029/1999JA000318

M. Nosé, K. Takahashi, K. Keika, L.M. Kistler, K. Koga, H. Koshiishi, H. Matsumoto, M. Shoji, Y. Miyashita, R. Nomura, Magnetic fluctuations embedded in dipolarization inside geosynchronous orbit and their associated selective acceleration of O+ ions. J. Geophys. Res. Space Phys. **119**(6), 4639–4655 (2014). doi:10.1002/2014JA019806

K. Nykyri, A. Otto, B. Lavraud, C. Mouikis, L.M. Kistler, A. Balogh, H. Rème, Cluster observations of reconnection due to the Kelvin–Helmholtz instability at the dawnside magnetospheric flank. Ann. Geophys. **24**(10), 2619–2643 (2006). doi:10.5194/angeo-24-2619-2006. http://www.ann-geophys.net/24/2619/2006/angeo-24-2619-2006.html

M. Øieroset, Global cooling and densification of the plasma sheet during an extended period of purely northward IMF on October 22–24, 2003. Geophys. Res. Lett. **32**(12), L12S07 (2005). doi:10.1029/2004GL021523

M. Øieroset, J. Raeder, T.D. Phan, S. Wing, J.P. McFadden, W. Li, M. Fujimoto, H. Rème, A. Balogh, Global cooling and densification of the plasma sheet during an extended period of purely northward IMF on October 22-24, 2003. Geophys. Res. Lett. **32**, 1–4 (2005). doi:10.1029/2004GL021523

Y. Obana, F.W. Menk, I. Yoshikawa, Plasma refilling rates for $L = 2.3$–3.8 flux tubes. J. Geophys. Res. **115**(A3), 03204 (2010). doi:10.1029/2009JA014191

Y. Ogawa, S.C. Buchert, R. Fujii, S. Nozawa, A.P. van Eyken, Characteristics of ion upflow and downflow observed with the European Incoherent Scatter Svalbard radar. J. Geophys. Res. **114**(A5), 05305 (2009). doi:10.1029/2008JA013817

Y. Ogawa, S.C. Buchert, A. Sakurai, S. Nozawa, R. Fujii, Solar activity dependence of ion upflow in the polar ionosphere observed with the European Incoherent Scatter (EISCAT) TromsøUHF radar. J. Geophys. Res. **115**(A7), 07310 (2010). doi:10.1029/2009JA014766

Y. Ono, M. Nosé, S.P. Christon, A.T.Y. Lui, The role of magnetic field fluctuations in nonadiabatic acceleration of ions during dipolarization. J. Geophys. Res. **114**(A5), 05209 (2009). doi:10.1029/2008JA013918

T.G. Onsager, J.D. Scudder, M. Lockwood, C.T. Russell, Reconnection at the high-latitude magnetopause during northward interplanetary magnetic field conditions. J. Geophys. Res. **106**(A11), 25467 (2001). doi:10.1029/2000JA000444

A. Opitz, J.-A. Sauvaud, A. Klassen, R. Gomez-Herrero, R. Bucik, L.M. Kistler, C. Jacquey, J. Luhmann, G. Mason, P. Kajdic, B. Lavraud, Solar wind control of the terrestrial magnetotail as seen by STEREO. J. Geophys. Res. Space Phys. **119**(8), 6342–6355 (2014). doi:10.1002/2014JA019988

S. Orsini, M. Candidi, M. Stockholm, H. Balsiger, Injection of ionospheric ions into the plasma sheet. J. Geophys. Res. **95**, 7915–7928 (1990)

A. Otto, D.H. Fairfield, Kelvin–Helmholtz instability at the magnetotail boundary: MHD simulation and comparison with Geotail observations. J. Geophys. Res. **105**(A9), 21175 (2000). doi:10.1029/1999JA000312

J.E. Ouellette, O.J. Brambles, J.G. Lyon, W. Lotko, B.N. Rogers, Properties of outflow-driven sawtooth substorms. J. Geophys. Res. Space Phys. **118**(6), 3223–3232 (2013). doi:10.1002/jgra.50309

I.L. Ovchinnikov, E.E. Antonova, Y.I. Yermolaev, Determination of the turbulent diffusion coefficient in the plasma sheet using the project INTERBALL data. Cosm. Res. **38**(6), 557–561 (2000). doi:10.1023/A:1026686600686. http://link.springer.com/article/10.1023/A%3A1026686600686

C.J. Owen, M.G.G.T. Taylor, I.C. Krauklis, A.N. Fazakerley, M.W. Dunlop, J.M. Bosqued, Cluster observations of surface waves on the dawn flank magnetopause. Ann. Geophys. **22**(3), 971–983 (2004). doi:10.5194/angeo-22-971-2004. http://www.ann-geophys.net/22/971/2004/angeo-22-971-2004.html

C.G. Park, Whistler observations of the interchange of ionization between the ionosphere and the protonosphere. J. Geophys. Res. **75**(22), 4249–4260 (1970). doi:10.1029/JA075i022p04249

G. Paschmann, G. Haerendel, N. Sckopke, H. Rosenbauer, P.C. Hedgecock, Plasma and magnetic field characteristics of the distant polar cusp near local noon: the entry layer. J. Geophys. Res. **81**(16), 2883–2899 (1976). doi:10.1029/JA081i016p02883

G. Paschmann, M. Øieroset, T. Phan, In-situ observations of reconnection in space. Space Sci. Rev. **178**(2-4), 385–417 (2013). doi:10.1007/s11214-012-9957-2. http://adsabs.harvard.edu/abs/2013SSRv..178..385P

R.J. Pellinen, W.J. Heikkila, Energization of charged particles to high energies by an induced substorm electric field within the magnetotail. J. Geophys. Res. **83**(A4), 1544 (1978). doi:10.1029/JA083iA04p01544

W.K. Peterson, L. Andersson, B.C. Callahan, H.L. Collin, J.D. Scudder, A.W. Yau, Solar-minimum quiet time ion energization and outflow in dynamic boundary related coordinates. J. Geophys. Res. **113**(A7), 07222 (2008). doi:10.1029/2008JA013059

W.K. Peterson, H.L. Collin, M.F. Doherty, C.M. Bjorklund, Extended (Bi-modal) ion conics at high altitudes, in *Space Plasmas: Coupling Between Small and Medium Scale Processes*. Geophysical Monograph, vol. 86 (1995). http://adsabs.harvard.edu/abs/1995GMS....86..105P

V. Pierrard, J. Cabrera, Comparisons between EUV/IMAGE observations and numerical simulations of the plasmapause formation. Ann. Geophys. **23**(7), 2635–2646 (2005). doi:10.5194/angeo-23-2635-2005. http://www.ann-geophys.net/23/2635/2005/angeo-23-2635-2005.html

V. Pierrard, J.F. Lemaire, Development of shoulders and plumes in the frame of the interchange instability mechanism for plasmapause formation. Geophys. Res. Lett. **31**(5) (2004). doi:10.1029/2003GL018919

V. Pierrard, G.V. Khazanov, J. Cabrera, J. Lemaire, Influence of the convection electric field models on predicted plasmapause positions during magnetic storms. J. Geophys. Res. **113**(A8), 08212 (2008). doi:10.1029/2007JA012612

V. Pierrard, J. Goldstein, N. André, V.K. Jordanova, G.A. Kotova, J.F. Lemaire, M.W. Liemohn, H. Matsui, Recent progress in physics-based models of the plasmasphere. Space Sci. Rev. **145**(1-2), 193–229 (2009). doi:10.1007/s11214-008-9480-7. http://link.springer.com/10.1007/s11214-008-9480-7

W.G. Pilipp, G. Morfill, The formation of the plasma sheet resulting from plasma mantle dynamics. J. Geophys. Res. **83**(A12), 5670 (1978). doi:10.1029/JA083iA12p05670

C.J. Pollock, M.O. Chandler, T.E. Moore, J.H. Waite, C.R. Chappell, D.A. Gurnett, A survey of upwelling ion event characteristics. J. Geophys. Res. **95**(A11), 18969 (1990). doi:10.1029/JA095iA11p18969

A.R. Poppe, R. Samad, J.S. Halekas, M. Sarantos, G.T. Delory, W.M. Farrell, V. Angelopoulos, J.P. McFadden, ARTEMIS observations of lunar pick-up ions in the terrestrial magnetotail lobes. Geophys. Res. Lett. **39**(17) (2012). doi:10.1029/2012GL052909

A. Posner, Association of low-charge-state heavy ions up to 200 R e upstream of the Earth's bow shock with geomagnetic disturbances. Geophys. Res. Lett. **29**(7), 1099 (2002). doi:10.1029/2001GL013449

H. Rème, C. Aoustin, J.M. Bosqued, I. Dandouras, B. Lavraud, J.A. Sauvaud, A. Barthe, J. Bouyssou, T. Camus, O. Coeur-Joly, A. Cros, J. Cuvilo, F. Ducay, Y. Garbarowitz, J.L. Medale, E. Penou, H. Perrier, D. Romefort, J. Rouzaud, C. Vallat, D. Alcaydé, C. Jacquey, C. Mazelle, C. D'Uston, E. Möbius,

L.M. Kistler, K. Crocker, M. Granoff, C. Mouikis, M. Popecki, M. Vosbury, B. Klecker, D. Hovestadt, H. Kucharek, E. Kuenneth, G. Paschmann, M. Scholer, N. Sckopke, E. Seidenschwang, C.W. Carlson, D.W. Curtis, C. Ingraham, R.P. Lin, J.P. McFadden, G.K. Parks, T. Phan, V. Formisano, E. Amata, M.B. Bavassano-Cattaneo, P. Baldetti, R. Bruno, G. Chionchio, A.D. Lellis, M.F. Marcucci, G. Pallocchia, A. Korth, P.W. Daly, B. Graeve, H. Rosenbauer, V. Vasyliunas, M. Mccarthy, M. Wilber, L. Eliasson, R. Lundin, S. Olsen, E.G. Shelley, S. Fuselier, A.G. Ghielmetti, W. Lennartsson, C.P. Escoubet, H. Balsiger, R. Friedel, J.-B. Cao, R.A. Kovrazhkin, I. Papamastorakis, R. Pellat, J. Scudder, B. Sonnerup, First multispacecraft ion measurements in and near the Earth's magnetosphere with the identical Cluster ion spectrometry (CIS) experiment. Ann. Geophys. **19**(10/12), 1303–1354 (2001). https://hal.archives-ouvertes.fr/hal-00329192/

W.T. Roberts, J.L. Horwitz, R.H. Comfort, C.R. Chappell, J.H. Waite, J.L. Green, Heavy ion density enhancements in the outer plasmasphere. J. Geophys. Res. **92**(A12), 13499 (1987). doi:10.1029/JA092iA12p13499

J.G. Roederer, On the adiabatic motion of energetic particles in a model magnetosphere. J. Geophys. Res. **72**(3), 981–992 (1967). doi:10.1029/JZ072i003p00981

J.G. Roederer, M. Schulz, Splitting of drift shells by the magnetospheric electric field. J. Geophys. Res. **76**(4), 1055–1059 (1971). doi:10.1029/JA076i004p01055

J.G. Roederer, H.H. Hilton, M. Schulz, Drift shell splitting by internal geomagnetic multipoles. J. Geophys. Res. **78**(1), 133–144 (1973). doi:10.1029/JA078i001p00133

H. Rosenbauer, H. Grünwaldt, M.D. Montgomery, G. Paschmann, N. Sckopke, Heos 2 plasma observations in the distant polar magnetosphere: the plasma mantle. J. Geophys. Res. **80**(19), 2723–2737 (1975). doi:10.1029/JA080i019p02723

Y. Saito, S. Yokota, K. Asamura, T. Tanaka, M.N. Nishino, T. Yamamoto, Y. Terakawa, M. Fujimoto, H. Hasegawa, H. Hayakawa, M. Hirahara, M. Hoshino, S. Machida, T. Mukai, T. Nagai, T. Nagatsuma, T. Nakagawa, M. Nakamura, K.-i. Oyama, E. Sagawa, S. Sasaki, K. Seki, I. Shinohara, T. Terasawa, H. Tsunakawa, H. Shibuya, M. Matsushima, H. Shimizu, F. Takahashi, In-flight performance and initial results of plasma energy angle and composition experiment (PACE) on SELENE (Kaguya). Space Sci. Rev. **154**(1-4), 265–303 (2010). doi:10.1007/s11214-010-9647-x. http://link.springer.com/10.1007/s11214-010-9647-x

B.R. Sandel, A.L. Broadfoot, C.C. Curtis, R.A. King, T.C. Stone, R.H. Hill, J. Chen, O.H.W. Siegmund, R. Raffanti, D.D. Allred, R.S. Turley, D.L. Gallagher, The extreme ultraviolet imager investigation for the image mission, in *The IMAGE Mission*, ed. by J.L. Burch (Springer, Berlin, 2000), pp. 197–242. doi:10.1007/978-94-011-4233-5_7

B.R. Sandel, J. Goldstein, D.L. Gallagher, M. Spasojevic, Extreme ultraviolet imager observations of the structure and dynamics of the plasmasphere. Space Sci. Rev. **109**(1-4), 25–46 (2003). doi:10.1023/B:SPAC.0000007511.47727.5b. http://link.springer.com/10.1023/B:SPAC.0000007511.47727.5b

J.-A. Sauvaud, R. Lundin, H. Rème, J.P. McFadden, C. Carlson, G.K. Parks, E. Möbius, L.M. Kistler, B. Klecker, E. Amata, A.M. Dilellis, V. Formisano, J.M. Bosqued, I. Dandouras, P. Décréau, M. Dunlop, L. Eliasson, A. Korth, B. Lavraud, M. Mccarthy, Intermittent thermal plasma acceleration linked to sporadic motions of the magnetopause, first Cluster results. Ann. Geophys. **19**(10/12), 1523–1532 (2001). https://hal.archives-ouvertes.fr/hal-00329207/

J.A. Sauvaud, P. Louarn, G. Fruit, H. Stenuit, C. Vallat, J. Dandouras, H. Rème, M. André, A. Balogh, M. Dunlop, L. Kistler, E. Möbius, C. Mouikis, B. Klecker, G.K. Parks, J. McFadden, C. Carlson, F. Marcucci, G. Pallocchia, R. Lundin, A. Korth, M. McCarthy, Case studies of the dynamics of ionospheric ions in the Earth's magnetotail. J. Geophys. Res. **109**(A), 1212 (2004)

R.W. Schunk, Time-dependent simulations of the global polar wind. J. Atmos. Sol.-Terr. Phys. **69**(16), 2028–2047 (2007). doi:10.1016/j.jastp.2007.08.009. http://www.sciencedirect.com/science/article/pii/S136468260700243X

N. Sckopke, G. Paschmann, H. Rosenbauer, D.H. Fairfield, Influence of the interplanetary magnetic field on the occurrence and thickness of the plasma mantle. J. Geophys. Res. **81**(16), 2687–2691 (1976). doi:10.1029/JA081i016p02687

K. Seki, M. Hirahara, T. Terasawa, I. Shinohara, T. Mukai, Y. Saito, S. Machida, T. Yamamoto, S. Kokubun, Coexistence of Earth-origin O+ and solar wind-origin H+/He++ in the distant magnetotail. Geophys. Res. Lett. **23**(9), 985–988 (1996). doi:10.1029/96GL00768

K. Seki, M. Hirahara, T. Terasawa, T. Mukai, S. Kokubun, Properties of He+ beams observed by Geotail in the lobe/mantle regions: comparison with O+ beams. J. Geophys. Res. **104**(A4), 6973 (1999). doi:10.1029/1998JA900142

K. Seki, General processes, in *Solar System Sources and Losses of Plasma* (2015)

K. Seki, T. Terasawa, M. Hirahara, T. Mukai, Quantification of tailward cold O+ beams in the lobe/mantle regions with Geotail data: constraints on polar O+ outflows. J. Geophys. Res. **103**(A), 29371–29382 (1998)

K. Seki, M. Hirahara, M. Hoshino, T. Terasawa, R.C. Elphic, Y. Saito, T. Mukai, H. Hayakawa, H. Kojima, H. Matsumoto, Cold ions in the hot plasma sheet of Earth's magnetotail. Nature **422**(6932), 589–592 (2003). doi:10.1038/nature01502. http://dx.doi.org/10.1038/nature01502

K. Seki, A. Nagy, C.M. Jackman, F. Crary, D. Fontaine, P. Zarka et al., A review of general physical and chemical processes related to plasma sources and losses for solar system magnetospheres. Space Sci. Rev. (2015). doi:10.1007/s11214-015-0170-y

E.G. Shelley, W.K. Peterson, A.G. Ghielmetti, J. Geiss, The polar ionosphere as a source of energetic magnetospheric plasma. Geophys. Res. Lett. **9**(9), 941–944 (1982). doi:10.1029/GL009i009p00941

D.G. Sibeck, R.W. McEntire, A.T.Y. Lui, R.E. Lopez, S.M. Krimigis, Magnetic field drift shell splitting: cause of unusual dayside particle pitch angle distributions during storms and substorms. J. Geophys. Res. **92**(A12), 13485 (1987). doi:10.1029/JA092iA12p13485

G.L. Siscoe, E. Sanchez, An MHD model for the complete open magnetotail boundary. J. Geophys. Res. **92**(A7), 7405 (1987). doi:10.1029/JA092iA07p07405

G.L. Siscoe, G.M. Erickson, B.U.O. Sonnerup, N.C. Maynard, K.D. Siebert, D.R. Weimer, W.W. White, Relation between cusp and mantle in MHD simulation. J. Geophys. Res. **106**(A6), 10743 (2001). doi:10.1029/2000JA000385

G. Siscoe, Z. Kaymaz, Spatial relations of mantle and plasma sheet. J. Geophys. Res. **104**(A7), 14639 (1999). doi:10.1029/1999JA900113

J.A. Slavin, E.J. Smith, P.W. Daly, T.R. Sanderson, K.-P. Wenzel, R.P. Lepping, Magnetic configuration of the distant plasma sheet: ISEE 3 observations, in *Magnetotail Physics* (1987), pp. 59–63. http://adsabs.harvard.edu/abs/1987magp.book...59S

J.A. Slavin, R.P. Lepping, J. Gjerloev, D.H. Fairfield, M. Hesse, C.J. Owen, M.B. Moldwin, T. Nagai, A. Ieda, T. Mukai, Geotail observations of magnetic flux ropes in the plasma sheet. J. Geophys. Res. Space Phys. **108**(A1), 1015 (2003). doi:10.1029/2002JA009557

J.A. Slavin, E.J. Smith, D.G. Sibeck, D.N. Baker, R.D. Zwickl, S.-I. Akasofu, An ISEE 3 study of average and substorm conditions in the distant magnetotail. J. Geophys. Res. **90**(A11), 10875 (1985). doi:10.1029/JA090iA11p10875

R. Smets, G. Belmont, D. Delcourt, L. Rezeau, Diffusion at the Earth magnetopause: enhancement by Kelvin–Helmholtz instability. Ann. Geophys. **25**(1), 271–282 (2007). doi:10.5194/angeo-25-271-2007. http://www.ann-geophys.net/25/271/2007/angeo-25-271-2007.html

P. Song, C.T. Russell, Model of the formation of the low-latitude boundary layer for strongly northward interplanetary magnetic field. J. Geophys. Res. **97**(A2), 1411 (1992). doi:10.1029/91JA02377

B.U.O. Sonnerup, Transport mechanisms at the magnetopause, in *Dynamics of the Magnetosphere*, ed. by S.-I. Akasofu (Springer, Berlin, 1980), pp. 77–100. 978-94-009-9519-2. doi:10.1007/978-94-009-9519-2_5

T.W. Speiser, Plasma density and acceleration in the tail from the reconnection model, in *Earth's Particles and Fields*, ed. by B.M. McCormac, New York, NY (1968)

H.E. Spence, M.G. Kivelson, Contributions of the low-latitude boundary layer to the finite width magnetotail convection model. J. Geophys. Res. **98**(A9), 15487 (1993). doi:10.1029/93JA01531

M. Stepanova, V. Pinto, J.A. Valdivia, E.E. Antonova, Spatial distribution of the eddy diffusion coefficients in the plasma sheet during quiet time and substorms from THEMIS satellite data. J. Geophys. Res. Space Phys. **116**(A5) (2011). doi:10.1029/2010JA015887

R. Strangeway, J.R.E. Ergun, Y.J. Su, C.W. Carlson, R.C. Elphic, Factors controlling ionospheric outflows as observed at intermediate altitudes. J. Geophys. Res. **110**(A3), 03221 (2005). doi:10.1029/2004JA010829

Y.-J. Su, J.L. Horwitz, T.E. Moore, B.L. Giles, M.O. Chandler, P.D. Craven, M. Hirahara, C.J. Pollock, Polar wind survey with the thermal ion dynamics Experiment/Plasma source instrument suite aboard POLAR. J. Geophys. Res. **103**(A12), 29305 (1998). doi:10.1029/98JA02662

Y.-J. Su, M.F. Thomsen, J.E. Borovsky, J.C. Foster, A linkage between polar patches and plasmaspheric drainage plumes. Geophys. Res. Lett. **28**(1), 111–113 (2001). doi:10.1029/2000GL012042

S. Taguchi, H. Kishida, T. Mukai, Y. Saito, Low-latitude plasma mantle in the near-Earth magnetosphere: Geotail observations. J. Geophys. Res. **106**(A2), 1949 (2001). doi:10.1029/2000JA900100

K. Takagi, C. Hashimoto, H. Hasegawa, M. Fujimoto, R. TanDokoro, Kelvin–Helmholtz instability in a magnetotail flank-like geometry: three-dimensional MHD simulations. J. Geophys. Res. **111**(A8), 08202 (2006). doi:10.1029/2006JA011631

K. Takahashi, B.J. Anderson, S.-i. Ohtani, G.D. Reeves, S. Takahashi, T.E. Sarris, K. Mursula, Drift-shell splitting of energetic ions injected at pseudo-substorm onsets. J. Geophys. Res. **102**(A10), 22117 (1997). doi:10.1029/97JA01870

S. Takahashi, T. Iyemori, M. Takeda, A simulation of the storm-time ring current. Planet. Space Sci. **38**(9), 1133–1141 (1990). doi:10.1016/0032-0633(90)90021-H. http://www.sciencedirect.com/science/article/pii/003206339090021H

S.W.Y. Tam, T. Chang, V. Pierrard, Kinetic modeling of the polar wind. J. Atmos. Sol.-Terr. Phys. **69**(16), 1984–2027 (2007). doi:10.1016/j.jastp.2007.08.006. http://www.sciencedirect.com/science/article/pii/S1364682607002428

T. Tanaka, Y. Saito, S. Yokota, K. Asamura, M.N. Nishino, H. Tsunakawa, H. Shibuya, M. Matsushima, H. Shimizu, F. Takahashi, M. Fujimoto, T. Mukai, T. Terasawa, First in situ observation of the Moon-originating ions in the Earth's magnetosphere by MAP-PACE on SELENE (KAGUYA). Geophys. Res. Lett. **36**(22), 22106 (2009). doi:10.1029/2009GL040682

M.G.G.T. Taylor, H. Hasegawa, B. Lavraud, T. Phan, C.P. Escoubet, M.W. Dunlop, Y.V. Bogdanova, A.L. Borg, M. Volwerk, J. Berchem, O.D. Constantinescu, J.P. Eastwood, A. Masson, H. Laakso, J. Soucek, A.N. Fazakerley, H.U. Frey, E.V. Panov, C. Shen, J.K. Shi, D.G. Sibeck, Z.Y. Pu, J. Wang, J.A. Wild, *Spatial Distribution of Rolled up Kelvin–Helmholtz Vortices at Earth's Dayside and Flank Magnetopause* (2012). http://eprints.lancs.ac.uk/60570/1/angeo_30_1025_2012.pdf

M.G.G.T. Taylor, B. Lavraud, C.P. Escoubet, S.E. Milan, K. Nykyri, M.W. Dunlop, J.A. Davies, R.H.W. Friedel, H. Frey, Y.V. Bogdanova, A. Å snes, H. Laakso, P. Trávnícek, A. Masson, H. Opgenoorth, C. Vallat, A.N. Fazakerley, A.D. Lahiff, C.J. Owen, F. Pitout, Z. Pu, C. Shen, Q.G. Zong, H. Rème, J. Scudder, T.L. Zhang, The plasma sheet and boundary layers under northward IMF: a multi-point and multi-instrument perspective. Adv. Space Res. **41**(10), 1619–1629 (2008). doi:10.1016/j.asr.2007.10.013. http://www.sciencedirect.com/science/article/pii/S0273117707010368

T. Terasawa, M. Fujimoto, T. Mukai, I. Shinohara, Y. Saito, T. Yamamoto, S. Machida, S. Kokubun, A.J. Lazarus, J.T. Steinberg, R.P. Lepping, Solar wind control of density and temperature in the near-Earth plasma sheet: WIND/GEOTAIL collaboration. Geophys. Res. Lett. **24**(8), 935–938 (1997). doi:10.1029/96GL04018

A. Teste, D. Fontaine, J.-A. Sauvaud, R. Maggiolo, P. Canu, A. Fazakerley, CLUSTER observations of electron outflowing beams carrying downward currents above the polar cap by northward IMF. Ann. Geophys. **25**(4), 953–969 (2007). doi:10.5194/angeo-25-953-2007. http://www.ann-geophys.net/25/953/2007/angeo-25-953-2007.html

A. Teste, D. Fontaine, P. Canu, G. Belmont, Cluster observations of outflowing electron distributions and broadband electrostatic emissions above the polar cap. Geophys. Res. Lett. **37**(3) (2010). doi:10.1029/2009GL041593

E.G. Thomas, J.B.H. Baker, J.M. Ruohoniemi, L.B.N. Clausen, A.J. Coster, J.C. Foster, P.J. Erickson, Direct observations of the role of convection electric field in the formation of a polar tongue of ionization from storm enhanced density. J. Geophys. Res. Space Phys. **118**(3), 1180–1189 (2013). doi:10.1002/jgra.50116

R.M. Thorne, Radiation belt dynamics: the importance of wave-particle interactions. Geophys. Res. Lett. **37**(22) (2010). doi:10.1029/2010GL044990

K. Torkar, A.I. Eriksson, P.-A. Lindqvist, W. Steiger, Long-term study of active spacecraft potential control. IEEE Trans. Plasma Sci. **36**(5), 2294–2300 (2008). doi:10.1109/TPS.2008.2003134. http://ieeexplore.ieee.org/lpdocs/epic03/wrapper.htm?arnumber=4663151

K.J. Trattner, J.S. Mulcock, S.M. Petrinec, S.A. Fuselier, Location of the reconnection line at the magnetopause during southward IMF conditions. Geophys. Res. Lett. **34**(3), 03108 (2007a). doi:10.1029/2006GL028397

K.J. Trattner, J.S. Mulcock, S.M. Petrinec, S.A. Fuselier, Probing the boundary between antiparallel and component reconnection during southward interplanetary magnetic field conditions. J. Geophys. Res. **112**(A8), 08210 (2007b). doi:10.1029/2007JA012270

K.J. Trattner, S.M. Petrinec, S.A. Fuselier, T.D. Phan, The location of reconnection at the magnetopause: testing the maximum magnetic shear model with THEMIS observations. J. Geophys. Res. Space Phys. **117**(A1) (2012). doi:10.1029/2011JA016959

B.T. Tsurutani, E.J. Smith, R.R. Anderson, K.W. Ogilvie, J.D. Scudder, D.N. Baker, S.J. Bame, Lion roars and nonoscillatory drift mirror waves in the magnetosheath. J. Geophys. Res. **87**(A8), 6060 (1982). doi:10.1029/JA087iA08p06060

N.A. Tsyganenko, Modeling the Earth's magnetospheric magnetic field confined within a realistic magnetopause. J. Geophys. Res. **100**(A4), 5599 (1995). doi:10.1029/94JA03193

J. Tu, P. Song, B.W. Reinisch, J.L. Green, Smooth electron density transition from plasmasphere to the subauroral region. J. Geophys. Res. **112**(A5), 05227 (2007). doi:10.1029/2007JA012298

C. Twitty, Cluster survey of cusp reconnection and its IMF dependence. Geophys. Res. Lett. **31**(19), 19808 (2004). doi:10.1029/2004GL020646

R.J. Walker, M. Ashour-Abdalla, T. Ogino, V. Peroomian, R.L. Richard, Modeling Magnetospheric Sources. Geophys. Monogr. **133** (2003). doi:10.1029/133GM03. http://192.102.233.13/books/gm/v133/133GM03/133GM03.pdf

B.M. Walsh, J.C. Foster, P.J. Erickson, D.G. Sibeck, Simultaneous ground- and space-based observations of the plasmaspheric plume and reconnection. Science **343**(6175), 1122–1125 (2014). doi:10.1126/science.1247212. http://www.sciencemag.org/content/343/6175/1122.short

C.-P. Wang, Modeling the transition of the inner plasma sheet from weak to enhanced convection. J. Geophys. Res. **109**(A12), 12202 (2004). doi:10.1029/2004JA010591
C.-P. Wang, L.R. Lyons, V. Angelopoulos, Properties of low-latitude mantle plasma in the Earth's magnetotail: ARTEMIS observations and global MHD predictions. J. Geophys. Res. Space Phys. **119**, 7264–7280 (2014). doi:10.1002/2014JA020060
C.-P. Wang, L.R. Lyons, T. Nagai, J.M. Weygand, R.W. McEntire, Sources, transport, and distributions of plasma sheet ions and electrons and dependences on interplanetary parameters under northward interplanetary magnetic field. J. Geophys. Res. **112**(A10), 10224 (2007). doi:10.1029/2007JA012522
C.P. Wang, L.R. Lyons, R.A. Wolf, T. Nagai, J.M. Weygand, A.T.Y. Lui, Plasma sheet Pv5/3and nν and associated plasma and energy transport for different convection strengths and AE levels. J. Geophys. Res. Space Phys. **114**, 1–2 (2009). doi:10.1029/2008JA013849
C.-P. Wang, L.R. Lyons, T. Nagai, J.M. Weygand, A.T.Y. Lui, Evolution of plasma sheet particle content under different interplanetary magnetic field conditions. J. Geophys. Res. **115**(A6), 06210 (2010). doi:10.1029/2009JA015028
C.-P. Wang, M. Gkioulidou, L.R. Lyons, V. Angelopoulos, Spatial distributions of the ion to electron temperature ratio in the magnetosheath and plasma sheet. J. Geophys. Res. **117**(A8), 08215 (2012). doi:10.1029/2012JA017658
C.-P. Wang, M. Gkioulidou, L.R. Lyons, X. Xing, R.A. Wolf, Interchange motion as a transport mechanism for formation of cold-dense plasma sheet. J. Geophys. Res. Space Phys. **119**, 8318–8337 (2014). doi:10.1002/2014JA020251
D.T. Welling, M.W. Liemohn, Outflow in global magnetohydrodynamics as a function of a passive inner boundary source. J. Geophys. Res. Space Phys. **119**(4), 2691–2705 (2014). doi:10.1002/2013JA019374
D.T. Welling, A.J. Ridley, Exploring sources of magnetospheric plasma using multispecies MHD. J. Geophys. Res. **115**(A4), 04201 (2010). doi:10.1029/2009JA014596
D.T. Welling, S.G. Zaharia, Ionospheric outflow and cross polar cap potential: what is the role of magnetospheric inflation? Geophys. Res. Lett. **39**(23) (2012). doi:10.1029/2012GL054228
D.T. Welling, V.K. Jordanova, S.G. Zaharia, A. Glocer, G. Toth, The effects of dynamic ionospheric outflow on the ring current. J. Geophys. Res. **116**, 1–19 (2011). doi:10.1029/2010JA015642
J.M. Weygand, Plasma sheet turbulence observed by Cluster II. J. Geophys. Res. **110**(A1), 01205 (2005). doi:10.1029/2004JA010581
B.A. Whalen, S. Watanabe, A.W. Yau, Observations in the transverse ion energization region. Geophys. Res. Lett. **18**(4), 725–728 (1991). doi:10.1029/90GL02788
M. Wiltberger, W. Lotko, J.G. Lyon, P. Damiano, V. Merkin, Influence of cusp O+ outflow on magnetotail dynamics in a multifluid MHD model of the magnetosphere. J. Geophys. Res. **115**(June), 1–5 (2010). doi:10.1029/2010JA015579
M. Wiltberger, Review of global simulation studies of effect of ionospheric outflow on magnetosphere-ionosphere system dynamics, in *Magnetotails in the Solar System* (Wiley, Hoboken, 2015), pp. 373–392. Chap. 22. doi:10.1002/978111884232
S. Wing, J.R. Johnson, P.T. Newell, C.I. Meng, Dawn-dusk asymmetries, ion spectra, and sources in the northward interplanetary magnetic field plasma sheet. J. Geophys. Res. Space Phys. **110**(A8), 08205 (2005). doi:10.1029/2005JA011086
S. Wing, J.R. Johnson, M. Fujimoto, Timescale for the formation of the cold-dense plasma sheet: a case study. Geophys. Res. Lett. **33**(23), 23106 (2006). doi:10.1029/2006GL027110
R.M. Winglee, Multi-fluid simulations of the magnetosphere: the identification of the geopause and its variation with IMF. Geophys. Res. Lett. **25**(24), 4441–4444 (1998). doi:10.1029/1998GL900217
R.M. Winglee, Global impact of ionospheric outflows on the dynamics of the magnetosphere and cross-polar cap potential. J. Geophys. Res. **107**(A9), 1237 (2002). doi:10.1029/2001JA000214
R.M. Winglee, E. Harnett, Influence of heavy ionospheric ions on substorm onset. J. Geophys. Res. **116**(A11), 11212 (2011). doi:10.1029/2011JA016447
G.Q. Yan, F.S. Mozer, C. Shen, T. Chen, G.K. Parks, C.L. Cai, J.P. McFadden, Kelvin–Helmholtz vortices observed by THEMIS at the duskside of the magnetopause under southward interplanetary magnetic field. Geophys. Res. Lett. (2014). doi:10.1002/2014GL060589
Y. Yao, C.C. Chaston, K.-H. Glassmeier, V. Angelopoulos, Electromagnetic waves on ion gyro-radii scales across the magnetopause. Geophys. Res. Lett. **38**(9) (2011). doi:10.1029/2011GL047328
A.W. Yau, M. André, M. Andre, Sources of ion outflow in the high latitude ionosphere. Space Sci. Rev. **80**(1-2), 1–25 (1997). doi:10.1023/A:1004947203046. http://link.springer.com/article/10.1023/A%3A1004947203046
A.W. Yau, W.K. Peterson, E.G. Shelley, Quantitative parametrization of energetic ionospheric ion outflow, in *Washington DC American Geophysical Union Geophysical Monograph Series* (1988), pp. 211–217
A.W. Yau, B.A. Whalen, A.G. McNamara, P.J. Kellogg, W. Bernstein, Particle and wave observations of low-altitude ionospheric ion acceleration events. J. Geophys. Res. **88**(A1), 341 (1983). doi:10.1029/JA088iA01p00341

A.W. Yau, B.A. Whalen, W.K. Peterson, E.G. Shelley, Distribution of upflowing ionospheric ions in the high-altitude polar cap and auroral ionosphere. J. Geophys. Res. **89**(A7), 5507 (1984). doi:10.1029/JA089iA07p05507

A.W. Yau, T. Abe, W.K. Peterson, The polar wind: recent observations. J. Atmos. Sol.-Terr. Phys. **69**(16), 1936–1983 (2007). doi:10.1016/j.jastp.2007.08.010. http://www.sciencedirect.com/science/article/pii/S1364682607002416

A.W. Yau, A. Howarth, W.K. Peterson, T. Abe, Transport of thermal-energy ionospheric oxygen (O+) ions between the ionosphere and the plasma sheet and ring current at quiet times preceding magnetic storms. J. Geophys. Res. **117**(A7), 07215 (2012). doi:10.1029/2012JA017803

I. Yoshikawa, Which is a significant contributor for outside of the plasmapause, an ionospheric filling or a leakage of plasmaspheric materials?: Comparison of He II (304 Å) images. J. Geophys. Res. **108**(A2), 1080 (2003). doi:10.1029/2002JA009578

Y. Yu, A.J. Ridley, Exploring the influence of ionospheric O+ outflow on magnetospheric dynamics: dependence on the source location. J. Geophys. Res. Space Phys. **118**(4), 1711–1722 (2013). doi:10.1029/2012JA018411

J. Zhang, M.W. Liemohn, D.L. De Zeeuw, J.E. Borovsky, A.J. Ridley, G. Toth, S. Sazykin, M.F. Thomsen, J.U. Kozyra, T.I. Gombosi, R.A. Wolf, Understanding storm-time ring current development through data-model comparisons of a moderate storm. J. Geophys. Res. **112**(A4), 04208 (2007). doi:10.1029/2006JA011846

Y. Zheng, T.E. Moore, F.S. Mozer, C.T. Russell, R.J. Strangeway, Polar study of ionospheric ion outflow versus energy input. J. Geophys. Res. **110**(A7), 07210 (2005). doi:10.1029/2004JA010995

X.-Z. Zhou, V. Angelopoulos, A.R. Poppe, J.S. Halekas, ARTEMIS observations of lunar pickup ions: mass constraints on ion species. J. Geophys. Res., Planets (2013). doi:10.1002/jgre.20125

L. Zhu, R.W. Schunk, J.J. Sojka, Polar cap arcs: a review. J. Atmos. Sol.-Terr. Phys. **59**(10), 1087–1126 (1997). doi:10.1016/S1364-6826(96)00113-7. http://www.sciencedirect.com/science/article/pii/S1364682696001137

Q.-G. Zong, B. Wilken, S.Y. Fu, T.A. Fritz, A. Korth, N. Hasebe, D.J. Williams, Z.-Y. Pu, Ring current oxygen ions escaping into the magnetosheath. J. Geophys. Res. **106**(A11), 25541 (2001). doi:10.1029/2000JA000127

S. Zou, M.B. Moldwin, A.J. Ridley, M.J. Nicolls, A.J. Coster, E.G. Thomas, J.M. Ruohoniemi, On the generation/decay of the storm-enhanced density plumes: role of the convection flow and field-aligned ion flow. J. Geophys. Res. Space Phys. **119**(10), 8543–8559 (2014). doi:10.1002/2014JA020408

R.D. Zwickl, D.N. Baker, S.J. Bame, W.C. Feldman, J.T. Gosling, E.W. Hones, D.J. McComas, B.T. Tsurutani, J.A. Slavin, Evolution of the Earth's distant magnetotail: ISEE 3 electron plasma results. J. Geophys. Res. **89**(A12), 11007 (1984). doi:10.1029/JA089iA12p11007